

**NUMERICAL PREDICTION OF DUCTILE FRACTURE
DUE TO MOVING LOAD**

by

© Md Abdullah, B.Eng.

A thesis submitted to the School of Graduate Studies
in partial fulfillment of the requirements for the degree of

Master of Engineering

Faculty of Engineering and Applied Science

Memorial University of Newfoundland

October 2017

St. John's

Newfoundland and Labrador

Canada

Abstract

This study investigates the effect of moving load on ductile fracture of shipbuilding metals through numerical simulation. Quinton [1,2] and Alsos [3] investigated moving load's effect on metals, in the plastic regime, and found that moving load results in a significant reduction in plastic capacity of metals. This study complements their work by extending the scope of the work up to ductile fracture initiation which was accomplished by implementing state-of-art ductile fracture model in moving loading scenario.

A state-of-art ductile fracture model has been implemented in this study by incorporating the knowledge acquired by research in the fracture mechanics arena. A stress state based fracture locus with strain rate and temperature effects has been selected as the ductile fracture criteria accordingly. Finite Element Method with Explicit Time Integration scheme deemed appropriate for numerical simulation and LS-DYNA has been chosen to accomplish this consequently.

This study attempts to mitigate two significant limitations of maritime structural assessment techniques associated with ship-ice interaction; undue simplification of load definition and over conservatism on fracture strain selection. Ship-ice interaction is considered as stationary loading scenario while it should be categorised as moving loading condition in accidental overloading situations. In addition, these techniques also regard fracture strain to be constant and independent of stress state, whereas studies show that ductile fracture initiation is highly dependent on the stress state.

This study provides a method to incorporate stress-state dependent state-of-art ductile fracture model for numerical investigation of moving load.

Acknowledgements

Firstly, I would like to express my deepest appreciation to both of my supervisors Dr. Bruce Quinton and Dr. Brian Veitch for providing me with the opportunity to work on this project and their support and encouragement throughout my stay at the Memorial University of Newfoundland. I am grateful to Dr. Bruce Quinton for his continual guidance and constructive discussions.

I am also grateful to Lloyd's Register Foundation for providing the financial support necessary to complete this work.

Finally, I would like to thank my mother who believed in me all along. Her constant support was the source of strength and motivation throughout this study.

Table of Contents

Abstract	ii
Acknowledgements	iii
Table of Contents	iv
List of Tables	viii
List of Figures	viii
List of Appendices	xi
Chapter 1 Introduction	1
Chapter 2 Literature Review	4
2.1 Collision and Grounding Analysis	5
2.1.1 Empirical Method	6
2.1.2 Analytical Method	6
2.1.3 Simplified Finite Element Method.....	7
2.1.4 Nonlinear FEM	9
2.2 Moving Load.....	11
2.3 Ductile Fracture	12
2.3.1 Void Nucleation	13
2.3.2 Void Growth	13
2.3.3 Void Coalescence and crack initiation.....	13

2.4	Implementation of Stress State based fracture criteria in Finite Element Analysis 14	
Chapter 3	Methodology	18
3.1	Fracture Criteria	19
3.2	Strain Rate & Temperature	20
3.3	Element Formulation	21
3.4	Material Model.....	22
3.5	Mesh Size Sensitivity.....	23
3.6	Contact Algorithm	24
3.7	Geometry & Boundary Condition.....	25
3.8	Model Validation	26
Chapter 4	Numerical Simulation	29
4.1	Geometry and Mesh.....	29
4.1.1	Mesh Elements.....	29
4.1.2	Mesh Quality.....	33
4.1.3	Initial Condition	34
4.2	Material Models	35
4.2.1	MAT_S01 Spring Elastic for Discrete Elements	35
4.2.2	MAT_020 Rigid for Solid Elements.....	36
4.2.3	MAT_224 Tabulated Johnson-Cook.....	36
4.3	Constraints	40

4.4	Load	41
4.5	Contact Algorithm	42
4.6	Output Control	44
4.6.1	Termination Control.....	44
4.6.2	Output Results Control	44
Chapter 5	Results and Discussions	46
5.1	Strain Rate Effect.....	48
5.1.1	Simulations with shell elements.....	49
5.1.2	Simulations with solid elements	51
5.2	Moving load capacity of the plate.....	53
5.2.1	Moving load capacity calculation with shell elements model	54
5.2.2	Comparison of moving load capacity between solid and shell elements model	56
5.3	State of stress during fracture initiation between stationary and moving loading scenario	59
5.4	Loading angle effects.....	64
5.5	Mesh convergence study.....	72
Chapter 6	Conclusions and Future Works	76
6.1	Conclusions.....	76
6.2	Future work.....	77
	Bibliography	79

Appendices..... 84

List of Tables

Table 3-1: Model parameters for validation simulations	27
Table 5-1: Summary of investigated effects	47
Table 5-2: Model parameters pertaining to strain rate effect (shell elements)	49
Table 5-3: Summarized results of strain rate effect (shell elements).....	50
Table 5-4: Model parameters pertaining to strain rate effect (solid elements)	51
Table 5-5: Summarized results of strain rate effect (solid elements)	52
Table 5-6: Parameters of stationary load effect simulations (shell elements)	54
Table 5-7: Parameters of stationary load effect models (solid vs shell)	56
Table 5-8: Results comparison between solid and shell elements models (fractured)	58
Table 5-9: Model parameters for state of stress effect.....	60
Table 5-10: Summary of results for state of stress	63
Table 5-11: Model parameters for loading angle effects (shell elements).....	66
Table 5-12: Summary of results for loading angle effects.....	68
Table 5-13: Model parameters for mesh convergence study	73
Table 5-14: Results obtained from mesh convergence study	74

List of Figures

Figure 2-1: Ductile damage evolution, a) initial state; b) void nucleation c) void growth; d) void coalescence [44]	12
Figure 2-2: Butterfly Specimen [9][6]	15
Figure 2-3: 3D fracture surface postulated by Wierzbicki and Bai [9].....	16

Figure 3-1: Vertical Force Vs Horizontal Displacement comparison for model validation.....	28
Figure 4-1 Shell elements (Aluminium Plate)	30
Figure 4-2 Solid Elements (Rigid Indenter).....	31
Figure 4-3: Solid Elements (Aluminium Plate)	31
Figure 4-4 Discrete Elements are shown at the corners of the plate (1)	32
Figure 4-5 Discrete Elements (2)	33
Figure 4-6 Mesh quality check of shell elements	34
Figure 4-7 Rigid body initial position.....	35
Figure 4-8 Strain rate dependent stress-strain relation	37
Figure 4-9 Temperature dependent stress-strain relation.....	38
Figure 4-10 Strain rate dependent fracture strain.....	38
Figure 4-11 Temperature dependent fracture strain.....	39
Figure 4-12: Stress state (fracture strain-triaxiality-Lode) dependent fracture strain..	39
Figure 4-13 Mesh size dependent fracture strain	40
Figure 4-14 Constrained Nodal Rigid Body (Boundary Condition).....	41
Figure 4-15 Indenter Vertical Motion.....	42
Figure 4-16 Indenter Horizontal Motion.....	42
Figure 4-17 Master Surface Mesh.....	43
Figure 4-18 Slave Surface Mesh.....	43
Figure 5-1: Prescribed motion (in-along-out) of the indenter.....	46
Figure 5-3: Vertical Force Vs Horizontal Displacement comparison with shell elements	50

Figure 5-4: Vertical Force Vs Horizontal Displacement comparison with solid elements	52
Figure 5-5: Vertical Force Vs Horizontal Displacement comparison	55
Figure 5-6: Resultant Force Vs Horizontal Displacement comparison	56
Figure 5-7: Vertical Force Vs Horizontal Displacement comparison (solid and shell elements models)	57
Figure 5-8: Resultant Force Vs Horizontal Displacement comparison	58
Figure 5-9: Triaxiality comparison between stationary and moving load	61
Figure 5-10: Lode comparison between stationary and moving load.....	61
Figure 5-11: Plastic Failure Strain comparison between stationary and moving load.	62
Figure 5-12: Von-Mises Stress comparison between stationary and moving load.....	63
Figure 5-13: Prescribed motion for loading angle effect	65
Figure 5-14: Resultant Force Vs Resultant Displacement comparison for loading angle effects	67
Figure 5-15: Vertical Force Vs Horizontal Displacement comparison for loading angle effects	67
Figure 5-16: Resultant Force Vs Resultant displacement at Fracture for different Loading Angles	69
Figure 5-17: Resultant Force at Fracture Vs Loading Angle.....	70
Figure 5-18: Resultant Force Vs Resultant displacement at Fracture for different Loading Angles	71
Figure 5-19: Vertical Force at Fracture Vs Loading Angle	72
Figure 5-20: Vertical Force Vs Horizontal Displacement for mesh convergence.....	74

List of Appendices

Appendix A Simulation Results for Strain Rate Effect (Plots).....	85
Appendix A1 Simulation Results (Plots) with Shell Elements.....	86
Appendix A2 Simulation Results (Plots) with Solid Elements	88
Appendix B Moving Load Capacity of the Plate Simulations Results (Plots)	90
Appendix B1 Shell Elements Model Results (Plots)	91
Appendix B2 Shell and Solid Elements Models Results Comparison (Plots).....	93
Appendix C Stress State Simulations Results (Moving Load and Stationary Load Results' Comparison Curves)	95
Appendix D Mesh Convergence Study Simulation Results (Plots).....	99

Chapter 1 Introduction

Structural response due to moving load differs significantly than that of stationary load. Here, stationary load refers to a load which acts perpendicular to the structure and does not slide along the structure, whereas moving load relates to the load which is acting perpendicular and moving at the same time. As the nature of the loads differ, their effects on the structure vary consequently. Metal's plastic capacity lowers significantly under moving load compared to stationary load. Therefore, moving load's effect on ductile fracture has been investigated in this study implementing state-of-art finite element analysis technique.

The effect of stationary load had been studied thoroughly over the years through collision and grounding analyses. Estimation of structural damage during collision and grounding started with an empirical formula which eventually ascended in the era of nonlinear finite element analysis with the advent of computational capability. Consequently, method for predicting fracture due to stationary load has been improved over the years.

This work focuses on ductile fracture prediction due to moving load and is inspired by moving ice loads on the hull of a ship; as ship-ice interaction scenarios are almost explicitly moving loading events. During ship-ice interaction or ice impact, the ship continues advancing as it crushes the ice, causing the load acting on the hull to move as ships pass through the ice. Traditionally, ship-ice interaction events were analysed as stationary loading problem similar to collision and grounding analysis. It was assumed that a load acting perpendicular to the structure results the maximum damage. However, Quintion [1,2] and Alsos's [3] work showed that moving load has a severely detrimental

effect on the plastic capacity of a structure than stationary load. Besides, the energy to initiate ductile fracture during ice impact is significant compared to total collision energy; whereas the fracture initiating energy is inconsequential compared to total collision energy during ship to ship collision and grounding events. Therefore, to understand and predict structural response during accidental loading accurately, we should consider both moving and stationary overloading scenarios.

Steel plate may fail in the manner of ductile fracture under accidental over loading scenarios. Therefore, to predict structural response accurately through numerical simulation, (i.e. nonlinear finite element method) appropriate selection of failure criteria of the material should be warranted. A commonly used failure criteria in nonlinear finite element modelling of ship collision is the effective plastic strain to fracture (i.e. fracture strain). The elements are considered to be failed and taken out of calculation when effective plastic strain of the element reaches a particular value. The major drawback of this method is the inability to incorporate state of stress as represented by triaxiality and Lode parameter.

Researchers in fracture mechanics arena had shown the strong influence of stress state with fracture strain. Therefore, nonlinear FEM analysis associated with ductile fracture should also be introduced with stress state based failure criteria to ascertain its accuracy. Although relationship between fracture strain and hydrostatic stress was observed back in 1968 by McClintock [4], Rice & Tracey [5], commercial explicit finite element software were still using effective plastic strain as failure criteria. Wierzbicki et al. [6,7], [8], [9-14] worked to find out a way to correlate fracture strain with stress state and also how to implement that in commercial explicit finite element code. Two parameters were used to describe state of stress: stress triaxiality and Lode parameter. Consequently, a

3D fracture surface was generated in fracture strain-stress triaxiality-Lode parameter dimension to express failure criteria for material. Wierzbicki et al. postulated the tests and procedures necessary to create 3D fracture surface for any material.

This study revisits the nonlinear finite element analysis of ship hull's ductile fracture for both stationary and moving load with the implementation of 3D fracture surface as the failure criteria. The finite element analysis (FEA) has been conducted to identify the effect of the moving load on the ductile fracture initiation of an Aluminium (Al2024) plate. A commercial Finite element analysis code LS-DYNA with explicit time integration scheme has been used by implementing state-of-the-art FEA techniques. A stress-state (as measured by the triaxiality and the Lode parameter) based failure criteria was incorporated in a elastic-viscoplastic material model (MAT_TABULATED_JOHNSON_COOK) to account any changes in the stress-state due to the moving load. In addition, strain-rate, temperature, and mesh size effects were also included the material model. Moreover, Quinton's experimental and numerical work on the moving load has been referred to define the geometry, boundary conditions, and application of the load to ensure compatibility of current model's results with experimental results from Quinton's moving load apparatus. From the simulation results, factors affecting the ductile fracture initiation due to the moving load were identified. The study was conducted only through numerical simulations, therefore, a practical experiment needs to be conducted to corroborate these findings.

Chapter 2 Literature Review

The objective of this study is to understand structural response (i.e. ductile fracture initiation) of ship's hull due to stationary load and moving load. Extensive work has been carried in past years to predict structural failure due to stationary load, but a little has been understood about the structural response due to moving load. This literature review work focused on four major sub divisions: methodologies implemented until now for collision analysis, the detrimental effect of moving load, the mechanism of ductile fracture initiation, and implementation of stress state based material failure criteria in nonlinear FEM analysis.

Collision and grounding analysis section briefly summarises all the methods associated with collision and grounding analysis. Minorsky's empirical method, Pedersen's theoretical model, simple nonlinear finite element analysis and nonlinear FEM analysis have been discussed in this section. Major drawbacks of those methodologies have also been reviewed accordingly.

Moving load effect section reviews mainly the detrimental effect of moving load in place of stationary load. Since not much research had been carried out in this area, Quinton's and Alsos's work on accidental moving load scenarios have been referred mainly.

The third section explains the micromechanics associated with ductile fracture initiation. Void nucleation, void growth, and void coalescence and crack initiation process were discussed accordingly.

Finally, the fourth section represents the procedure to develop 3D fracture locus for different ship building material and how to incorporate that in commercial explicit finite element code.

2.1 Collision and Grounding Analysis

Several review article has been written in the area of collision analysis. The widest ranged review was written by Ge Wang [15] where he listed all the work that had been carried out (till that date) focusing three fields: definition of accident scenario, analysis methodologies, and acceptance criteria for collision resistance ship structure. Although the review covered a broad range of topics, it did not focus on providing deeper understanding of the methodologies. Later on, Pedersen [16] wrote another review paper which focused on collision analysis procedure necessary for risk analysis of ship collision. To the recent time Miguel et al. [17,18] published two review papers. The first paper focused on explaining different analysis methodologies related ship collision, and the second paper focused on different material failure criteria used in FEM analysis of ship collision.

Similar review article has been published by Ehlers [19] where he highlighted complexities associated with FEM analysis of structural damage due to ship collision; mesh size effect on accuracy of FEM analysis result was considered significant while strain rate effect was deemed negligible. In addition, he explained the external dynamics associated with collision along with various assessment methodologies related to external mechanics of ship collision.

The study of the ship collision analysis started in 1950s focusing on ships carrying radioactive material. The scope of the study expanded for hull structures in general over

the years. During these years several analysis methods have been developed namely: empirical, analytical, and finite element method.

2.1.1 Empirical Method

The first person to work on the prediction of hull fracture was Minorsky [20]. He analysed 50 maritime accidents data, and developed a simple linear relationship between the damage extent and the energy released during the collision. Though his method provides an excellent approximation of the damage extent for high energy collisions, it fails to predict the damage extent during the low energy collisions. Several researchers had worked on this model to improve its credibility. Wosin [21] is one of them who established Minorsky's method's validation. Few other researchers had also worked on this method's modifications: Vaughan [22], Reardon & Sprung [23] and Maestro & Marino [24]. All these researchers contributed to the development of an empirical model for prediction of ship's damage during ship collisions.

2.1.2 Analytical Method

P T Pedersen and his student M J Petersen [25] are the pioneer researchers to understand the necessity of working on a prediction based on theoretical approach. They worked on a numerical prediction method based on outer dynamics (external mechanics of ship collision). They calculated the added mass, damping, and unit response function based on an approximation method, and the deformation of the ship structures during the collisions are modelled as nonlinear springs.

Pedersen and Simonsen [26,27] worked on the development of a theoretical model based on both external and internal mechanics to capture the hull response during grounding. The external mechanics incorporated the hydrodynamic effect due to surge,

heave, and pitch motion and the internal mechanics incorporated the inelastic damage estimation based on energy dissipation rate of assumed mode of deformation.

Pedersen and Zhang [28] developed a prediction model which considered hydrodynamic effect for the surge, sway and yaw motion of the ship. It also incorporated the friction between the contact surface and the sliding motion induced from it. All these models considered the ships as rigid bodies and only considered the inelastic damage caused during the collision. Later Pedersen and Li [29] worked on a numerical model to calculate the elastic energy stored during the elastic vibration of the ship hull during the collision.

2.1.3 Simplified Finite Element Method

Ito et al. [30-32] worked on the development of a simplified finite element model for collision analysis. A simplified method to obtain the overall response of double hull structure during collision scenario has been developed from the result of scaled collision experiment results. For simplicity of the formulation, the shell plate was considered as plastic membrane element while the transverse web & side stringers were assumed as buckling members, and the striking ship was considered as rigid body. With this assumptions, a matrix equation to relate penetration distance with penetration load was developed. The accuracy of the model had been validated with experimental results. Later on, he carried out research [32] to find out the most influential parameter that affects energy absorption during collision and concluded that transverse web thickness contributes most in changing the energy absorption.

J K Paik and Pedersen [33] worked on developing a simplified finite element model based on the idealised structural unit method (ISUM) to calculate the structural response

during collision. The calculation had been carried out based on internal mechanics during collision incorporating yielding, crushing and rupture of the plates. A major challenge had been overcome in this study using nonlinear finite element method by coupling the local and global failure of the structure. A double hull structure's response had analysed considering both inner and outer shell plate as membrane plate while all other plates had considered as usual plate. Strain rate sensitivity had also been incorporated in the material model to account the dynamic strength of the plates.

Several joint efforts had been made to develop tools/software for grounding analysis since Exxon Valdez accident [34]. "Protection of oil spills from crude oil tankers" by AISIS in Japan, grounding experiments conducted by NSWCCD and MIT- Joint Industry project on tanker safety in the USA are few notable joint project in that time. International ship and offshore structures congress reviewed state-of-art of research related to collision and grounding [35] and concluded nonlinear finite element analysis was capable of predicting structural damage during grounding fairly accurately. However, that method demands high level of expertise and very time consuming, therefore, was not very suitable for designing or regulatory purposes. A simplified method which is less time consuming and more suitable for designers and regulators. A software developed by MIT-joint industry project on tanker safety (DAMAGE) and an analytical method developed by Dr. Wang are two most successful tools that had been developed as simplified damage evaluation tools. The idea expanded in collision analysis as well and few simplified collision analysis tools were developed; SIMCOL, DAMAGE, APS/SCOL, DTU model are the results of such efforts.

2.1.4 Nonlinear FEM

Jorgen Amdahl [36] laid out the foundation of nonlinear finite element analysis in ship collision. Energy dissipation mechanism associated ship collision and their closed form solutions are implemented to basic elements and the whole structure had been considered as the integration of those elements. Energy dissipation for each structural component was calculated and force-displacement curve during collision for the whole system had been derived by summing results for all elements. He had derived a closed form equation for the average crushing strength of the bow. The total crushing force is calculated by multiplying the crushing stress with cross sectional area. The results obtained with this method were compared with experimental results and satisfactory concordance was observed, especially for isolated angle elements.

Due to the demand of high computational power nonlinear finite element analysis did not become very popular until early 1990s. However, with the advent of high computational power collision analysis were mainly focused on nonlinear finite element analysis method. It serves the purpose of both conducting quantitative analysis of crashworthiness and validation of simplified method as well. O Kitamura [37] pointed several uncertain factors involved in simplified analytical approach. He examined seven large scale nonlinear finite element analysis carried out by Regulation Research panel of Japan and pointed out different concerns associated with it. Effect of time integration formulation, mesh size and time increment on the analysis result were discussed for nonlinear finite element analysis.

A continuous effort has been employed for last two decades in improving the nonlinear finite element analysis of ship collision. All those parameters mentioned above greatly affect the result and they are also interrelated. For example, two types of time integration

formulations are applied, name Eulerian formulation (implicit analysis) and backward Eulerian formulation (explicit analysis). In the implicit analysis, equation of motion is solved for each state using the values at the present state and the next state as well. Consequently, each time step requires a series of trial solutions to obtain the value which yields results within appropriate tolerance. For this reason, computation expense for each time step is very high in implicit analysis. In addition, it requires an advanced iterative solution technique. Whereas, in the explicit analysis, solution for each time step is calculated based on values from the previous state. Consequently, it requires only one solution for each step and uses simple solution technique. However, the time step must be less than Courant time step (time taken by a sound wave to pass across an element) which mandates the time step to be very small in explicit analysis. Therefore, explicit analysis technique require an enormous amount of calculation compared to implicit analysis.

The choice of solver (implicit or explicit) mainly depends on the type of the problem with regard to dynamics, namely: static and dynamic. Static problems do not involve any inertia or damping effect whereas dynamic problems are associated with it. Static problem can be solved by implicit solver only and dynamic problems can be solved using implicit or explicit solver. However, as mentioned earlier computational expense for each time step is very high for implicit solver, especially for large models. In contrast, computational cost is lower in explicit solver. In addition, explicit solvers handles nonlinearities more efficiently than implicit solvers.

In addition to time integration scheme, material model definition plays a significant role on the numerical results, especially the selection of failure criteria in the material model. Miguel [18] did a state-of-art review on material failure modelling regarding ship

collision analysis. He discussed major failure criteria: strain based failure criteria, tri-axial state based failure criteria, and forming limit diagram based failure criteria. The most commonly used failure criterion is strain based failure criteria where elements are removed from the calculation once it reaches a certain value of plastic strain. Although it provides a convenient estimation of structural damage during collision, even used by regulatory authorities, it significantly compromises the accuracy of the results. Therefore, intensive research are being carried out to improve the results by incorporating stress state.

2.2 Moving Load

In conjunction with previous studies regarding ship collision (stationary load) analysis, this study focuses numerical prediction of ductile fracture due to moving load as well. Although not much work had been carried out on moving load, Quinton [1,2,38-41] and Alsos's [3] works have proved compelling importance on studying moving load. Moving load cause considerably more plastic damage than stationary load. Quinton carried out several experimental and numerical investigations [2] on moving load's effect on hull structure's plastic capacity. He found a significant drop of plastic capacity of structure under moving loading scenarios. Since ship-ice interaction scenarios are mainly moving loading scenarios, therefore, this effect should be considered during ice classed ship design [39].

Alsos's work also resulted in similar conclusion regarding the effect of moving load. He calculated contact force during two grounding scenarios, a) where the ship is static and b) the ship is moving, and found a significant decrease in contact forces [42,43] during horizontal sliding motion of the ship during grounding (moving) scenario.

2.3 Ductile Fracture

Fracture refers to the separation of a solid body into pieces due to stress at temperatures below the melting point. Ductile fracture occurs to materials which can sustain large deformation before fracture. Material heterogeneity is the precursor for the initiation of ductile fracture. Heterogeneity refers to the inclusion of second-phase particles and metal alloys during metal formation. Heterogeneity incites nucleation of micro voids which grow due to external stress, coalesce with adjacent micro voids which lead to the formation of macro crack and fracture eventually. The process is schematically showed in Figure 2-12-1

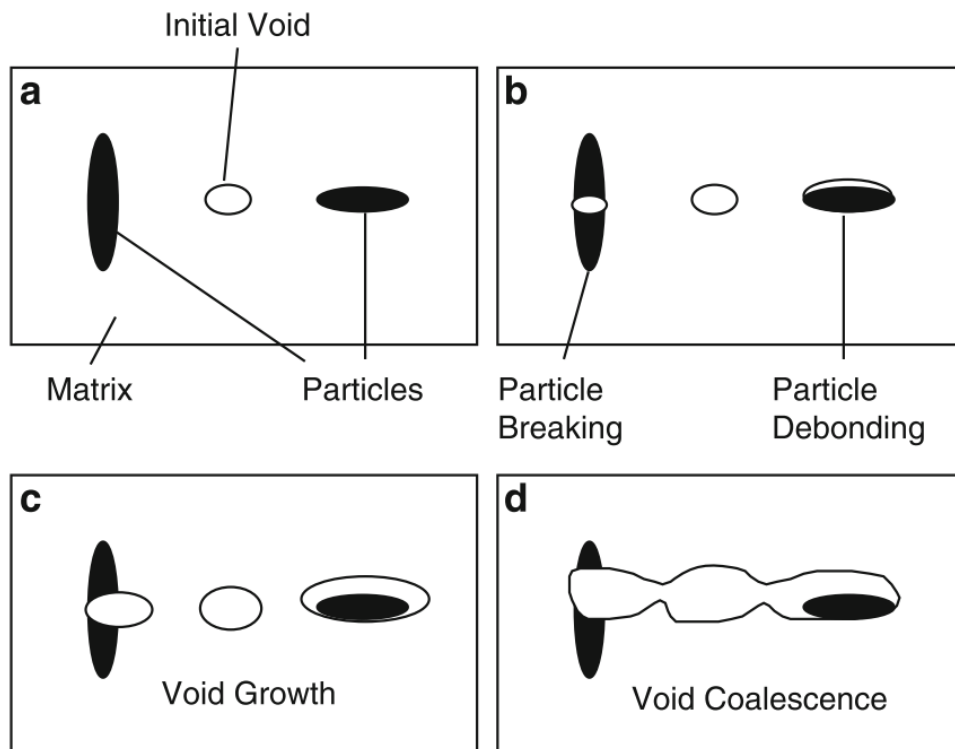


Figure 2-1: Ductile damage evolution, a) initial state; b) void nucleation c) void growth; d) void coalescence [44]

The micromechanics of the ductile fracture involves void nucleation, void growth, and void coalesce and the process is highly dependent on each state [43]. It is governed by

several factors such as second-phase particle/void distribution, void geometry, stress state, strain rate, material hardening and temperature [45].

2.3.1 Void Nucleation

Void nucleation occurs when the second phase particles crack or debond during plastic deformation which largely depends on the size and shape of the particles. Metal with larger second phase particle tends to crack at lower strain than metals with smaller second phase particles. Several other factors govern the mechanism such as stress state, temperature and strength of the particle [46-48], [45,49-51].

2.3.2 Void Growth

The micro voids, after nucleation, continue to grow larger due to external stress and it is relatively the stable phase of deformation. It is a continuum plastic deformation which mainly depends on the stress triaxiality [4,5] and size of the void [52]. Stress triaxiality represents the intensity of hydrostatic stress and calculated as the ratio of hydrostatic to effective stress.

2.3.3 Void Coalescence and crack initiation

Void coalescence is a sudden and rapid event where micro voids in the material coalesce together to form micro crack which propagates throughout the material and yields sudden failure. It depends on several factors such as initial porosity, stress triaxiality, void size, shape, spacing and material hardening [5,53]. There are three mechanisms of void coalescence i) primary void impingement, failure of inter-void ligament due to ii) shearing or iii) necking. Inter-ligament necking and shearing occur at low to moderate stress triaxialities and necking coalescence occurs exclusively at high stress triaxialities.

2.4 Implementation of Stress State based fracture criteria in Finite Element Analysis

Research had been carried out to develop a material yield criterion which can be coupled with the micromechanical process of ductile fracture (i.e. accounts material softening and evolution of stress state with progressive damage).

Gurson [54] was the first to propose a damage-based yield criterion and flow rules; he formulated the way to determine maximum macroscopic stresses required to sustain plastic flow. However, Gurson model did not consider void shape evolution which was later included in the model by Tvergaard [53]. Later on, Tvergaard and Needleman [55] extended Gurson-Tvergaard model to include coalescence by modifying void volume fraction and it is widely known as the Gurson-Tvergaard-Needleman (GTN) yield criterion. The GTN model could not be successfully implemented in industrial application due to large number of coefficients to be determined, and those parameters are strongly coupled [6].

Therefore, in spite of decades of research on ductile fracture and strong dependency of ductile fracture process on the state of stress, commercial FEM codes such ABAQUS, LS-DYNA, PAM-CRASH were still using primitive material failure criteria.

Wierzbicki and Bao revisited [6,7] this problem to find a way to develop stress state based fracture criteria which could be implemented in commercial nonlinear Finite Element Modelling codes. It was found out already that ductile fracture mechanism primarily depends on hydrostatic stress (McClintock, Rice and Tracey) and again hydrostatic stress intensity can be expressed as stress triaxiality [8]. Bao & Wierzbicki noticed a major limitation of previous studies. All those studies were carried out by pre-

notched round tensile specimen and upsetting specimen. Therefore, data acquired through these experiments were limited to negative stress triaxiality zone and high stress triaxiality zone only. Bao and Wierzbicki conducted several experiments covering a wide range of stress triaxiality to develop a procedure to find out the fracture locus for different material. With all these experimental results and numerical results fracture locus based on equivalent fracture strain and stress triaxiality had been derived.

This results can be easily incorporated into current finite element analysis. It made a remarkable contribution to determine material's fracture criteria, but critical strain to fracture for Bao's compression tests was somewhat higher than the conventional upsetting test on cylinders for the same amount of triaxialities. Later on, Bai & Wierzbicki revisited [9-14] this study and confirmed that another parameter (Lode Parameter) also govern the ductile fracture mechanism. He postulated biaxial tensile test with butterfly specimen (Figure 2-22-2) with changing the loading condition to calculate 3D fracture locus in fracture strain-stress triaxiality-Lode parameter dimension.

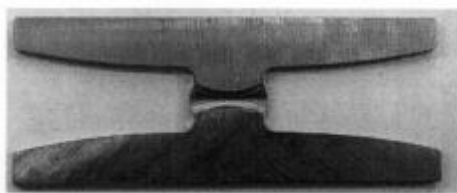


Figure 2-2: Butterfly Specimen [9][6]

The key advantage of this specimen is it covers a wide range of stress state from pure tension through tension/shear, shear, shear/compression, and all the way to axial compression. Therefore, only one type of specimen is required for carrying out all the test necessary and consequently it is much more convenient to couple with numerical

experiment as well. It negates the mesh size effect since the mesh remains same only the boundary conditions change. Another advantage is all the crack occurs at the centre of the gauge section. A typical fracture locus is given in Figure 2-32-3 below

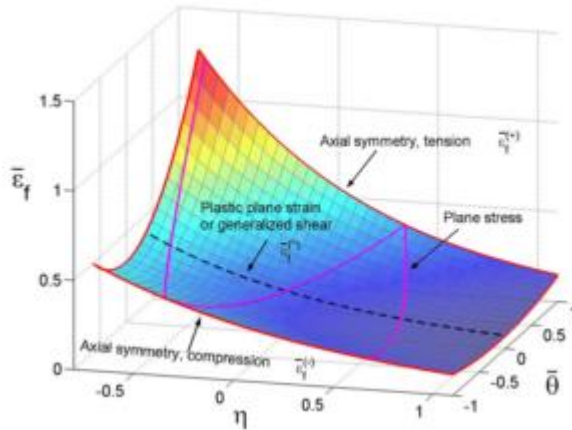


Figure 2-3: 3D fracture surface postulated by Wierzbicki and Bai [9]

It was also found that the Lode parameter is insensitive for some material where as it varies significantly for other material. Therefore, both stress triaxiality and Lode parameter should be included to define fracture characteristics of any metal.

To implement stress-state based fracture locus in commercial finite element modelling software, such as LS-DYNA with MAT_224, triaxiality versus fracture strain for different Lode parameter should be extracted from 3D fracture locus. All these curves should be incorporated as load curves in LS-DYNA and finally, a table is to be created to incorporate all those load curves. This results in a fracture surface in three-dimensional space of stress triaxiality, Lode parameter and fracture strain. Although above mentioned 3D fracture locus is associated with solid elements, shell elements uses a 2D fracture locus in the dimension of stress triaxiality and fracture strain. The Lode parameter is not considered in the calculation for shell elements in MAT_224, which makes the fracture criteria for shell elements independent of the Lode parameter.

Consequently, numerical results obtained using shell elements with MAT_224 differs from the results obtained from solid elements.

Chapter 3 Methodology

Quinton [1] and Alsos's [3] work showed that moving load affects the structural capacity in the plastic regime. The investigations were carried out by numerical simulations where the numerical models were verified by experimental results obtained in stationary load experiment. Later on, Quinton [2] continued his work and obtained experimental results from his novel moving load experiment. Quinton showed from experimental result [2] that moving load severely reduces the plastic capacity of ship structure which was predicted from numerical experiment [1].

This study investigates the influence of moving load on ductile fracture initiation of Aluminium 2024 plate through numerical simulations. Experimental setup and numerical model described in Quinton's [2] work were referred to define model parameters for this investigation. The experiment involves applying the load to a plate with rigid indenter by controlling the displacement. A 1500X400mm flat plate (thickness: 6.35mm) is subjected to load through a spherical (radius: 25.4cm) rigid indenter. In addition, current study's numerical model is very similar to Quinton's validated numerical model except for the material model; the material model was adopted from LS-DYNA Aerospace Working Group. Eventually, the model was used to predict ductile fracture initiation of the Aluminium plate due to moving load.

The numerical modeling of this study includes geometric and material nonlinearity. The model involves application of load through contact force from rigid indenter, large deformation, and fracture of metal. Hence, a time integration scheme (implicit or explicit) that is efficient in handling dynamic problem with contact and material nonlinearities should be used to solve this problem. As mentioned in 2.1.4, explicit

solver is more suitable for this type of problem. Accordingly, the numerical simulation has been carried out by commercially available explicit time integration finite element modelling software LS-DYNA. In the development of the numerical model state-of-art material model has been implemented to improve the accuracy of numerical simulation result. Since the state of stress dictates largely the ductile fracture phenomenon, therefore, state-of-art stress-state dependent material failure model has been incorporated into the numerical model [6,9]. The material model MAT_224 has been implemented in LS-DYNA and this material model data had been adopted from LS-DYNA Aerospace Working Group website: <http://awg.lstc.com>.. Finally, this validated numerical model had been used to investigate the influence of moving load during the ductile fracture initiation of Aluminium 2024 plate.

The underlining methodology of this study constitutes creating and optimising finite element model with fracture locus surface. The modelling is done in such a way that it can be regenerated in any other equivalent finite element code. The optimisation is achieved considering both accuracy and computational cost of the numerical model.

Several factors influence the accuracy of the numerical result and those factors have been studied and incorporated accordingly in this investigation. These factors are described elaborately in the following sections.

3.1 Fracture Criteria

Appropriate failure definition plays the most significant role in the numerical simulation involving ductile fracture initiation. Although constant fracture strain is widely used in the industries because of its simplicity, it severely underestimates the plastic capacity of metals in certain cases. As it has been discussed in the literature review section that

fracture strain changes with changes in stress state, stress state dependent fracture strain should be incorporated to improve the accuracy of the numerical result. Bao and Bai's work [6,9] postulates the method to implement stress-state dependent fracture criteria in commercially available finite element modelling code. The stress state can be represented by two parameters: stress triaxiality and Lode parameter.

Stress triaxiality refers to the hydrostatic pressure and Lode parameter relates to the direction of shear stress. For solid elements, the range of stress triaxiality is $-\infty \sim +\infty$, but a range of $-1 \sim +1$ (here negative sign represents tension) is sufficient to account for structural simulation. Bao also showed a cut-off value of triaxiality below which fracture never happens. The cut-off value of triaxiality is $1/3$. Although Lou et al. [56] mentioned about a changeable cut-off value of triaxiality in his research, in our study the fracture occurs when the triaxiality value is in the range of $0 \sim -2/3$ (pure shear to tension). Therefore, further study on the changeable cut-off value of stress triaxiality has been purposely avoided. For Lode parameter the range is between -1 to $+1$.

A three-dimensional fracture surface, in the space of stress triaxiality, Lode parameter and equivalent plastic strain, has been selected as the failure criteria for this study. The stress triaxiality value ranges from $-1/3 \sim +1$ and Lode parameter ranges from $-1 \sim +1$ in the defined fracture locus of this model.

3.2 Strain Rate & Temperature

Strain rate and temperature have considerable effect on the yield strength of metals. Although the strain rate sensitivity varies among different materials (for example, steel is highly susceptible to strain rate sensitivity whereas aluminium is relatively insensitive to strain rate), generally yield strength is higher for higher strain rate. On the contrary,

the higher temperature lowers yield strength. Johnson-Cook expressed the strain rate and temperature effect through following equation [57]

$$\sigma_y = (A + B\varepsilon^{-p^n})(1 + C \cdot \ln\dot{\varepsilon}^*)(1 - T^*{}^m)$$

Johnson-Cook constitutive model comprised of three components; Strain hardening, Strain rate hardening and Thermal softening.

Strain Hardening: $(A + B\varepsilon^{-p^n})$

Strain Rate Hardening: $(1 + C \cdot \ln\dot{\varepsilon}^*)$

Thermal Softening: $(1 - T^*{}^m)$

Although strain rate and temperature effect on Aluminium is insignificant during stationary load, strain rate effect during moving load should be examined. Therefore, strain rate hardening and thermal softening have also been incorporated in this model.

3.3 Element Formulation

Element selection plays a key role in the accuracy and computational cost of numerical simulation. If computational cost was not an issue, then we could use solid elements with sufficiently smaller size to accurately account both macroscopic and microscopic deformations. Microscopic deformation refers to the internal changes happening in the plate during necking and fracture. Macroscopic change addresses large geometrical deformation of the structure. Due to the higher computational cost of solid elements, shell elements are widely used in the industry. Another type of elements has been developed and being used in finite element modelling is thick shell elements. TShell elements are somewhat like solid elements and the difference between Shell and TShell elements is that in shell elements thickness is a parameter, we put the thickness in the

shell section definition. But in TShell we can model the thickness geometrically. Therefore, the deformation going on along the thickness of the plate can also be easily calculated. The computational efficiency of TShell elements makes it a suitable alternative to Solid elements. However, MAT_224 is not compatible with TShell yet. Therefore, only solid and shell elements have been used in this study to compare the accuracy and computational cost.

3.4 Material Model

Incorporating influence of various factors in the numerical prediction of ductile fracture initiation depends on the selection of appropriate material model. For example, stress state based fracture criteria cannot be implemented in LS-DYNA with MAT_03 (MAT_PLASTIC_KINEMATIC) although it is very a cost effective material model. Therefore, an appropriate material model should be selected, to include all necessary factors affecting results, for accurate numerical prediction of fracture. MAT_03 or MAT_24 does not have the capability to incorporate 3D fracture locus as the failure criteria, but those material models can be coupled with MAT_ADD_EROSION to enhance their capability. We could use those models for our study. However, LS-DYNA Aerospace Working Group has developed a new material model MAT_TABULATED_JOHNSON_COOK (MAT_224) to conduct aerospace impact analysis. This elastic-viscoplastic material model has been developed in a joint research by Federal Aviation Administration (FAA), National Aeronautics and Space Administration (NASA), George Washington University (GMU), Ohio State University (OSU), and George Mason University (GMU) [58][59]. This tabulated thermo-viscoplastic material model can be used to predict modes of failure and damage, incorporating the influence of all necessary factors relevant to our study.

The failure criterion is based on accumulated damage parameter defined by:

$$F = \int \frac{\dot{\varepsilon}_p}{\varepsilon_{pf}} dt$$

Where, F is the damage parameter, $\dot{\varepsilon}_p$ is plastic strain rate and ε_{pf} is plastic failure strain which is calculated by:

$$\varepsilon_{pf} = f(\eta, \theta)g(\dot{\varepsilon}_p)h(T)i(l_c)$$

Where, η is triaxiality, θ is Lode parameter, $\dot{\varepsilon}_p$ is plastic strain rate, T is temperature and l_c is element characteristic size. When the value of damage parameter reaches one the element is considered failed and it gets deleted from the calculation.

Although both triaxiality and Lode parameter is considered in defining the stress-state for solid elements, only triaxiality is considered in case of shell element. Lode parameter is considered constant in shell elements, therefore, fracture criteria is independent of Lode parameter. Consequently, results obtained from solid elements models vary from shell elements models' results.

The effect of strain rate, temperature and mesh size, details are given section 4.2.3, can also be incorporated in this material model. Therefore, MAT_224 has been incorporated in this model.

3.5 Mesh Size Sensitivity

Mesh size sensitivity is an embedded drawback associated with finite element analysis. Stress and strain are computed averaging the stress, strain over the element integration points. Therefore, the size of element dictates resultant of stress and strain in areas of high stress/strain gradient. Mesh size effects should be accounted in the FEA to obtain

objective solution (i.e. mesh-independent solution). The current study investigates the effect of moving load on ductile fracture of ship building steel, therefore mesh size effects should be addressed elaborately for following reasons. Firstly, ductile fracture phenomenon is a complicated analysis to conduct by FEA due to the required size of elements to be in the scale of micrometer to properly model localization, necking and fracture. Which warrants analysis with solid elements. Secondly, the computational cost of solid elements nullifies the possibility of conducting FEA with solid elements in the industrial applications, which forces industries to apply shell elements. Finally, shell element comes with an innate limitation on the size of the elements; edge length cannot be smaller than thickness, which is justified by the type of analysis carried out with shell elements. Shell elements are widely used in the industry to carry out analysis of large scale structures due to its cost effectiveness. Since analysis with shell elements deemed appropriate for current study, mesh size effects associated with shell elements were investigated carefully. Fracture strain with different mesh size has been calculated and incorporated in the model accordingly.

3.6 Contact Algorithm

Load has been applied in this model as a contact between a rigid body and deformable plate. Consequently, appropriate contact algorithm influence the fidelity of the model. Since penalty based contact definition is suitable for contact between separate bodies, penalty contact has been used accordingly. Contact compatibility was ensured to prevent interpenetration of colliding bodies. Interpenetration prevention is achieved by placing a virtual spring between colliding bodies. The virtual spring exerts interface force which equal spring constant and penetration distance. The automatic contact algorithm in LS-DYNA has been proven its accuracy over the years.

Automatic_Single_Surface contact card has been used to implement accurate penalty based contact algorithm in this model.

3.7 Geometry & Boundary Condition

Finally, the geometry and boundary condition should be set in such a way that it resembles the experimental setup. The geometry of the plate and the indenter has been selected accordingly. The sides of the plate are clamped in the moving load apparatus, therefore, all the edges of the plate should be fixed. This could be numerically achieved by setting a fixed boundary condition along the node of the edged elements. However, Quinton [2] explained that numerical results of stationary/moving loads are very highly dependent on boundary condition stiffness. Fixed numerical boundary conditions incited unrealistically high force results when compared with similar experiments. This is because the vertical support and hydraulics go through a recoverable elastic deformation when the load is applied. On the contrary, fixed boundary condition, during finite element analysis, assumes an infinitely stiff clamping and all the energy is transferred to the plate. Quinton suggested using a constrained nodal rigid body using linear springs of known stiffness as the boundary condition, to recreate practical experimental setup. After conducting a design of experiment analysis with response surface method, Quinton quantified the optimum stiffness (for his moving load apparatus) which yields results concordant with experimental results. Therefore, Constrained Nodal Rigid Body (CNRB) with Quinton's suggested stiffness constant value was implemented in this simulation to obtain more realistic results that are comparable with Quinton's experimental setup.

3.8 Model Validation

Quinton's validated numerical model together with state-of-the-art FEM techniques were employed in this model to ensure the accuracy of the results. Quinton's moving load experiment and numerical model were referred to define the problem of this study; geometry, boundary condition and load were implemented accordingly. However, materials were different: Quinton worked with commercial steel whereas Aluminium (Al2024) was used in current model. Commercial steel plate with yield strength 379MPa had been used in Quinton's experiment. But stress state based fracture criteria (3D fracture surface) is not available for the type of steel Quinton used in his moving load experiment. In addition, generating data of stress-state based fracture criteria for any material requires enormous number of tests with at least 21 specimen to cover a wide range of triaxiality and Lode parameter [58,60]. However, stress-state based fracture criteria for Aluminium (Al2024) has been generated by LS-DYNA Aerospace working group and it is publicly available at their website (<http://awg.lstc.com>). For that reason Al 2024 has been used in this study instead of commercial steel. As a result, quantitative validation of this model cannot be conducted with Quinton's results. Regardless, a qualitative model validation has been conducted by comparing the force-displacement curve obtained from the current model with Quinton's validated numerical model's results.

Table 3-1 shows the parameters for both models; only material and associated material model differed, rest of the parameters are identical.

Table 3-1: Model parameters for validation simulations

Parameters	Quinton's Model	Current Model
Material	Steel	Aluminium 2024
Material Model	MAT_03	MAT_224
Plate Thickness (mm)	6.35	6.35
Element Type for Plate	Shell	Shell
Element Size (mm)	6.35	6.35
Vertical Indentation (mm)	40	40
Vertical Indentation Time (s)	2	2
Vertical Indentation Speed (mm/s)	20	20
Horizontal Indentation (mm)	567	567
Horizontal Indentation Time (s)	2.85	2.85
Horizontal Indentation Speed (mm/s)	198.95	198.95

Vertical force versus horizontal displacement curve for both models is represented and compared in Figure 3-13-1.

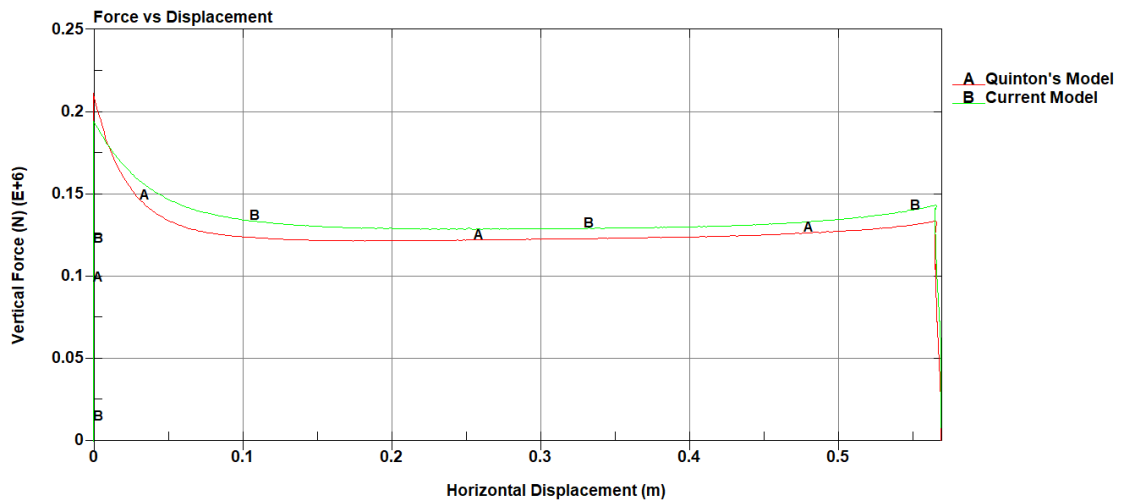


Figure 3-1: Vertical Force Vs Horizontal Displacement comparison for model validation

It can be seen from Figure 3-13-1 that, vertical force versus horizontal displacement curves of Quinton's model and current model showed a similar trend. To conclude, qualitative verification was conducted for the current numerical model with Quinton's results and good agreement was found between both numerical results.

Chapter 4 Numerical Simulation

Numerical simulations were carried out to predict ductile fracture of Aluminium 2024 when moving load is applied. A rigid indenter is used to apply load on the plate through prescribed rigid body motion. The movement of the indenter is controlled by prescribed displacement of the indenter in both vertical (Y axis) and horizontal (X axis) direction. The vertical displacement of the rigid indenter creates stationary load on the plate which is followed by the horizontal travel of the indenter. Therefore during horizontal travel of the indenter both vertical and horizontal force is experienced by the plate which is by definition, the moving load. This numerical representation of the problem represents the experimental set up implemented in Quinton's [2] moving load numerical model and experiment.

Explicit finite element modelling code LS-DYNA has been used for numerical simulation and different components of the numerical model has been briefly discussed below.

4.1 Geometry and Mesh

The geometry was created in Rhino 3D, a CAD program, with absolute tolerance being .001m and angular tolerance being 0.1° . The geometry was then imported into LS-PrePost and mesh was created using Auto_Mesher tool accordingly.

4.1.1 Mesh Elements

Three types of elements had been used in this model; Shell or Solid elements for Aluminium plate (depending on the numerical model), Solid elements for rigid indenter and discrete element at the corners of the aluminium plate to set a boundary condition on rigid body motion of the plate.

4.1.1.1 Shell Elements

Four node quadrilateral Belytschko-Tsay shell elements had been used for meshing the aluminium plate (1500mmX400mm) with thickness being 6.35mm (quarter inch) and incorporating warpage control. The mesh of the plate is given below:

Quarter Inch Sample

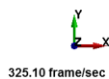
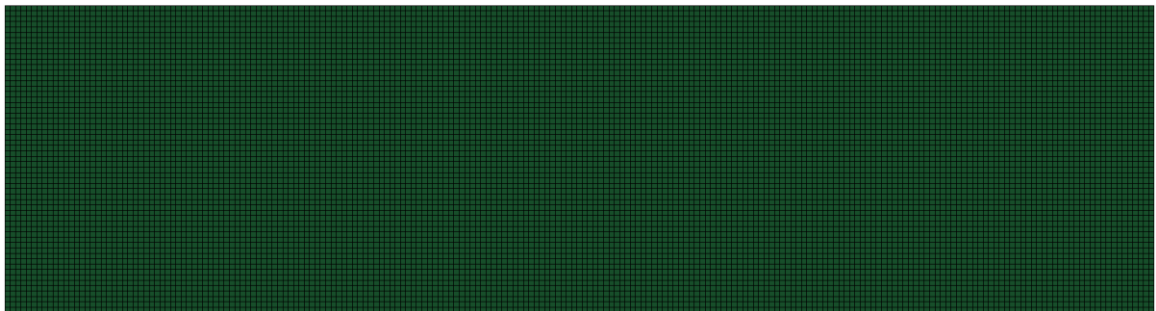


Figure 4-1 Shell elements (Aluminium Plate)

The nodes at the edge of the plate are constrained by CONSTRAINED_NODAL_RIGID_BODY_SPC (CNRB_SPC). The nodes act as a rigid body with only one degree of freedom: z (vertical) displacement, all other rotational and translational degrees are freedoms are constrained.

4.1.1.2 Solid Elements

Hexahedral solid elements had been used to model the rigid indenter, and in some cases, the aluminium plate. The mesh of rigid indenter is given below:

Quarter Inch Sample



Figure 4-2 Solid Elements (Rigid Indenter)

The rigid indenter has two degrees of freedoms: z and x-translational degree of freedom, all other translational and rotational motions were constrained. The motion of the indenter was achieved by controlling its displacement.

Hexahedral solid elements were also employed for meshing the Aluminium plate in several numerical models. The mesh of solid aluminium plate is given below:

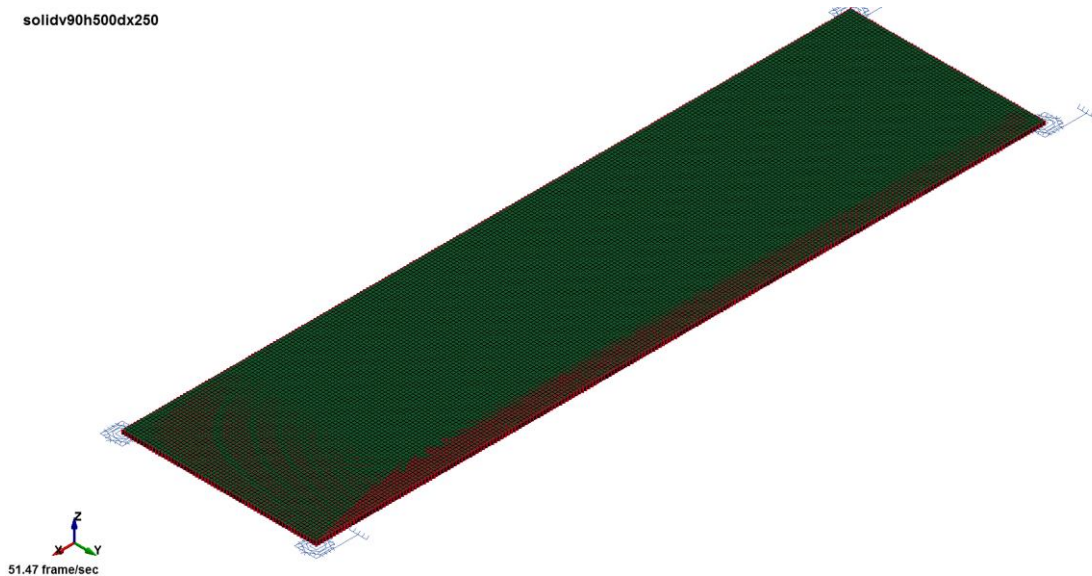


Figure 4-3: Solid Elements (Aluminium Plate)

Similar to shell plate, nodes at the edge of the solid plate are also constrained by CNRB_SPC. The nodes act like a rigid body with only one degree of freedom: z (vertical) displacement, all other rotational and translational degrees are freedom are constrained.

4.1.1.3 Discrete Elements

Four discrete elements have been used at the four corners of the plate to restrain vertical (z-axis) motion. They behave like translational elastic spring with a spring constant of $6.338 \times 10^6 \text{N/m}$. The details are given below:

Quarter Inch Sample

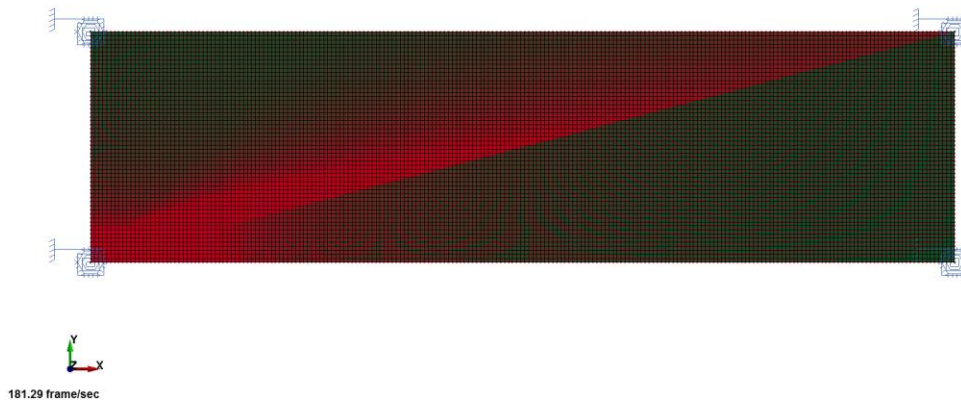


Figure 4-4 Discrete Elements are shown at the corners of the plate (1)

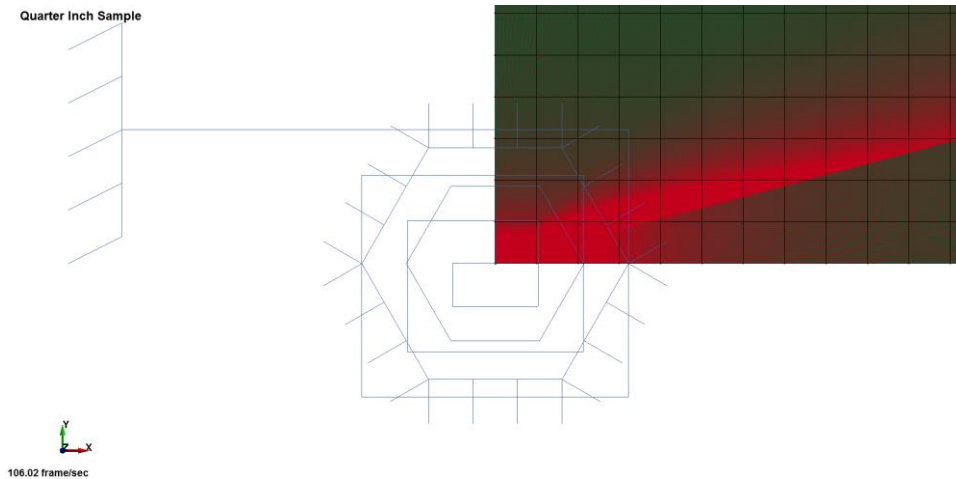


Figure 4-5 Discrete Elements (2)

4.1.2 Mesh Quality

Among several measures warpage, aspect ratio, skew, and jacobian are four primary measures to assess element quality. These measures have been inspected to ensure they are in the acceptable range mentioned in [61]. *Warpage* quantifies the deviation of an element, for shell element or element face for solid element, from being planar; 10° warpage is acceptable. *Aspect ratio* is the ratio of the longest edge of an element to its shortest edge, and it should be less than 5. *Skew* is the minimum angle between two lines joining the opposite mid-sides of an element, or element face for solid elements, and should be less than 60° . *Jacobian* determines an element's deviation from its ideal shape, and it should be in the range of 0.6~1.0 (where 1.0 represents ideally shaped element).

The summary of Shell element quality check report is given below:

SHELL ELEMENT QUALITY CHECK SUMMARY:

File Name: C:\~\mat224_a12024_shell_rev1.k|

Quality Name	Min. val	Max. val	Allowable	#Violated(%)
Min side length	0	0	0	0(0%)
Max side length	0	0	0	0(0%)
Aspect Ratio	1.01	1.01	10	0(0%)
Warpage	0	0	10	0(0%)
Min Quad Angle	0	0	0	0(0%)
Max Quad Angle	0	0	0	0(0%)
Min Tria Angle	0	0	0	0(0%)
Max Tria Angle	0	0	0	0(0%)
Taper	0	0	0	0(0%)
Skew	0	0.00813	45	0(0%)
Jacobian	1	1	0.6	0(0%)
Char. length	0	0	0	0(0%)
Area	0	0	0	0(0%)
Feature angle	0	0	0	0(0%)
TimeStep	0	0	0	0(0%)

#QUADS(%):12255(100%), #TRIAS(%):0(0%), #TOTAL OF FAILED(%):0(0%)

Figure 4-6 Mesh quality check of shell elements

Figure 4-64-6 shows that warpage (0), aspect ratio (1.01), skew (0), and jacobian (1) values are satisfactory, in fact, close to their ideal values.

4.1.3 Initial Condition

The rigid indenter is moved to 3.175mm (half of shell thickness) below the Aluminium plate at the initial condition. Shell elements thickness creates a virtual boundary on both sides keeping the element at the mid-plane. Therefore, the roller is placed at 3.175mm below the z axis and the inner plate's mid-plane is kept along the z axis.

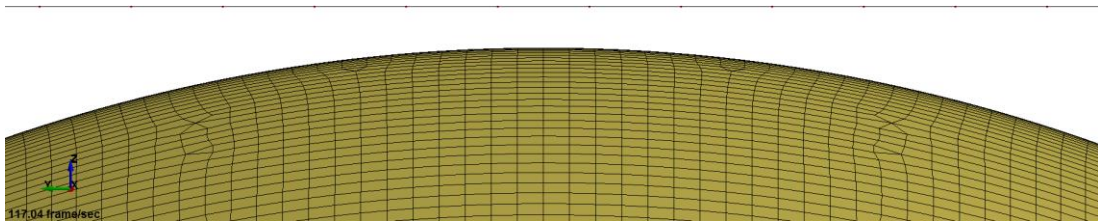


Figure 4-7 Rigid body initial position

4.2 Material Models

Three material models have been used for three types of elements in this model. Discrete element has been used to define an elastic spring at the edge of plate; solid elements have been used to represent rigid indenter; and, shell or solid solid elements have been used model the Aluminium plate. The details of these material models are discussed below. The elements for plate used state-of-the-art ductile fracture material model. The fracture criteria is defined by a three dimensional fracture surface in the dimension of stress triaxiality, Lode parameter and fracture strain. These material models have been described in the following sections.

4.2.1 MAT_S01 Spring Elastic for Discrete Elements

The discrete elements are incorporated to spring elastic material model with elastic stiffness being $6.338 \times 10^6 \text{N/m}$. Fixed boundary condition can be used in lieu of elastic spring. However, normal boundary stiffness has significant influence on moving load experiment results [2]. All the energy, during indentation, is not absorbed by indented plate; a portion of energy is lost, causing recoverable elastic deformation of supporting

structure and hydraulics system of moving load apparatus. Quinton incorporated this phenomenon in numerical model by inclusion of elastic spring with spring constant being $6.338 \times 10^6 \text{N/m}$, after conducting design of experiment analysis with series of numerical simulation results. Therefore, same spring constant value was used in the simulation of this study since it represents more realistic experimental condition.

4.2.2 MAT_020 Rigid for Solid Elements

The steel indenter's solid element meshes are incorporated to rigid body material with following properties:

Density: 7850kg/m^3

Young's Modulus: 2.07×10^{11}

Poisson's Ratio: 0.3

4.2.3 MAT_224 Tabulated Johnson-Cook

MAT_224 is a newly developed material model which is capable of predicting ductile fracture initiation during impact and crash analysis [59]. This material model has been incorporated with elements for Aluminium plate (both solid and shell elements depends on the element used to model Aluminium plate) to appropriately model ductile fracture with strain rate, temperature, stress state (effective fracture strain, load and triaxiality based 3D fracture model), and mesh size effects. Development of material model data for MAT_224 for any material requires a vast number of experiments which demand copious amount of time and resources. Since material data development was out of scope of this study and there was limitation in time and resources, material data of Aluminium for MAT_224 was not developed by the author. However, MAT_224 data for Aluminium 2024 has been generated by its developer and available through US

Aerospace Working Group Website: <http://awg.lstc.com>. Therefore, that data has been employed in present research. Various components of the material model have been discussed below.

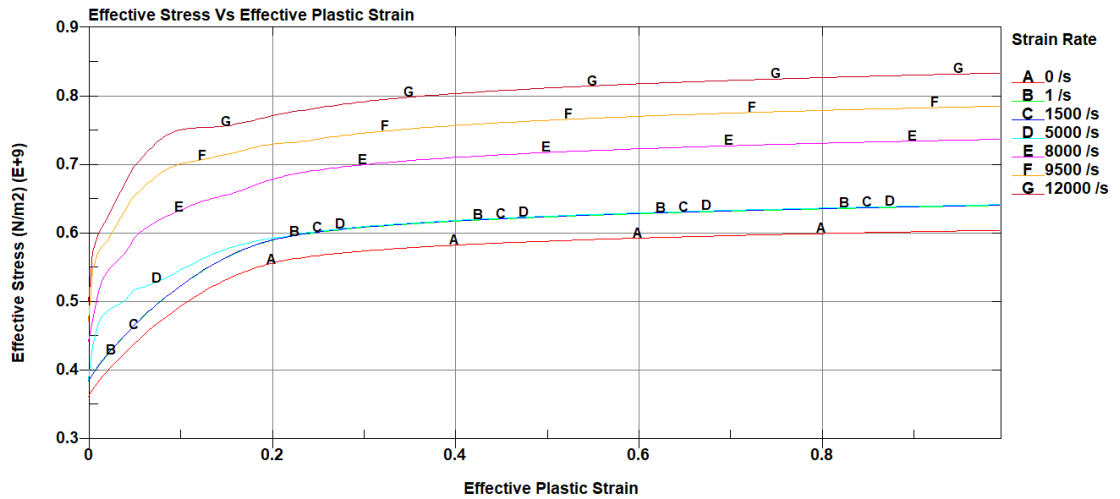


Figure 4-8 Strain rate dependent stress-strain relation

Figure 4-84-8, shows how strain rate is incorporated into plastic flow stress calculation for the elements. It can be seen that effective stress increases as strain rate increases. This relationship has been incorporated in simulations so that strain rate dependency can be accounted in the moving load simulations.

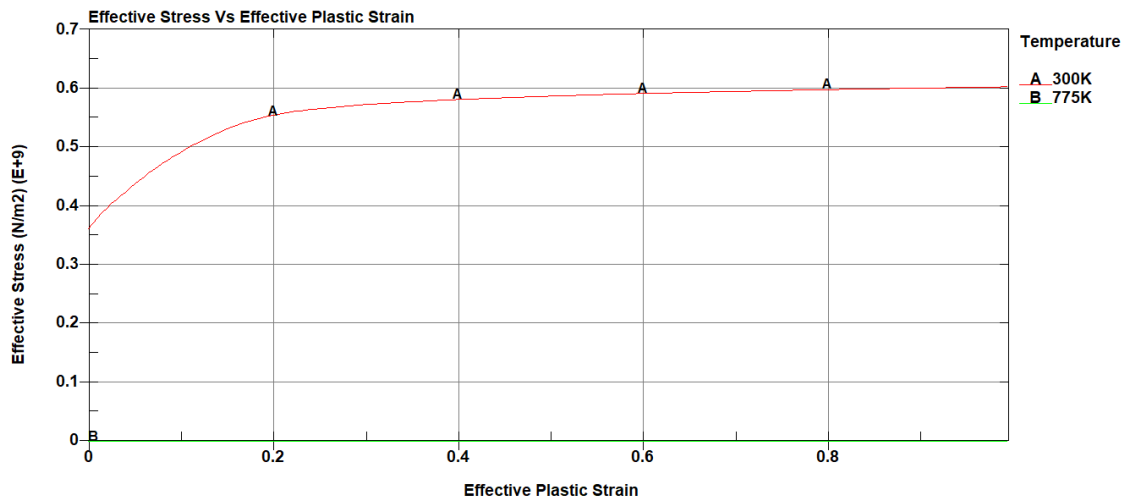


Figure 4-9 Temperature dependent stress-strain relation

Effective stress versus effective plastic strain relationship is shown in Figure 4-94-9 with temperature dependency. It is noticeable that no stress is expected to develop at 775K as it is close to Aluminium's melting point. The plastic work causes a raise in temperature, therefore, this relationship was included in the final model to incorporate thermal softening and changes in fracture strain of Aluminium 2024 during moving load simulations.

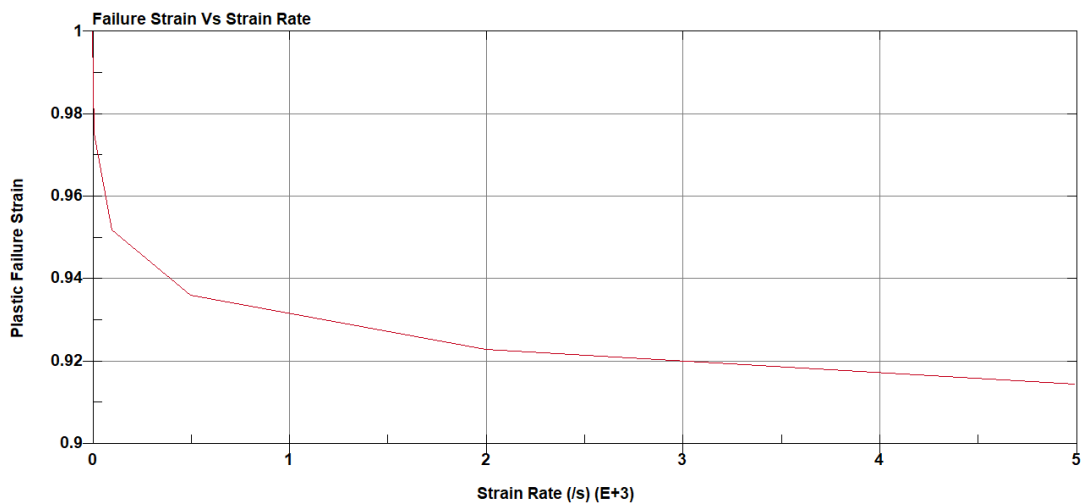


Figure 4-10 Strain rate dependent fracture strain

Figure 4-104-10 shows effect of strain rate on fracture strain. Strain rate is likely to vary among elements during moving load simulations, and its effect on elements failure strain will be accounted through this relationship.

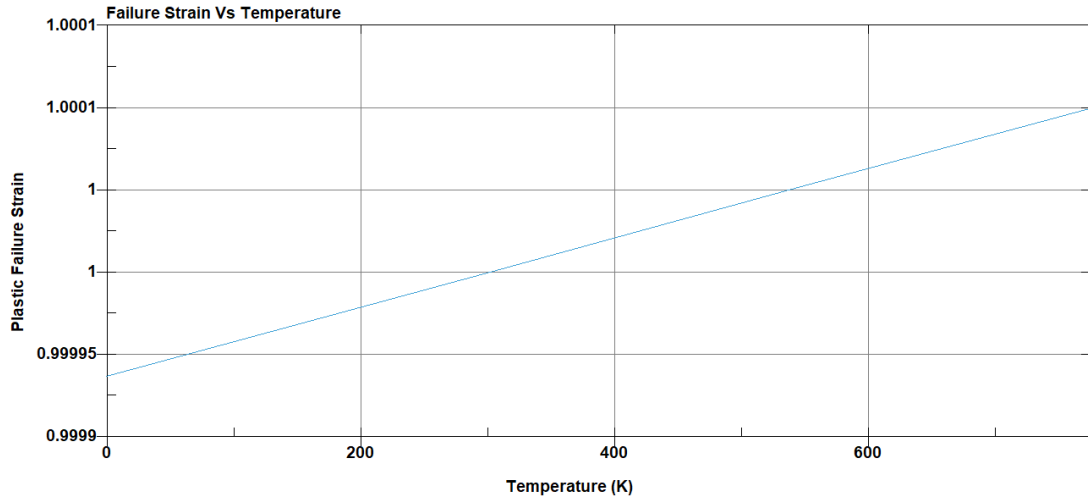


Figure 4-11 Temperature dependent fracture strain

Influence of temperature on fracture strain is shown in Figure 4-114-11, and changes in fracture strain of elements due to changes in temperature, during moving load simulations, are incorporated through this relationship.

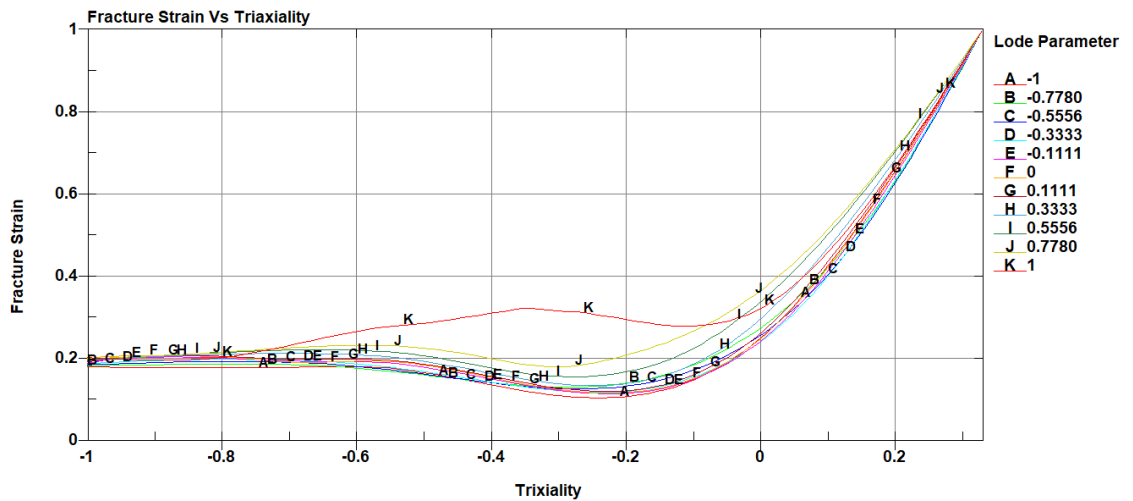


Figure 4-12: Stress state (fracture strain-triaxiality-Lode) dependent fracture strain

The state of stress is defined by triaxiality (η) and Lode parameter (θ), and they affect the fracture strain of material. Figure 4-124-12: represents a 3D surface where each curve represents fracture strain versus triaxiality relationship for certain values of the Lode parameter. A large number of tests with different types of specimen need to be carried out to generate 3D fracture surface for any material. In addition, the specimen and tests should be selected in a way so that it covers a wide range of triaxiality and Lode parameter [58]. In total 21 specimen were tested to generate above 3D fracture surface for Al 2024 [60]. State of stress based fracture criteria is incorporated in the moving load simulations through this relationship.

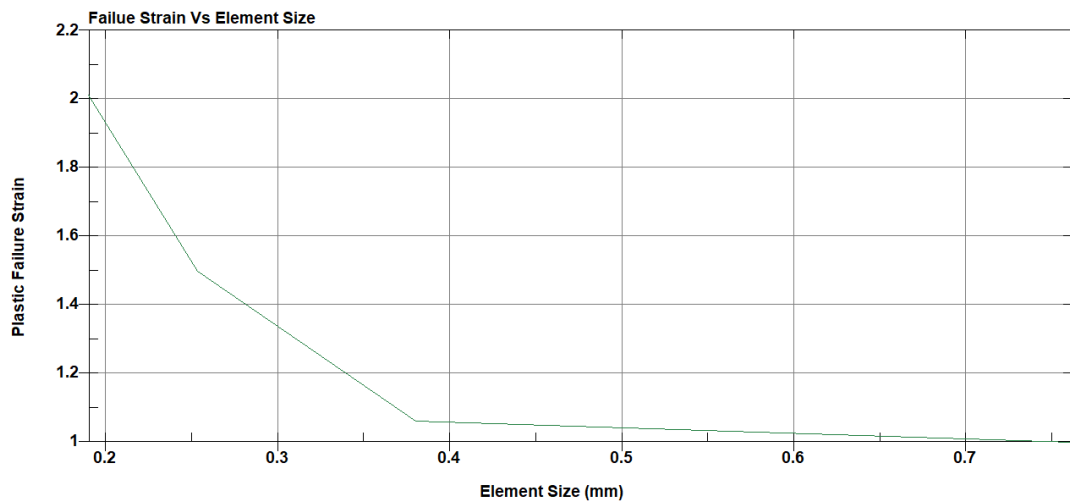


Figure 4-13 Mesh size dependent fracture strain

Mesh size sensitivity for Aluminium 2024 is shown in Figure 4-134-13, and it is incorporated in the moving load simulations accordingly.

4.3 Constraints

Constrained nodal rigid body boundary condition has been applied on node set (comprised of all the nodes at the edge of the plate) in global direction. Those nodes are constrained in translational degrees of freedom in x and y direction and also constrained in rotational degrees of freedom in all direction (x, y & z). The translational degrees of

freedom in z direction is restricted by elastic spring with elastic stiffness being $6.338 \times 10^6 \text{ N/m}$.

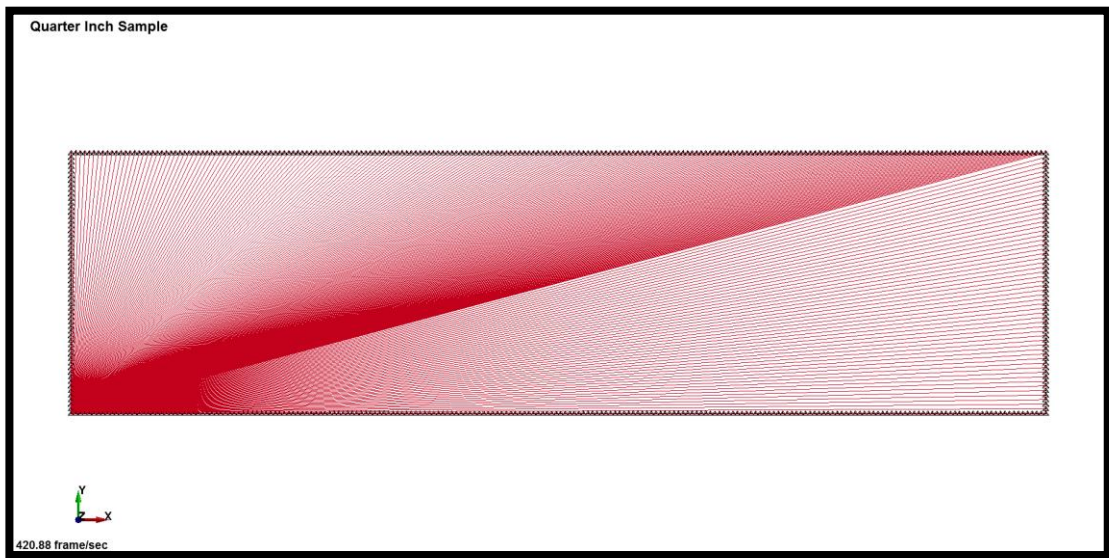


Figure 4-14 Constrained Nodal Rigid Body (Boundary Condition)

4.4 Load

Load is applied through prescribed motion of rigid indenter. The rigid indenter has the translational degrees of freedom in z & x direction and the motion is controlled by displacement; all other degrees of freedom (translational and rotational) are fixed. The vertical (z axis) and horizontal (x axis) motion of the rigid indenter is given in the following figures:

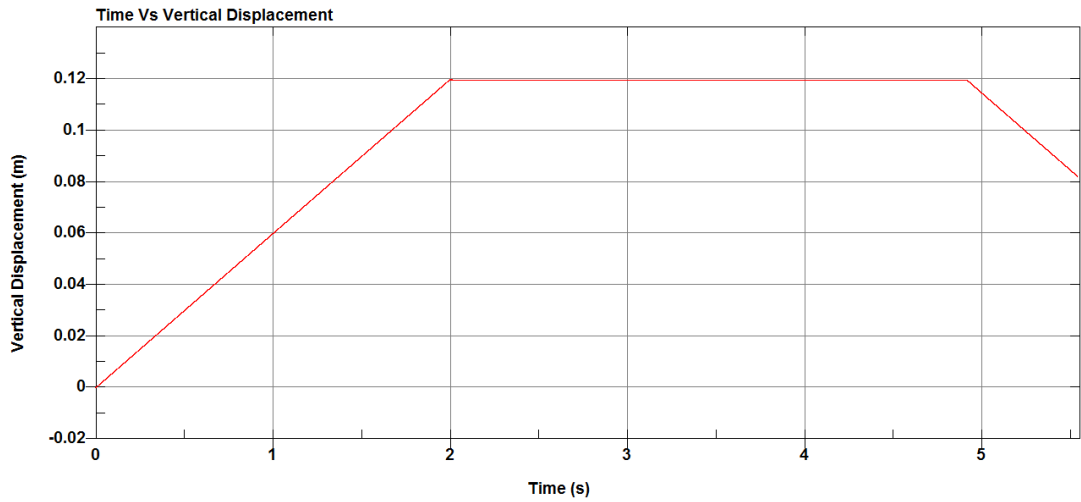


Figure 4-15 Indenter Vertical Motion

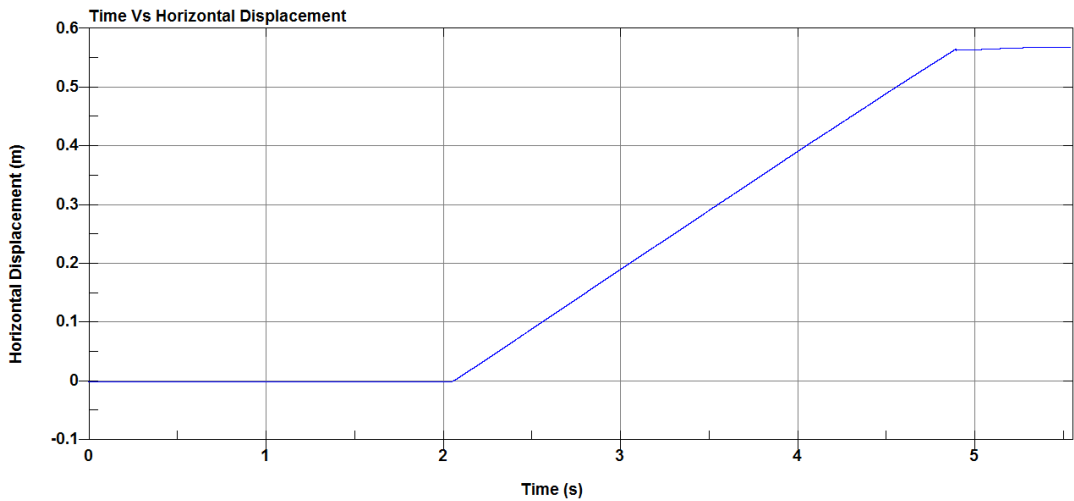


Figure 4-16 Indenter Horizontal Motion

4.5 Contact Algorithm

Current finite element analysis codes have improved and perfected their contact algorithm over years. Therefore, it is best to use automatic contact algorithm provided in today's FEA codes, due to complexity and maturity of contact algorithms. Consequently, in this study, LS-DYNA automatic single surface contact has been implemented with inner plate being the slave mesh and rigid body being the master. Since automatic single surface contact algorithm is used so all the contact surfaces are

selected in the automatic single surface contact card defining plate as the slave surface. A force transducer has been implemented between contact surfaces without considering friction. The slave and master surface are shown in the following figure:

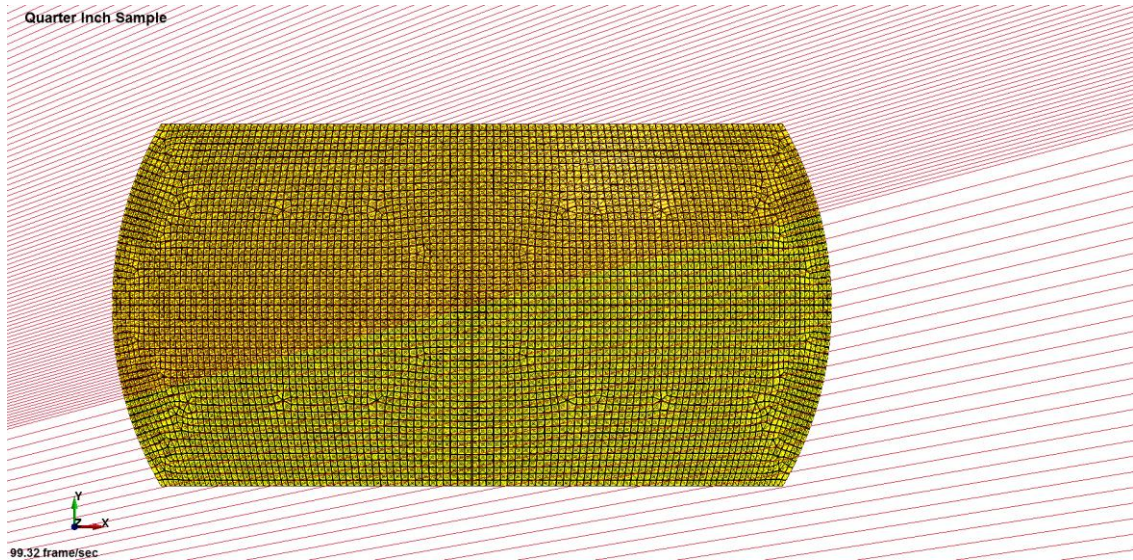


Figure 4-17 Master Surface Mesh

The nodes of this surface (Master Surface) can penetrate through the slave surface.

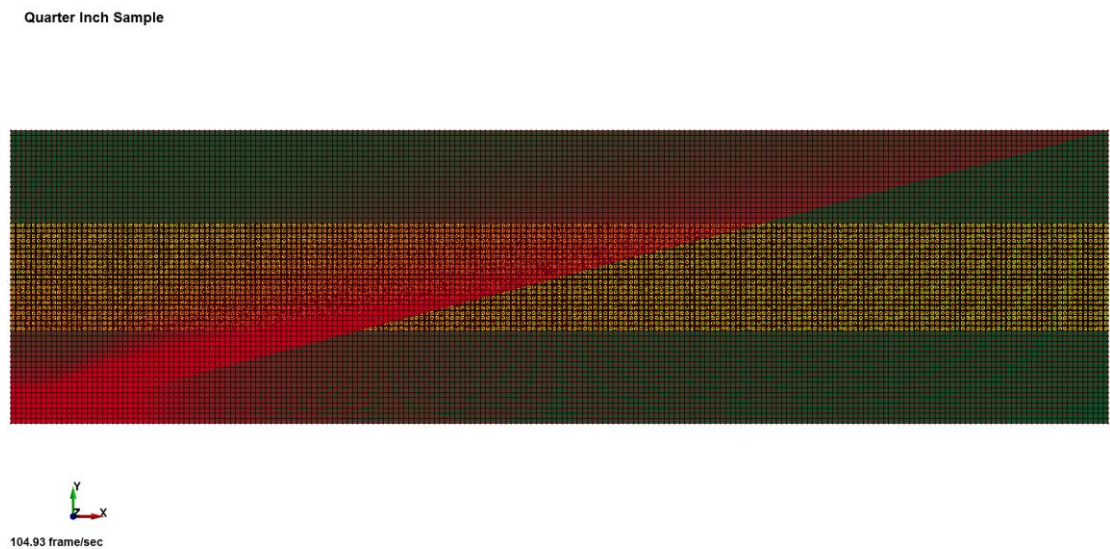


Figure 4-18 Slave Surface Mesh

The slave surface is shown in Figure 4-18, it's represented by the highlighted segments in the above figures. The nodes of this surface (Slave Surface) does not penetrate through the master surface.

4.6 Output Control

4.6.1 Termination Control

CONTROL_TERMINATION card has invoked to control the termination time of each simulation. Required simulation times varied due to objective (indentation speed, examined parameters, etc.) of the simulation, consequently, termination times have been varied as well. Termination time for each simulation is given in Table 5-1.

4.6.2 Output Results Control

DATABASE definitions are invoked to generate output files containing results information. The result information are written as two types of database: Binary and ASCII (American Standard Code for Information Interchange) database. DATABASE_BINARY_D3PLOT has invoked to obtain results of stress tensor, plastic strain, strain tensor, forces, etc., for entire model; the output can be post-processed graphically. In addition, DATABASE_EXTENT_BINARY has also invoked to obtain stress-state and fracture strain data, calculated through material model (MAT_224). The time interval between output states (DT) was varied for each simulation, to get the sufficient number of states.

ASCII databases were invoked to obtain specific output such as boundary condition forces and energy, global statistics, material energies, contact forces, and sliding forces. The time interval (DT) value was varied for each simulation; it was 25times smaller than DT in binary database.

Chapter 5 Results and Discussions

Several aspects of moving loading effect on ductile fracture have been investigated in this study: changing load, time and element type. The load is applied to the aluminium plate through contact with a rigid indenter. The vertical and horizontal motion of the indenter has been controlled by prescribed motion of the rigid indenter. The contact was conducted by in-along-out (Figure 5-1) for moving loading scenarios. The indenter travels a certain distance in the normal direction of the plate, then travels along the plate maintaining the vertical indentation to create moving load and then travels opposite direction of the initial indentation to withdraw the applied load.

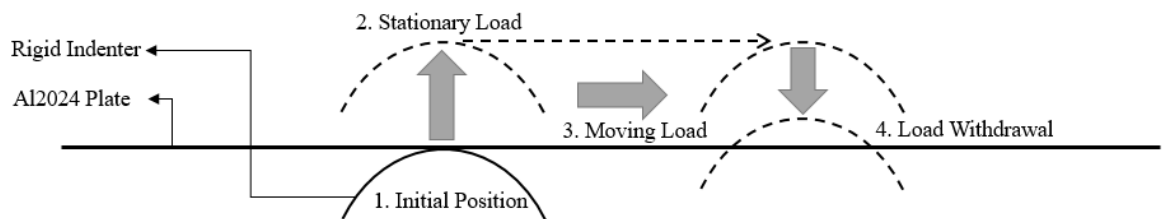


Figure 5-1: Prescribed motion (in-along-out) of the indenter

The effects investigated in this study could be broadly divided into two categories: effect of moving load on ductile fracture and effect of simulation technique on simulation results. Effect of stationary load, strain rate and loading angle have been investigated to find out how these affect ductile fracture initiation of Al2024 Aluminium plate. Effect of element selection (i.e. Shell and Solid elements) and element size for shell element have also been investigated accordingly. As mentioned in 4.6.1, the termination time for the simulations were varied based in studied factor. The summary of investigated effects is given in Table 5-1:

Table 5-1: Summary of investigated effects

Studied Effect	Element Type	Cases	Termination Time (S)
Strain Rate	Shell	SR1	0.2775
		SR2	0.555
		SR3	1.11
		SR4	1.85
		SR5	5.55
	Solid	SR1	0.2775
		SR2	0.555
		SR3	1.11
		SR4	1.850
		SR5	5.55
Stationary Load	Shell	V60	4.29
		V70	4.54
		V80	4.78
		V90	5.02
		V100	5.26
		V110	5.51
		V115	5.65
		V116	5.65
	Solid	V90	4.94
Stress State	Solid	Stationary Load	2.50
		Moving Load	5.55

Studied Effect	Element Type	Cases	Termination Time (S)
Loading Angle	Shell	15°	9.01
		30°	5.67
		45°	4.72
		60°	3.85
		75°	3.53
		90°	3.42
Element Type and Element Size	Shell	6.35mm	5.55
		9.5mm	5.55
		12.5mm	5.55
	Solid	6.35mm	5.55

In total, five parameters' effect on ductile fracture initiation due to moving load have been represented in this study, through numerical model results. Details of each investigated item are discussed further in the following sections.

5.1 Strain Rate Effect

Strain rate affects some metal's elastic and plastic capacity. Although strain rate effects are generally insignificant for Aluminium, its effect during moving load should be explored. Therefore, simulations were carried out in six different strain rate to find the effect of strain rate on ductile fracture initiation due to moving load. Strain rate was varied by changing the speed of the indenter. Simulations were carried out with both shell and solid elements.

5.1.1 Simulations with shell elements

The detail of the simulation parameters for shell elements' models are given in Table 5-2:

Table 5-2: Model parameters pertaining to strain rate effect (shell elements)

SN	Vertical indentation (mm)	Time for vertical indentation (s)	Speed of vertical indentation (mm/s)	Horizontal indentation (mm)	Time for horizontal indentation (s)	Speed of horizontal indentation (mm/s)
1	120	0.12	1000	567	0.145	3910.35
2	120	0.24	500	567	0.285	1989.50
3	120	0.48	250	567	0.579	979.27
4	120	0.8	150	567	0.967	586.35
5	120	2.4	50	567	2.85	198.95

Results obtained from above-mentioned simulations are discussed below. Vertical force versus horizontal displacement comparison curves are shown in Figure 5-25-1; all the plots generated from above simulations are given in Appendix A1.

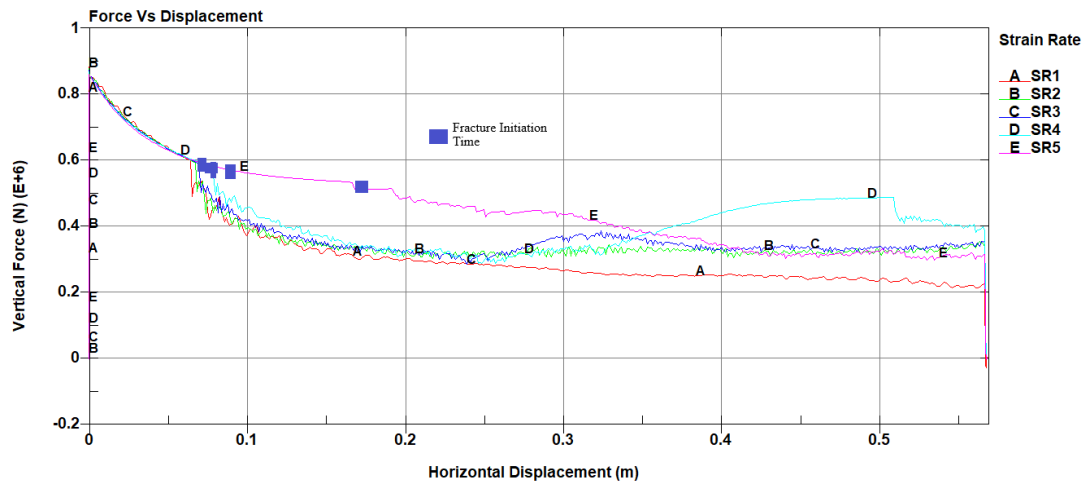


Figure 5-2: Vertical Force Vs Horizontal Displacement comparison with shell elements
 It can be noticed from vertical force versus horizontal displacement curves, horizontal displacement necessary to initiate fracture decreases as strain rate increases.

Results obtained from simulations (with shell elements) regarding strain rate effect on ductile fracture initiation due to moving load have been summarized in Table 5-3:

Table 5-3: Summarized results of strain rate effect (shell elements)

Cases	Horizontal Indentation Speed (mm/s)	Simulation Time (s)	Maximum Vertical Force (MN)	Vertical Force at Fracture (MN)	Horizontal Displacement at Fracture (mm)
SR1	3910.35	0.2775	0.88718	0.603	64.61
SR2	1989.50	0.555	0.88168	0.595	67.4
SR3	979.27	1.11	0.87706	0.592	69.7
SR4	586.35	1.85	0.87083	0.582	78.2
SR5	198.95	5.55	0.86507	0.535	167.0

It can be seen from above figure that the difference in the value of maximum vertical force is negligible among the models although vertical indentation speed varied significantly. This hints that strain rate has negligible effect on stationary load. However, it can also be seen from above table that vertical force and horizontal displacement at ductile fracture initiation varied with the changes in horizontal indentation speed. The results show that strain rate influences ductile fracture initiation due to moving load: as strain rate increases, horizontal displacement necessary to initiate fracture decreases. However, it has little effect on stationary (vertical) loading capacity.

5.1.2 Simulations with solid elements

Element selection plays a vital role on the fidelity of a numerical model. Therefore, same study has been conducted with solid elements (i.e. inner plate modeled with hexahedron solid elements) to reconfirm the conclusion of 5.1.1. Parameters of solid elements models are detailed in Table 5-4:

Table 5-4: Model parameters pertaining to strain rate effect (solid elements)

Cases	Vertical indentation (mm)	Vertical indentation Time (s)	Vertical indentation Speed (mm/s)	Horizontal indentation (mm)	Time for horizontal indentation (s)	Speed of horizontal indentation (mm/s)
SR1	100	0.1	1000	567	0.145	3910.35
SR2	100	0.2	500	567	0.285	1989.50
SR3	100	0.4	250	567	0.579	979.27
SR4	100	0.669	150	567	0.967	586.35

SR5	100	2.0	50	567	2.85	198.95
-----	-----	-----	----	-----	------	--------

Results obtained from above mentioned simulations are discussed below. Vertical force versus horizontal displacement comparison curves are shown in Figure 5-35-2; all the plots generated from above simulations are given in Appendix A2.

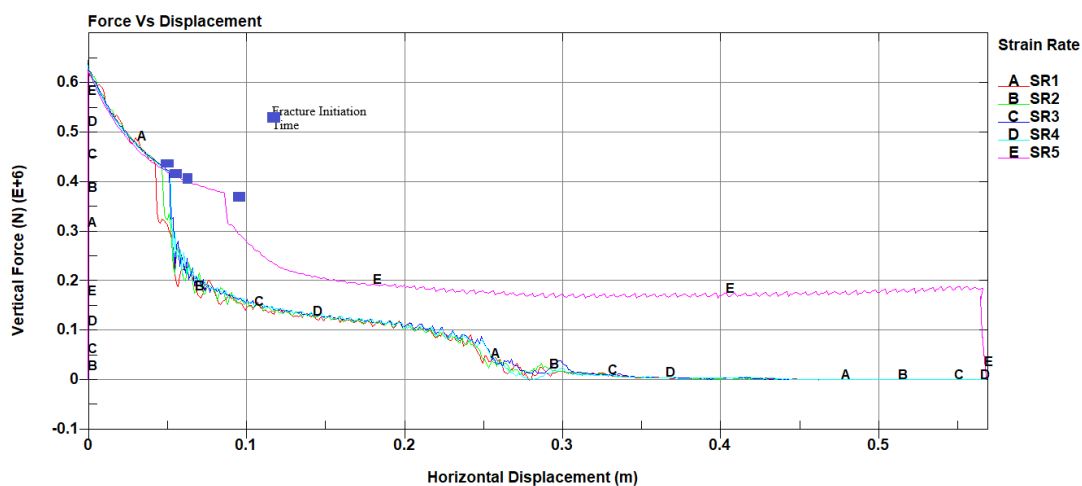


Figure 5-3: Vertical Force Vs Horizontal Displacement comparison with solid elements
 Figure 5-35-2 shows the comparison of vertical force versus horizontal displacement curves for different strain rate. It can be noticed that as strain rate increases, vertical force and horizontal displacement at fracture decreases.

Results obtained from simulations (with solid elements) regarding strain rate effect on ductile fracture initiation due to moving load have been summarized in Table 5-5:

Table 5-5: Summarized results of strain rate effect (solid elements)

Cases	Horizontal Indentation	Simulation Time (s)	Maximum Vertical Force (MN)	Vertical Force at	Horizontal Displacement

	Speed (mm/s)			Fracture (MN)	at Fracture (mm)
SR1	3910.35	0.2775	0.64579	0.446	41.4
SR2	1989.50	0.555	0.64278	0.430	47.1
SR3	979.27	1.11	0.64013	0.421	51.5
SR4	586.35	1.850	0.63610	0.418	51.7
SR5	198.95	5.55	0.62172	0.377	86.4

It can be seen from above table that horizontal displacement associated with fracture initiation increases as strain rate decreases whereas vertical force at fracture decreases. Comparing Table 5-3 and Table 5-5 it can be noticed that both solid and shell elements models results shows similar trend. However, vertical force at fracture and horizontal displacement at fracture values are higher for shell elements. As discussed in section 3.4, fracture criteria of shell elements is independent of the Lode parameter which causes a difference in results between shell and solid elements. Therefore, it should be considered carefully during modeling ductile fracture with shell elements model. In summary, solid elements models' results are concordant with shell elements models' results: moving load with high strain rate requires less horizontal indentation to initiate fracture.

5.2 Moving load capacity of the plate

Ship structures capacity to withstand damage due to moving load is different from stationary load. The plastic capacity of hull structure changes when the load starts moving. Consequently, the load to initiate fracture also should be different between

moving and stationary load. Here, moving load capacity term has used to refer the amount of moving load at which ductile fracture initiates in a hull structure. Moving load capacity of the plate has been identified in this section. The amount of moving load was varied by changing the vertical indentation of the plate, and the vertical indentation associated with ductile fracture initiation due to moving load was calculated.

5.2.1 Moving load capacity calculation with shell elements model

The vertical force acting on the plate varies as the vertical indentation changes which can be referred as the stationary load. As the indenter starts moving both vertical and horizontal forces act on the plate (i.e. moving load), therefore the amount of moving load varies as amount of vertical indentation changes. In this study, a series of simulations were conducted changing the vertical indentation, keeping the horizontal indentation constant, thereby changing the moving load, to find out vertical force and resultant force associated with initiation of ductile fracture due to moving load for current model.

A series of simulations have been conducted to find out how much force is necessary to initiate fracture due to moving load for current model. This investigation was carried out with shell element models and the parameters of simulations are given in Table 5-6:

Table 5-6: Parameters of stationary load effect simulations (shell elements)

Cases	Vertical indentation (mm)	Horizontal indentation
1	60	567
2	70	567
3	80	567
4	90	567

Cases	Vertical indentation (mm)	Horizontal indentation
5	100	567
6	110	567
7	115	567
8	116	567

Vertical force versus horizontal displacement and resultant force versus horizontal displacement comparison curves are shown in Figure 5-45-3 and Figure 5-55-4 respectively; all the plots generated from above simulations are given in Appendix B1

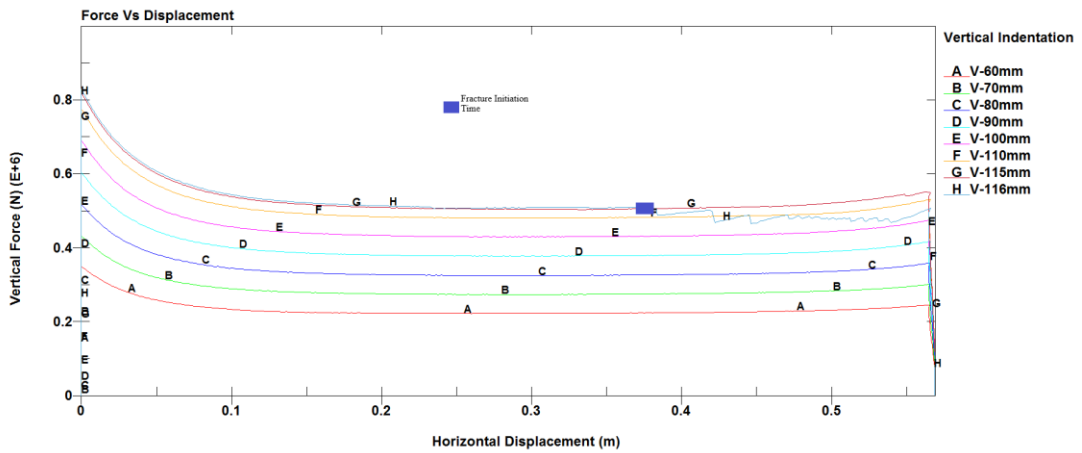


Figure 5-4: Vertical Force Vs Horizontal Displacement comparison

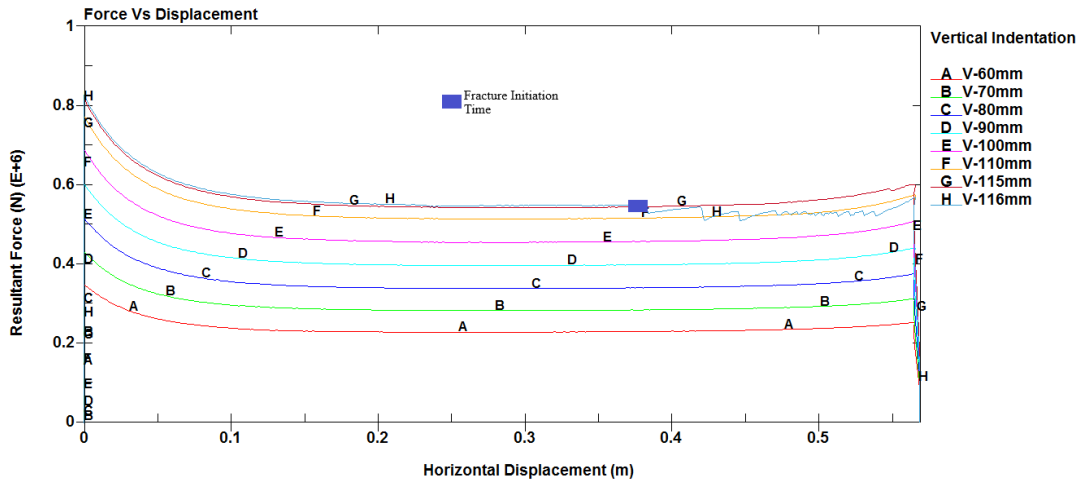


Figure 5-5: Resultant Force Vs Horizontal Displacement comparison

It can be seen from Figure 5-45-3 and Figure 5-55-4 that both vertical and resultant forces increase as vertical indentation increases and ductile fracture initiates for case 8 (i.e. vertical indentation:116mm). Vertical force and resultant force at fracture are 0.504MN and 0.545MN respectively.

5.2.2 Comparison of moving load capacity between solid and shell elements model

As mentioned in section 5.1.2, results for solid elements models differ from shell elements models. Numerical simulations have been carried out with solid elements to find out whether vertical indentation, associated with ductile fracture initiation due to moving load, is same for both solid and shell elements models. It was found that for solid element model ductile fracture due to moving load initiates when vertical indentation is 90mm while it's 116mm for shell elements model. Parameters of solid and shell elements models (fractured) have been shown in Table 5-7:

Table 5-7: Parameters of stationary load effect models (solid vs shell)

Element Type	Vertical indentation	Horizontal indentation
--------------	----------------------	------------------------

	(mm)	(mm)
Shell	116	567
Solid	90	567

Vertical force versus horizontal displacement and resultant force versus horizontal displacement comparison curves are shown in Figure 5-65-5 and Figure 5-75-6 respectively; all the plots generated from above simulations are compared and given in Appendix B2.

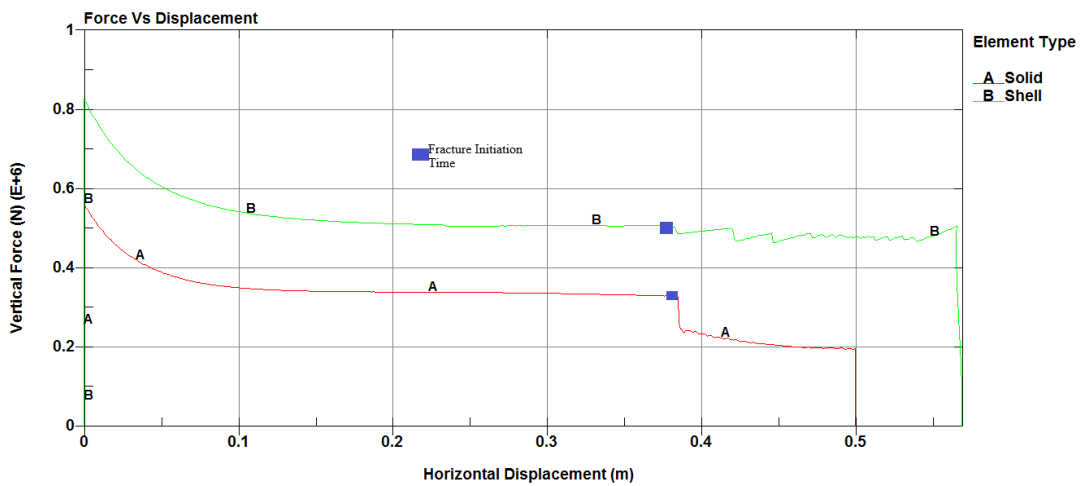


Figure 5-6: Vertical Force Vs Horizontal Displacement comparison (solid and shell elements models)

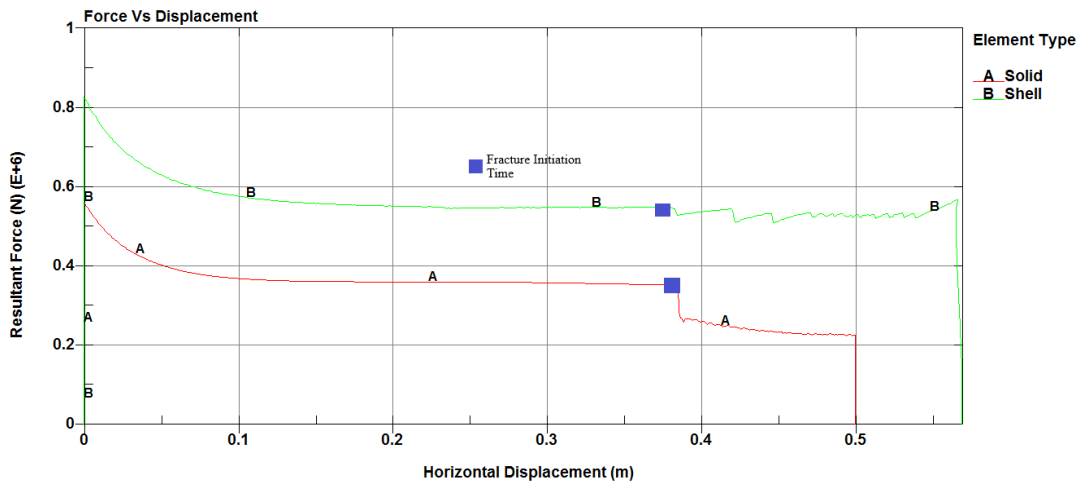


Figure 5-7: Resultant Force Vs Horizontal Displacement comparison

From above figures, it is apparent that moving load capacity calculated from both models are different. The vertical force and resultant force at fracture is much higher for shell elements model than solid elements model although fracture initiates almost same horizontal displacement.

The difference in results for shell and solid elements (fractured) models have been summarized in Table 5-8:

Table 5-8: Results comparison between solid and shell elements models (fractured)

Element Type	Vertical Indentation (mm)	Horizontal Displacement at Fracture (mm)	Resultant Displacement at Fracture (mm)	Vertical Force at Fracture (N)	Resultant Force at Fracture (N)
Solid	90	385	395	3.28×10^5	3.51×10^5
Shell	116	383	400	5.04×10^5	5.45×10^5

Table 5-8 shows: vertical force at fracture is 53.65% higher for shell elements compared to solid elements model; resultant force at fracture is 55.27% higher for shell elements compared to solid elements model. However, horizontal displacement is almost equal.

The difference in results between these two elements is likely due to the exclusion of Lode parameter calculation in shell elements. Lode parameter is not calculated in MAT_224 for shell elements, so state of stress has not been fully incorporated into the shell element models. Consequently, ductile fracture initiates at different load in shell elements than solid elements.

5.3 State of stress during fracture initiation between stationary and moving loading scenario

State of stress dictates plastic deformation and initiation of ductile fracture. Fracture strain for metals changes with the change in state of stress. Force capacity under plastic deformation due to sustained indentation during moving loads is significantly less than for stationary loads at the same indentation. Therefore, a comparison of state of stress and associated fracture strain, for stationary load and moving load, has carried out and represented in this section: to find out the root cause of moving load effects on ductile fracture initiation. Two simulations were carried out, one for stationary loading condition and another for moving loading condition. The vertical indentation speed was kept same for both case although the amount of vertical indentations were varied. This was to ensure that stationary loading model fractures during vertical indentation (under stationary load) and moving loading model fractures during horizontal indentation (i.e. under moving load). The details of compared models have been given in Table 5-9:

Table 5-9: Model parameters for state of stress effect

Load Type	Vertical indentation (mm)	Time for vertical indentation (s)	Horizontal indentation	Time for horizontal indentation (s)
Stationary Load	150	2.5	0	0
Moving Load	90	2.0	500	2.85

The time interval value (DT) for both binary (D3PLOT) and ASCII outputs were kept significantly smaller at fracture initiation time to accurately capture the fracture initiating elements. Fracture initiated at 2.016s for stationary load model; the DT of Binary_D3PLOT and ASCII were chosen to be 0.0005s and 0.00002s accordingly, during 2.00~2.05s of the simulation. Similarly, fracture initiated at 4.2001s for moving load model, and DT value of Binary_D3PLOT and ASCII had kept as 0.0005 and 0.00002s during 4.18~4.27s of the simulation accordingly.

Several parameters, related to state of stress (triaxiality and Lode) and fracture initiation (such as plastic strain, plastic strain rate, Von-Mises stress, fracture strain, etc.) of fracture initiating element (for both stationary and moving load) have been plotted and shown in Figure 5-85-7 ~ Figure 5-115-10. All the plots generated from above simulations are given in Appendix C.

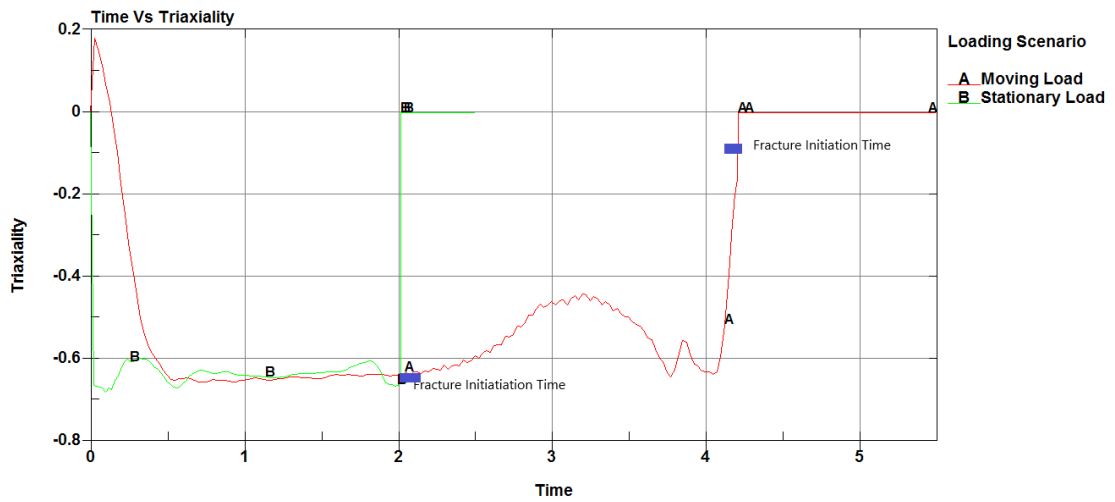


Figure 5-8: Triaxiality comparison between stationary and moving load

Figure 5-85-7 shows the progression of triaxiality value (over time) of fracture initiating elements for both moving and stationary loading condition. The fracture initiating time were marked for easy identification of the difference in values. It's worth mentioning that the sign of triaxiality in MAT_224 calculation is opposite to conventional calculation. Here, negative sign represents tension as opposed to conventional calculation where negative sign represents compression.

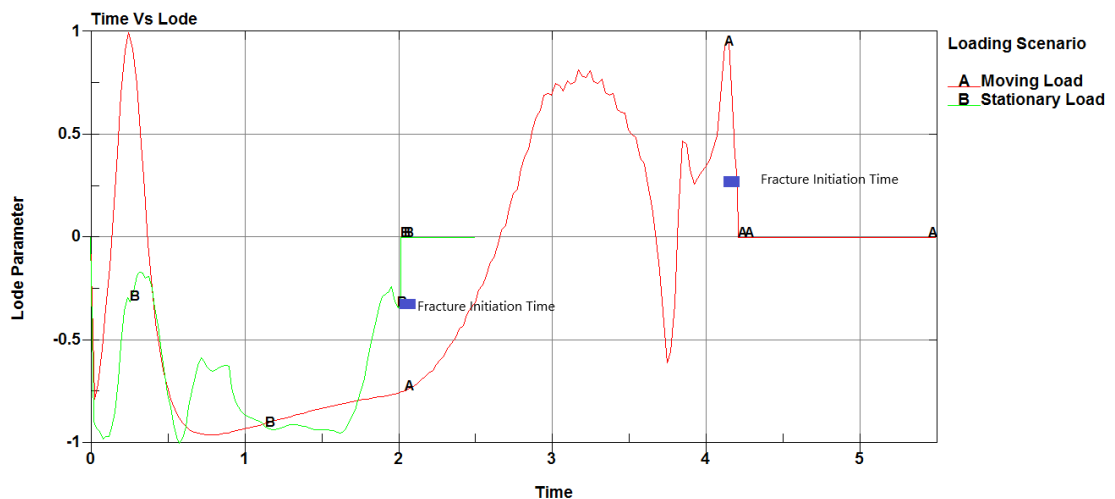


Figure 5-9: Lode comparison between stationary and moving load

Figure 5-95-8 shows the progression of Lode parameter (over time) of fracture initiating elements for both moving and stationary loading condition. The fracture initiating time were marked for easy identification of the difference in values.

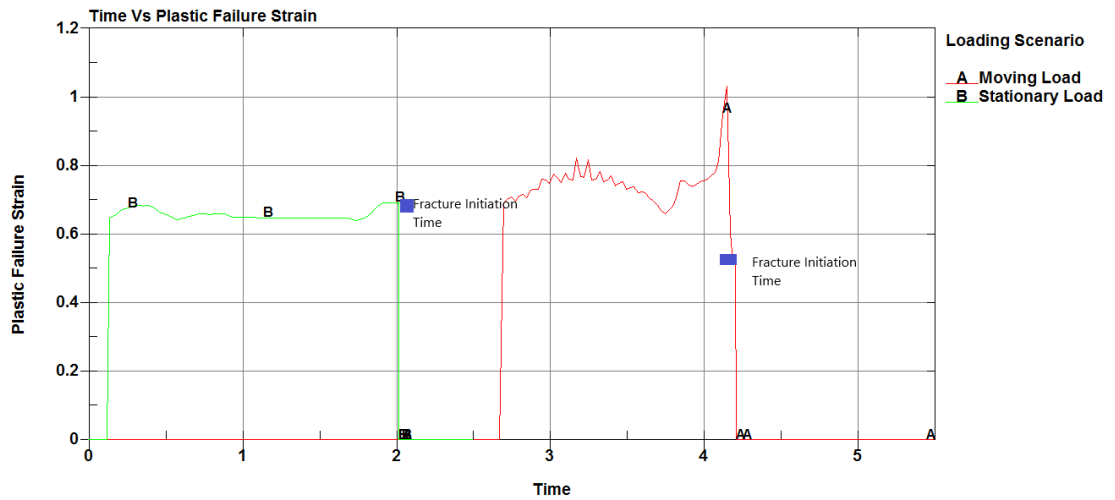


Figure 5-10: Plastic Failure Strain comparison between stationary and moving load

Figure 5-105-9 shows the plastic failure strain versus time curve of fracture initiating element for both moving and stationary loading condition. The fracture initiating time were marked for easy identification of the difference in values. The fracture strain for moving load is lower than stationary load.

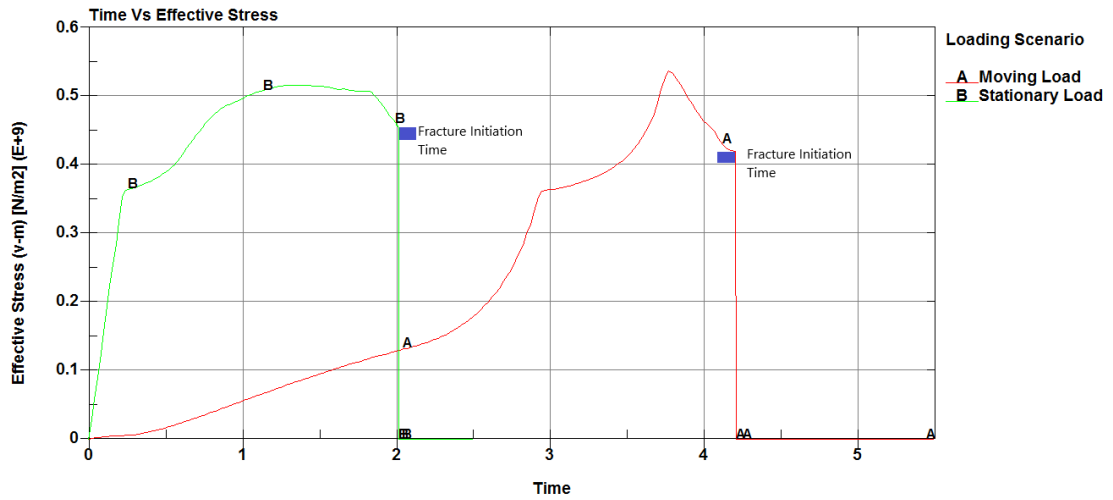


Figure 5-11: Von-Mises Stress comparison between stationary and moving load

Figure 5-115-10 shows the comparison of Von-Mises stress versus time curve between fracture initiating element of moving and stationary loading condition. The fracture initiating time were marked for easy identification of the difference in values. The Von-Mises stress for stationary load was higher than moving load.

Simulation results have been summarized in Table 5-10 below:

Table 5-10: Summary of results for state of stress

Parameters	Stationary Load	Moving Load
Fracture Initiating Element	H10073827	H10074081
Fracture Initiation Time	2.016s	4.2001s
Effective Plastic Strain	0.649641	0.73346
Von Mises Stress	$4.5581 \times 10^8 \text{ N/m}^2$	$4.2029 \times 10^8 \text{ N/m}^2$
Plastic Strain Rate	0.9896	0.2459
Plastic Failure Strain	0.69115	0.52706
Triaxiality	-0.65868	-0.15078
Lode Parameter	-0.32674	0.25325

Parameters	Stationary Load	Moving Load
Plastic Work	3.0682X10 ⁸	3.4101X10 ⁸
Plastic Strain to Plastic Failure Strain Ratio	0.99923	1.0
Temperature	431.12K	445.73K

It can be noted from the above table that Von-Mises stress is significantly higher in stationary loading condition compared to moving loading scenario. This means the fracture strain becomes lower during moving loading condition. Fracture strain during stationary load was 0.69115 whereas it was 0.52706 for moving load. Since fracture strain depends on the state of the stress, it indicates that fracture initiates at different stress-state in stationary loading condition compared to moving load. The state of stress is measured by the value of triaxiality and the Lode parameter. For stationary load, the triaxiality and the Lode parameter at fracture are -0.65868 and -0.32674; this represents an axisymmetric tension (equi-biaxial tension)[60]. For moving load, the triaxiality and Lode parameter at fracture were -0.15078 and 0.25325; this represents a combination of shear and tension [60]. Because of the change in state of stress, fracture initiates at lower force during moving load.

To conclude, the state of stress changes significantly between stationary and moving load scenarios which causes plates with moving load to fracture at lower vertical force.

5.4 Loading angle effects

In the above sections, vertical and horizontal loads were applied separately; vertical indentation is applied first, followed by horizontal indentation. On the contrary, in

practical moving loading incidence (such as ship-ice interaction), both vertical and horizontal load acts simultaneously. Therefore, this section describes effect of moving load when both vertical and horizontal indentation takes place simultaneously. In addition, the resultant loading angle has been varied changing vertical and horizontal indentation.

The effects of loading angle on ductile fracture initiation due to moving load have been investigated in this study. To accomplish this, both tangential and normal load were applied simultaneously to create an angle between indenter and steel plate. Furthermore, the tangential and normal load value has been changed to vary amount of applied load and loading angle (**Error! Reference source not found.**); loading angle 90° represents purely normal load and 0° represents purely tangential load.

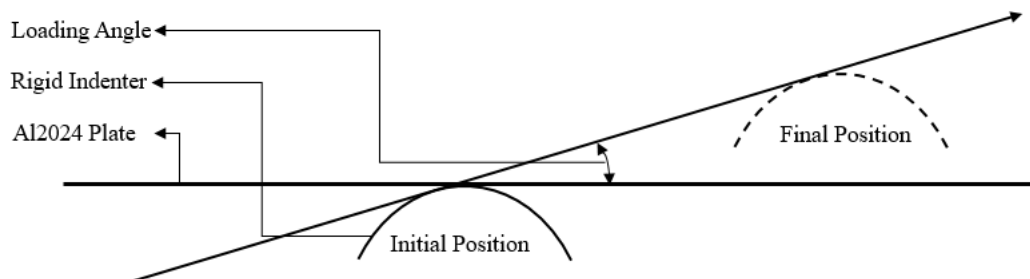


Figure 5-12: Prescribed motion for loading angle effect

Detail parameter of the simulations are given in Table 5-11 below:

Table 5-11: Model parameters for loading angle effects (shell elements)

Loading angle (Degree)	Simulation time (s)	Vertical indentation (mm)	Horizontal indentation (mm)	Resultant Indentation (mm)	Indentation speed (mm/s)
15	9.01	140	522	540.45	60.05
30	5.67	170	295	340.48	60.05
45	4.72	200	200	282.84	59.92
60	3.85	200	115	230.71	59.92
75	3.53	205	55	212.25	60.13
90	3.42	205	0	205	59.94

Vertical force versus horizontal displacement and resultant force versus horizontal displacement comparison curves are shown in Figure 5-135-11 and Figure 5-145-12 respectively.

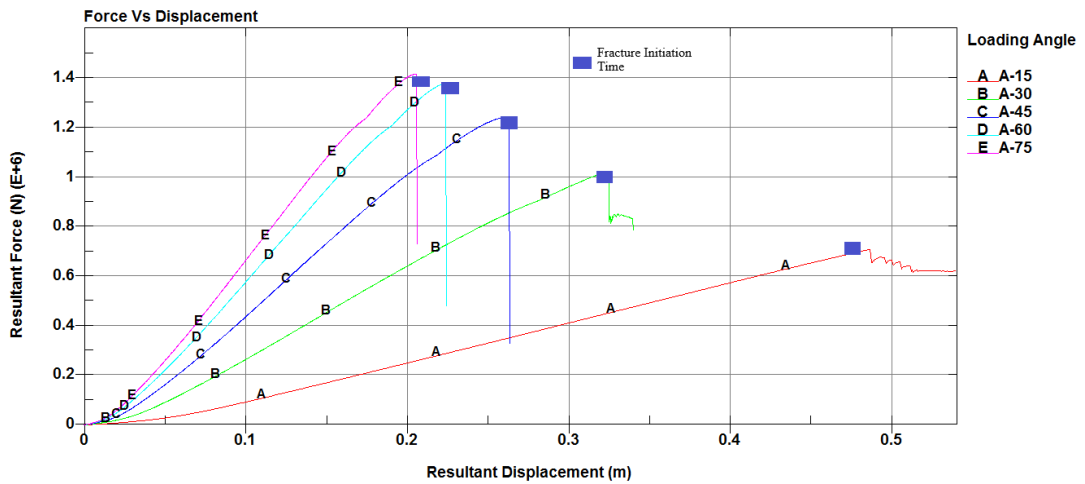


Figure 5-13: Resultant Force Vs Resultant Displacement comparison for loading angle effects

It can be seen from Figure 5-135-11 that both resultant displacement and resultant force at fracture is strongly dependent on loading angle: as loading angle increases, resultant force increases while resultant displacement decreases.

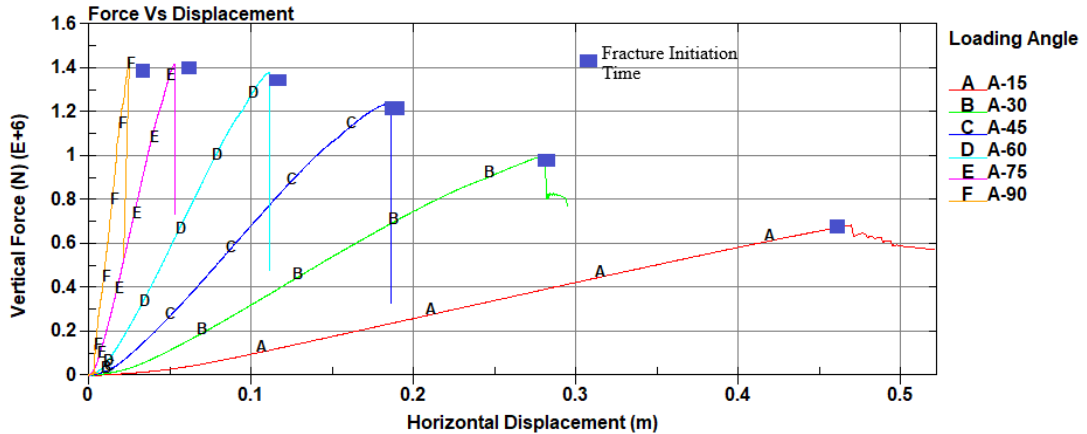


Figure 5-14: Vertical Force Vs Horizontal Displacement comparison for loading angle effects

Strong dependency on loading angle was observed for vertical force and horizontal displacement at fracture; vertical force increases as loading angle increases while horizontal displacement decreases as loading angle increases.

The results have been further summarised in Table 5-12 below:

Table 5-12: Summary of results for loading angle effects

Loading angle (Degree)	Simulation Time (s)	Vertical Displacement at Fracture (mm)	Horizontal Displacement at Fracture (mm)	Resultant Displacement at Fracture (mm)	Resultant Force at Fracture (N)
15	9.01	126	502	487	7.10×10^5
30	5.67	162	281	325	1.01×10^6
45	4.72	186	186	263	1.24×10^6
60	3.85	194	112	224	1.38×10^6
75	3.53	199	53.3	206	1.42×10^6
90	3.42	202	25.3	204	1.44×10^6

An exponential relationship was obtained by plotting the values of resultant force and resultant displacement at fracture, for different loading angle. The plot was obtained by Microsoft Excel with 99.4% data fits the trend line. It is shown in Figure 5-155-13 below

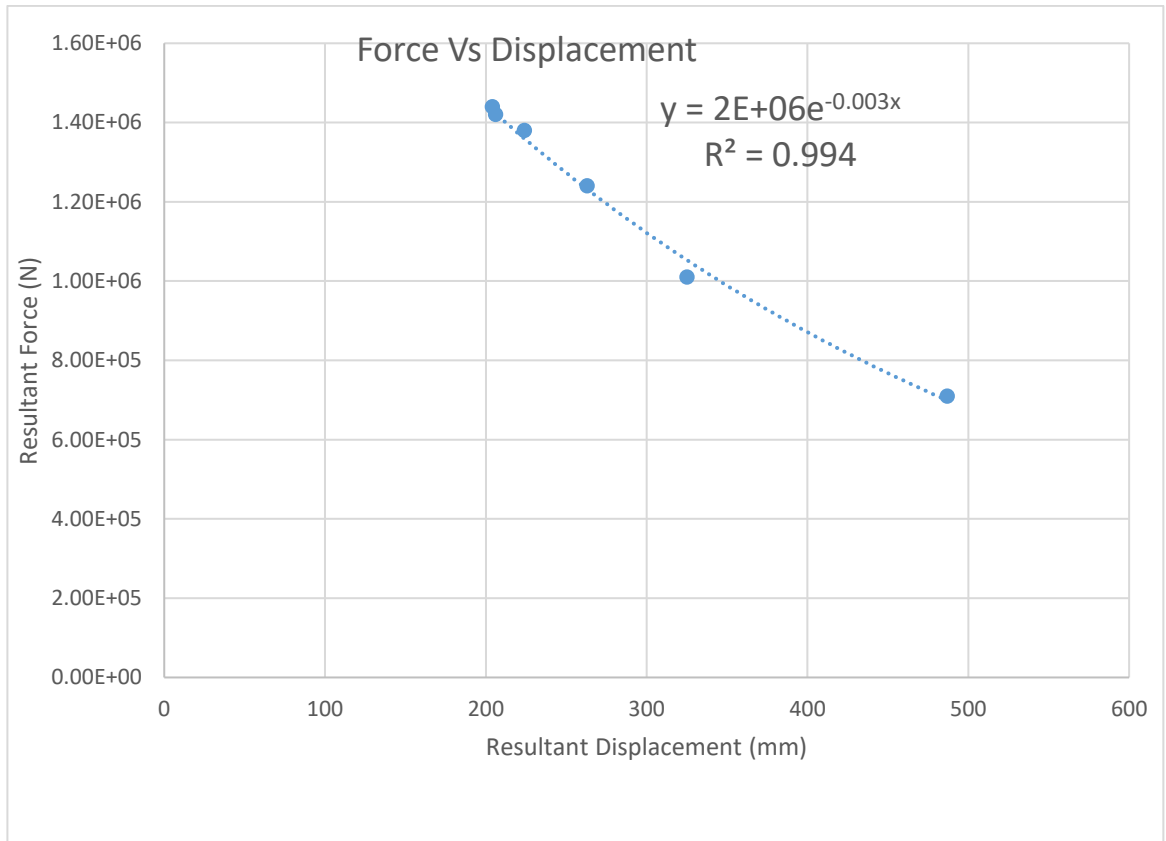


Figure 5-15: Resultant Force Vs Resultant displacement at Fracture for different Loading Angles

It can be concluded from Figure 5-155-13 that the relationship between resultant force and resultant displacement at fracture can be expressed by below equation

$$F_r = 2 \times 10^6 e^{-0.003 d_r}$$

In addition, resultant forces at fracture versus loading angles were plotted and shown in Figure 5-165-14 below:

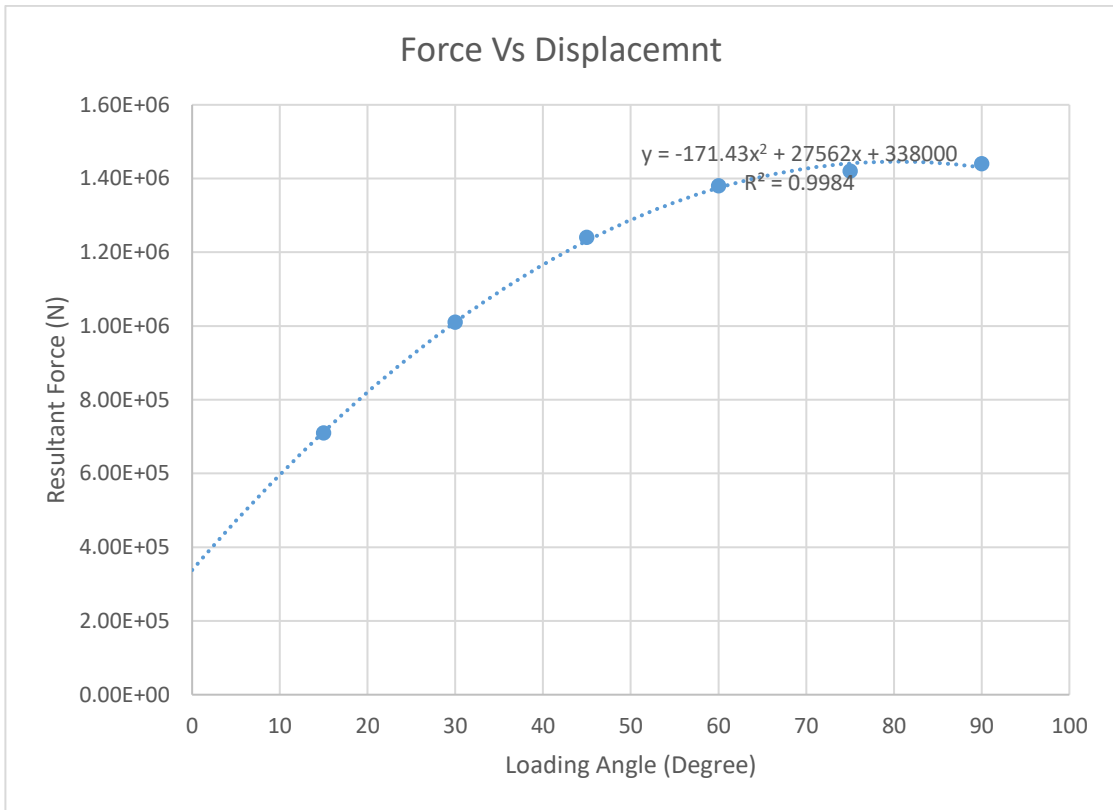


Figure 5-16: Resultant Force at Fracture Vs Loading Angle

A polynomial relationship was observed between resultant force at fracture and loading angle from above figure. As loading angle is decreased (i.e. horizontal indentation speed decreases) resultant force required to initiate ductile fracture decreases as well.

Again, vertical force versus horizontal displacement, at fracture, plotted as shown in Figure 5-175-15 below:

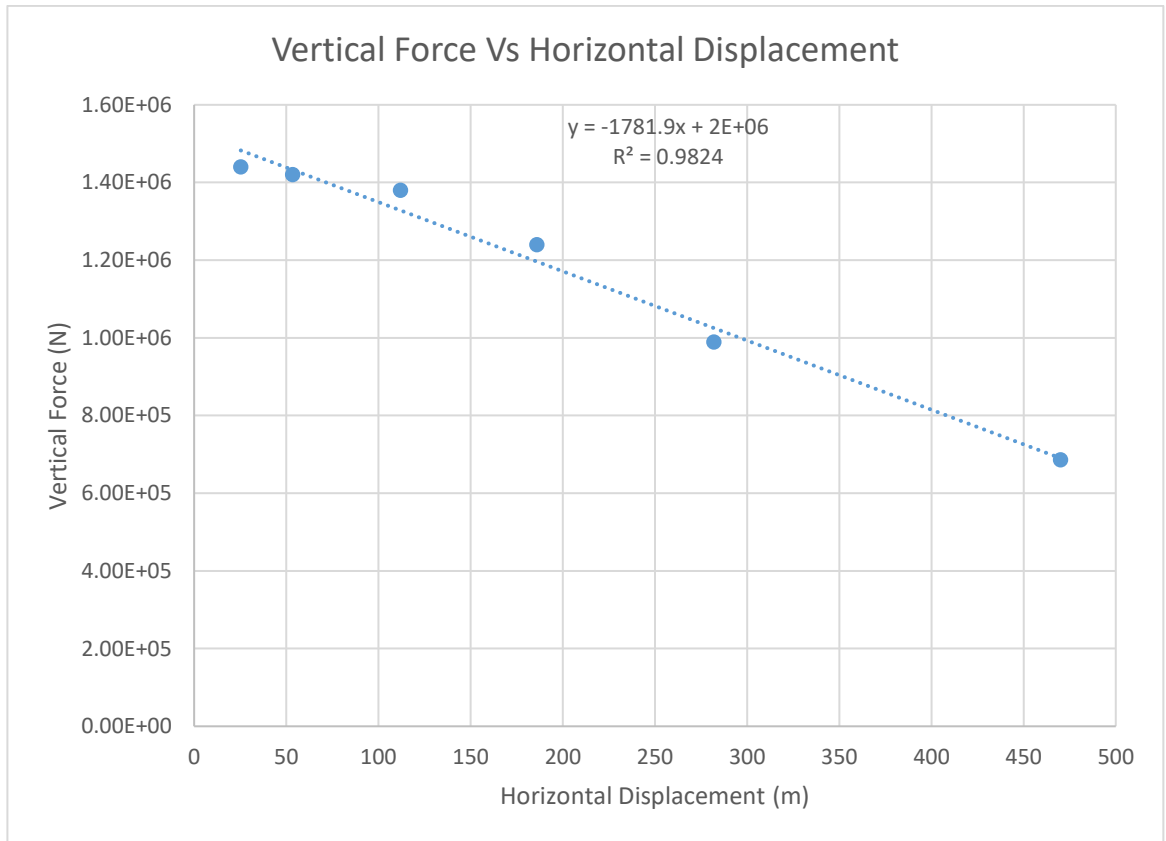


Figure 5-17: Resultant Force Vs Resultant displacement at Fracture for different Loading Angles

A linear relationship was observed between vertical force and horizontal displacement at fracture, with 98.24% data fits the trend line obtained by Microsoft Excel. The relationship can be expressed by below equation:

$$F_v = 2 \times 10^6 - 1781.9 d_x$$

Moreover, another polynomial relationship was found between vertical force at fracture and loading angle (Figure 5-185-16).

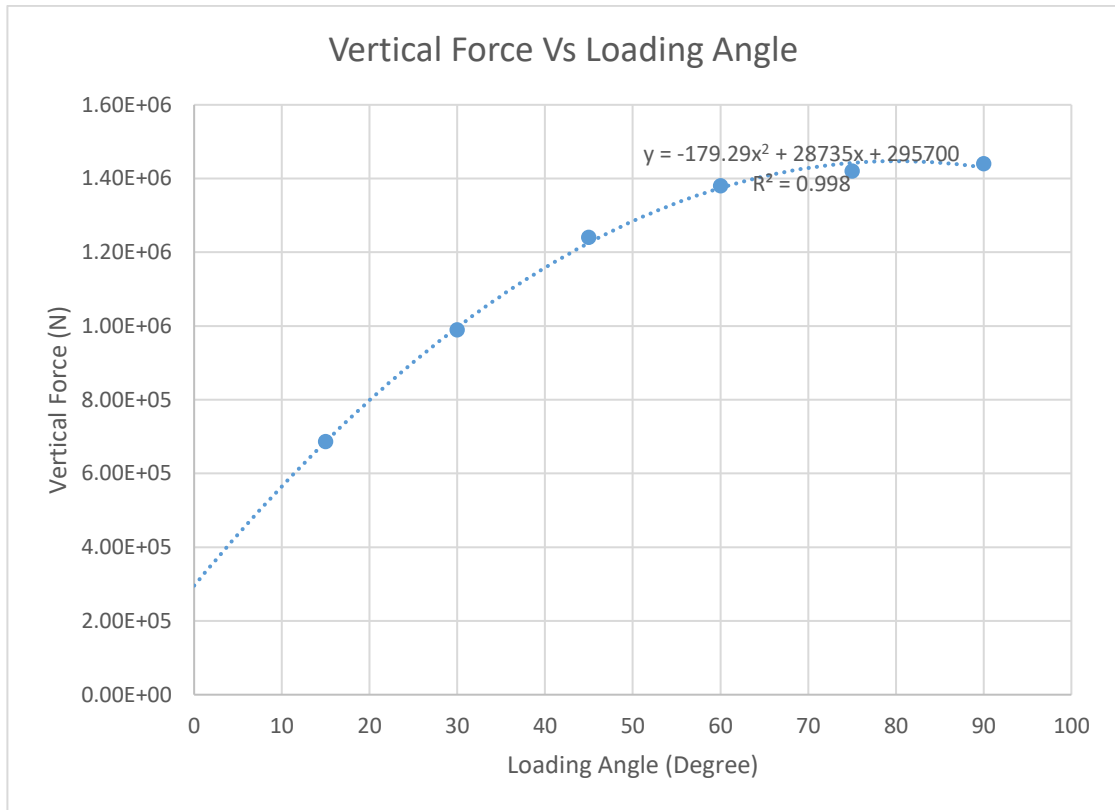


Figure 5-18: Vertical Force at Fracture Vs Loading Angle

It can be seen from above figure that vertical force required to initiate fracture increases as loading angle increases (i.e. horizontal indentation speed decreases).

5.5 Mesh convergence study

Finite element analysis is always associated with mesh sensitivity, therefore, mesh convergence study must be carried out to confirm that the result is mesh size independent. Models with shell element have element size of 6.35mm since the thickness of the plate is 6.35mm; shell elements' edge length cannot be smaller than plate thickness. Therefore, all the models have length to thickness of 1 ($l/t=1$). Two more models have been created with $l/t=1.5$ and $l/t=2$ to conduct the mesh convergence analysis. In addition, results obtained from solid element models were also compared with shell elements results. For solid elements, industrially proven best meshing method

(5 layers of solid element with element size equal to thickness of the plate) has been employed to reassure the accuracy of the model.

Since fracture initiation is dependent on element size, mesh convergence study was carried out without fracture initiation. The details of conducted simulation have been given in Table 5-13 below:

Table 5-13: Model parameters for mesh convergence study

Element size to thickness ratio	Element size (mm)	V-indentation (mm)	H-indentation (mm)	Simulation Time (s)
Shell (l/t=1)	6.35	40	567	5.55
Shell (l/t=1.5)	9.5	40	567	5.55
Shell (l/t=2)	12.5	40	567	5.55
Solid	6.35	40	567	5.55

Accordingly, vertical force versus horizontal displacement curves were compared and shown in Figure 5-195-17. All the results obtained from above simulations are given in Appendix D.

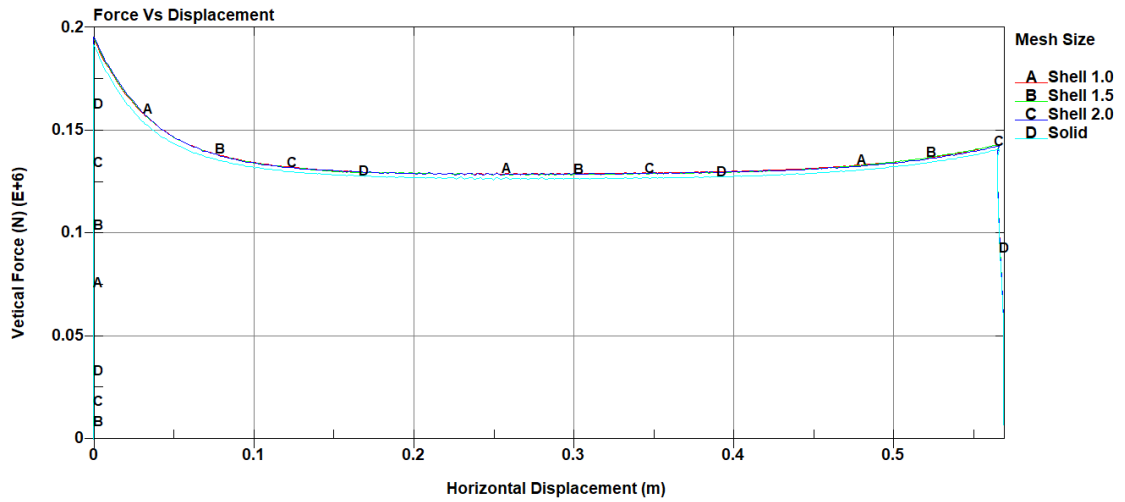


Figure 5-19: Vertical Force Vs Horizontal Displacement for mesh convergence

It can be seen from Figure 5-195-17 vertical force versus horizontal displacement curves for all the shell elements are identical. However, the vertical force for solid elements were slightly lower than shell elements models. Maximum vertical force obtained from above simulations were tabulated with corresponding computational time and shown in Table 5-14.

Table 5-14: Results obtained from mesh convergence study

Element size to thickness ratio	Element size (mm)	Maximum Vertical Force (MN)	Difference in results with Reference Model	Computation Time (s)
Shell (1/t=1)	6.35	0.193	Reference Model	9213
Shell (1/t=1.5)	9.5	0.193	0.0%	5113
Shell (1/t=2)	12.5	0.194	0.52%	3356
Solid	6.35	0.192	0.54%	72749

Here, shell element model with element size 6.35mm ($l/t=1$) has been selected as the reference model and other models' results were compared accordingly. Table 5-14 shows that the maximum difference in results from reference model is less than 0.54%. On the whole, results for subject meshes converged successfully.

Chapter 6 Conclusions and Future Works

6.1 Conclusions

This study investigated the effect of moving load on ductile fracture initiation of Aluminium 2024 by finite element analysis. The investigation explored several aspects of moving load's effect and following conclusions were drawn:

1. State of stress at fracture differs between stationary and moving loading conditions. Ductile fracture initiation occurred approximately under equi-biaxial tension for stationary load while it occurred under the combination of shear and tension for moving load. Since a combination of shear and tension stress had resulted during moving load, fracture initiated at a lower stress for moving load than stationary load.
2. Moving load's effect is intertwined with state of stress. Therefore, stress-state dependent fracture criteria is imperative to study moving load's effect. If a stress-state independent (for example, constant fracture strain) failure criteria is used, moving load's effect on fracture cannot be identified. An ideal failure model should account the relationship among triaxiality, Lode parameter and fracture strain.
3. Lode parameter is not calculated in MAT_224 which is likely the reason a difference in results were observed between solid and shell elements models. Inclusion of Lode parameter calculation in MAT_224 will probably improve the accuracy of results obtained with shell elements.

4. Strain rate has a substantial effect on fracture initiation due to moving load, especially on required horizontal indentation, to initiate fracture. Fracture initiates at higher horizontal indentation for lower strain rate and vice versa.
5. Moving loading angle has significant influence on ductile fracture initiation. As loading angle increases, i.e. resultant force gets closer to plate's normal direction, required resultant force to initiate fracture increases as well; however, resultant displacement to initiate fracture decreases. Furthermore, a relationship between resultant force and resultant displacement was derived given in the equation below:

$$F_r = 2X10^6 e^{-0.003d_r}$$

It was also found that vertical force to initiate fracture decreases significantly as loading angle decreases (as horizontal displacement increases); half amount of vertical force is sufficient to initiate for 15° loading angle, compared to 90° loading angle (stationary loading condition). Finally, a linear relationship was derived between vertical force and horizontal displacement to initiate fracture, with simulation results. The equation is given below:

$$F_v = 2X10^6 - 1781.9d_x$$

6.2 Future work

In this study, the effect of moving load on ductile fracture initiation for Aluminium 2024 was conducted with numerical method only. Consequently, conducting practical experiment to validate these results is a discernible extension of this work. In addition to that, further development of this study can be achieved through following research:

1. Since the complete material fracture model was available from MAT_224 developer, Aluminium 2024 was chosen for this study; it was impossible and

also out of scope of the study to generate fracture locus for any material, due to limited resources. Although Aluminium is used for high-speed craft, Steel is the common material for ship structure. Therefore, future study should be conducted with commonly used ship building steel such as mild steel.

2. Effect of loading angle was conducted maintaining constant indentation rate, both horizontal and vertical. However, strain rate has significant effect on moving load, therefore, strain rate should be varied in future study. In addition, the study should be extended to make connection with ship-ice interaction study. The horizontal displacement rate can be perceived as ship's speed and the vertical displacement can be coupled with practical ice load data; series of studies should be conducted to find out the critical horizontal displacement rate (ship's speed) that initiates fracture for certain vertical force (ice load). As a result, critical ship's speed, initiates ductile fracture at hull, can be identified for known ice-infested sea routes.
3. Finally, method for incorporating Lode parameter calculation in MAT_224 should be explored to improve the accuracy of results for shell elements. Shell elements are plane stress elements and for plane stress, triaxiality and Lode parameter is related by the following relationship:

$$\cos \left[\frac{\pi}{2} (1 - \bar{\theta}) \right] = -\frac{27}{2} \eta \left(\eta^2 - \frac{1}{3} \right)$$

This relationship can be used to further investigate and improve accuracy of MAT_224 with shell elements.

Bibliography

- [1] Quinton BWT. Progressive damage to a ship's structure due to ice loading. 2008.
- [2] Quinton BWT. Experimental and numerical investigation of moving loads on hull structures. 2015.
- [3] Alsos HS, Amdahl J. Analysis of bottom damage caused by ship grounding. 2008;2:829-36.
- [4] McClintock FA. A Criterion for Ductile Fracture by the Growth of Holes. J Appl Mech 1968;35:363.
- [5] Rice JR, Tracey DM. On the ductile enlargement of voids in triaxial stress fields*. J Mech Phys Solids 1969;17:201-17.
- [6] Bao Y. Prediction of ductile crack formation in uncracked bodies 2003.
- [7] Bao Y, Wierzbicki T. On fracture locus in the equivalent strain and stress triaxiality space. Int J Mech Sci 2004;46:81-98.
- [8] Johnson GR, Cook WH. Fracture characteristics of three metals subjected to various strains, strain rates, temperatures and pressures. Eng Fract Mech 1985;21:31-48.
- [9] Bai Y. Effect of loading history on necking and fracture 2007.
- [10] Bai Y, Wierzbicki T. A new model of metal plasticity and fracture with pressure and Lode dependence. Int J Plast 2008;24:1071-96.
- [11] Bai Y, Teng X, Wierzbicki T. On the application of stress triaxiality formula for plane strain fracture testing. J Eng Mater Technol Trans ASME 2009;131:0210021-02100210.
- [12] Bai Y, Wierzbicki T. Application of extended Mohr-Coulomb criterion to ductile fracture. Int J Fract 2010;161:1-20.
- [13] Bai Y, Wierzbicki T. A comparative study of three groups of ductile fracture loci in the 3D space. Eng Fract Mech 2014.
- [14] Bai Y, Wierzbicki T. A comparative study of three groups of ductile fracture loci in the 3D space. Eng Fract Mech 2015;135:147-67.
- [15] Wang G, Spencer J, Chen Y. Assessment of a ship's performance in accidents. Mar Struct 2002;15:313-33.

- [16] Pedersen PT. Review and application of ship collision and grounding analysis procedures. *Mar Struct* 2010;23:241-62.
- [17] 'Miguel Angel Gonzales Calle', 'Marcilio Alves'. *Ship Collision: A Brief Survey*. 21st Brazilian Congress of Mechanical Engineering October 2011.
- [18] Calle MAG, Alves M. A review- analysis on material failure modeling in ship collision. *Ocean Eng* 2015;106:20-38.
- [19] Ehlers S, Tabri K, Varsta P. Collision strength of ship structures-a state of the art review. *Mar Technol Eng* 2011;2:841-50.
- [20] Minorsky V. *An analysis of ship collisions with reference to protection of nuclear power plants* 1958.
- [21] Woisin G. *Design against collision*. : GKSS-Forschungszentrum, 1980.
- [22] Vaughan H. *Damage to Ships due to Collision and Grounding*. 1977.
- [23] Reardon P, Sprung J. Validation of Minorsky's ship collision model and use of the model to estimate the probability of damaging a radioactive material transportation cask during a ship collision. 1996;22:23.
- [24] Maestro M, Marino A. A predictive model for structural damages in ship collisions. *Tec Ital* 1995;60:149-62.
- [25] Petersen MJ. Dynamics of ship collisions. *Ocean Eng* 1982;9:295-329.
- [26] Simonsen BC. Ship grounding on rock - I. Theory. *Mar Struct* 1998;10:519-62.
- [27] Simonsen BC. Ship grounding on rock - II. Validation and application. *Mar Struct* 1998;10:563-84.
- [28] Pedersen PT, Zhang S. On impact mechanics in ship collisions. *Mar Struct* 1999;11:429-49.
- [29] Pedersen PT, Li Y. On the global ship hull bending energy in ship collisions. *Mar Struct* 2009;22:2-11.
- [30] Ito H, Kondo K, Yoshimura N, Kawashima M, Yamamoto S. A simplified method to analyse the strength of double hulled structures in collision. 1984;1984:283-96.
- [31] Ito H, Kondo K, Yoshimura N, Kawashima M, Yamamoto S. A simplified method to analyse the strength of double hulled structures in collision (2nd Report). *J SNAJ, Nihon zousen gakkai ronbunshu* 1985;1985:420-34.

- [32] Ito H, Kondo K, Yoshimura N, Kawashima M, Yamamoto S. A Simplified Method to Analyse the Strength of Double Hulled Structures in Collision (3rd Report). J SNAJ, Nihon zousen gakkai ronbunshu 1986;1986:266-74.
- [33] Paik JK, Pedersen PT. A simplified method for predicting ultimate compressive strength of ship panels. Int Shipbuild Prog 1996;43:139-57.
- [34] Samuel K. Skinner, William K. Reilly. The Exxon Valdez Oil Spill. 1989.
- [35] 'Ohtsubo, H.', 'Astrup, O.C.', 'Cazzulo, R.', 'Kim, O.H.', 'Lub, P.A.', Spangerberg, S.'. Structural design against collision and grounding. 1997.
- [36] Amdahl J. Energy absorption in ship-platform impacts [PhD thesis].[Trondheim (Norway)]: Department of Marine Technology. Norwegian University of Science and Technology 1983.
- [37] Kitamura O. FEM approach to the simulation of collision and grounding damage. Mar Struct 2002;15:403-28.
- [38] Quinton BWT, Daley CG, Gagnon RE. Effect of moving ice loads on the plastic capacity of a ship's structure. Int Conf Exhib Perform Ships Struct Ice, ICETECH 2010:146-53.
- [39] Quinton BWT, Daley CG, Gagnon RE. Realistic moving ice loads and ship structural response. Proc Int Offshore Polar Eng Conf 2012:1208-14.
- [40] Quinton BWT, Daley CG, Gagnon RE. Response of IACS URI ship structures to real-time full-scale operational ice loads. Int Conf Exhib Perform Ships Struct Ice, ICETECH 2012:89-95.
- [41] Quinton BWT, Daley CG, Gagnon RE. Response of IACS URI ship structures to real-time full-scale operational ice loads. Trans Soc Nav Archit Mar Eng 2013;120:203-9.
- [42] Alsos HS, Amdahl J. On the resistance to penetration of stiffened plates, Part I - Experiments. Int J Impact Eng 2009;36:799-807.
- [43] Alsos HS, Amdahl J, Hopperstad OS. On the resistance to penetration of stiffened plates, Part II: Numerical analysis. Int J Impact Eng 2009;36:875-87.
- [44] Chen Z. The role of heterogeneous particle distribution in the prediction of ductile fracture. , 2005.
- [45] Horstemeyer M, Ramaswamy S, Negrete M. Using a micromechanical finite element parametric study to motivate a phenomenological macroscale model for void/crack nucleation in aluminum with a hard second phase. Mech Mater 2003;35:675-87.

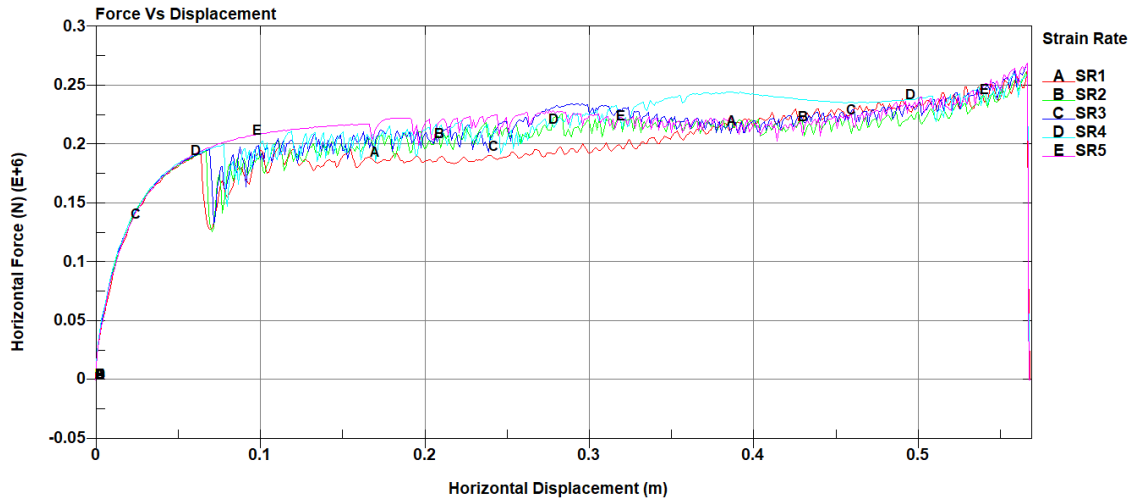
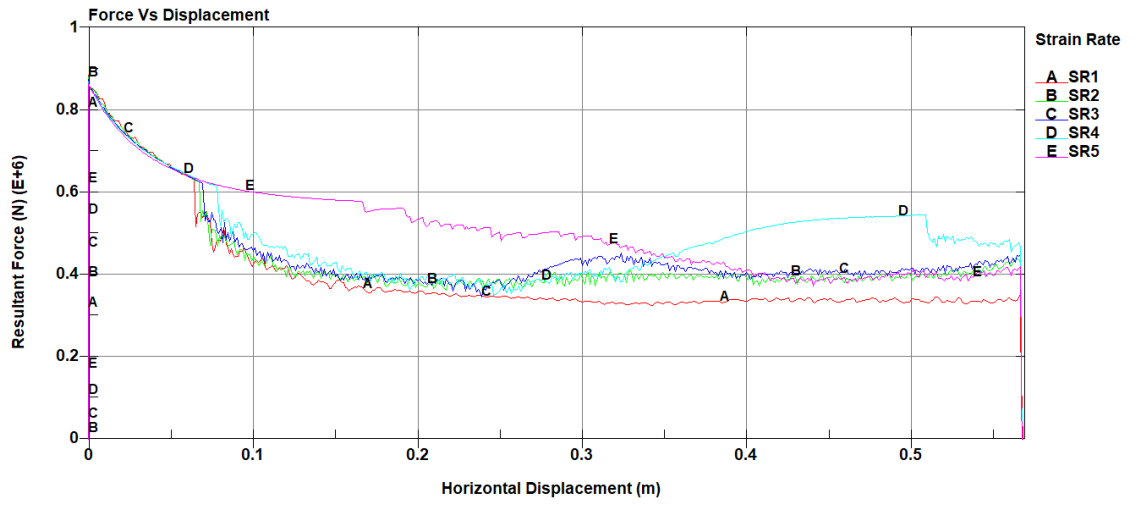
- [46] Gurland J, Plateau J. The mechanism of ductile rupture of metals containing inclusions 1963.
- [47] Gurland J. Observations on the fracture of cementite particles in a spheroidized 1.05% C steel deformed at room temperature. *Acta Metallurgica* 1972;20:735-41.
- [48] Cox TB, Low JR. An investigation of the plastic fracture of AISI 4340 and 18 Nickel-200 grade maraging steels. *Metallurgical Transactions* 1974;5:1457-70.
- [49] Brown WF. Review of developments in plane strain fracture toughness testing. : ASTM International, 1970.
- [50] Horstemeyer MF, Gokhale AM. A void-crack nucleation model for ductile metals. *Int J Solids Struct* 1999;36:5029-55.
- [51] Horstemeyer MF, Lathrop J, Gokhale AM, Dighe M. Modeling stress state dependent damage evolution in a cast Al-Si-Mg aluminum alloy. *Theor Appl Fract Mech* 2000;33:31-47.
- [52] Liu B, Qiu X, Huang Y, Hwang K, Li M, Liu C. The size effect on void growth in ductile materials. *J Mech Phys Solids* 2003;51:1171-87.
- [53] Tvergaard V. Influence of voids on shear band instabilities under plane strain conditions. *Int J Fract* 1981;17:389-407.
- [54] Gurson AL. Continuum theory of ductile rupture by void nucleation and growth: Part I—Yield criteria and flow rules for porous ductile media. *Journal of engineering materials and technology* 1977;99:2-15.
- [55] Tvergaard V, Needleman A. Analysis of the cup-cone fracture in a round tensile test bar. *Acta Metall* 1984;32:157-69.
- [56] Lou Y, Yoon JW, Huh H. Modeling of shear ductile fracture considering a changeable cut-off value for stress triaxiality. *Int J Plast* 2014;54:56-80.
- [57] Johnson GR, Cook WH. A constitutive model and data for metals subjected to large strains, high strain rates and high temperatures. 1983;21:541-7.
- [58] 'LS-DYNA Aerospace Working Group'. *MAT_224 User Guide*. 2017.
- [59] Buyuk M. Development of a tabulated thermo-viscoplastic material model with regularized failure for dynamic ductile failure prediction of structures under impact loading 2013.
- [60] 'Murat B. Development of a new material model in LS-DYNA, Part 2: Development of a tabulated thermo-viscoplastic material model with regularized failure for dynamic ductile failure prediction of structures under impact loading. 2014.

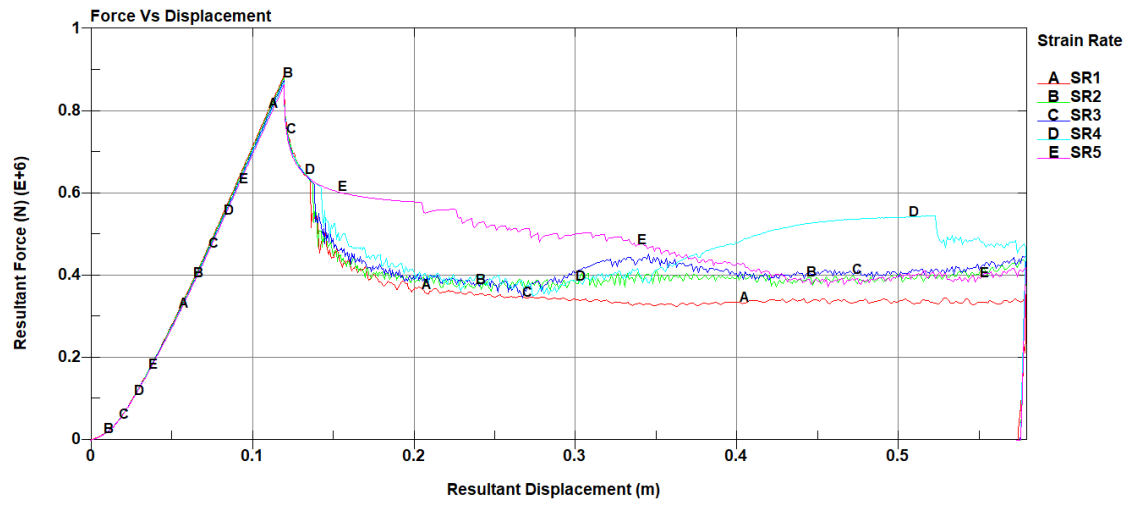
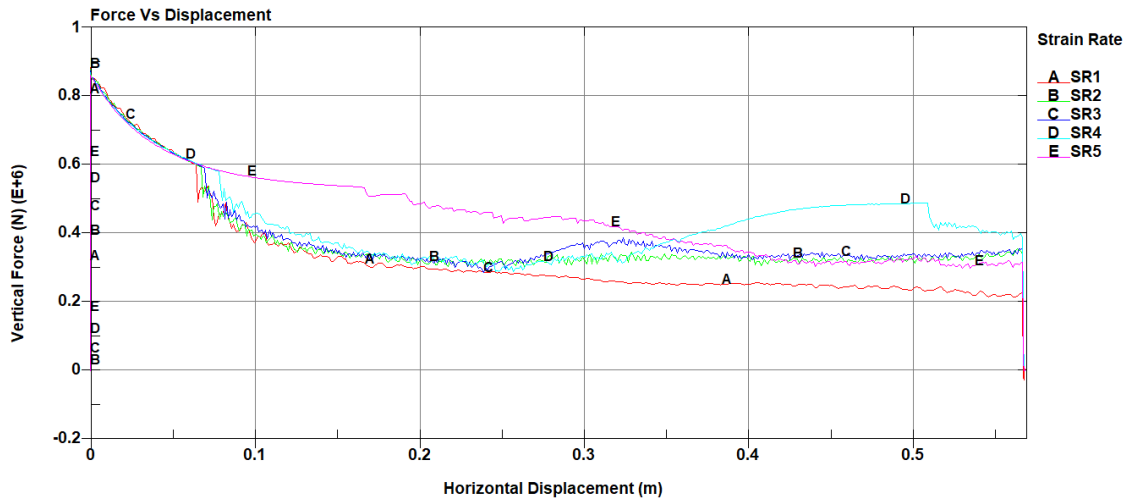
[61] Gokhale NS. Practical finite element analysis. : Finite to infinite, 2008.

Appendices

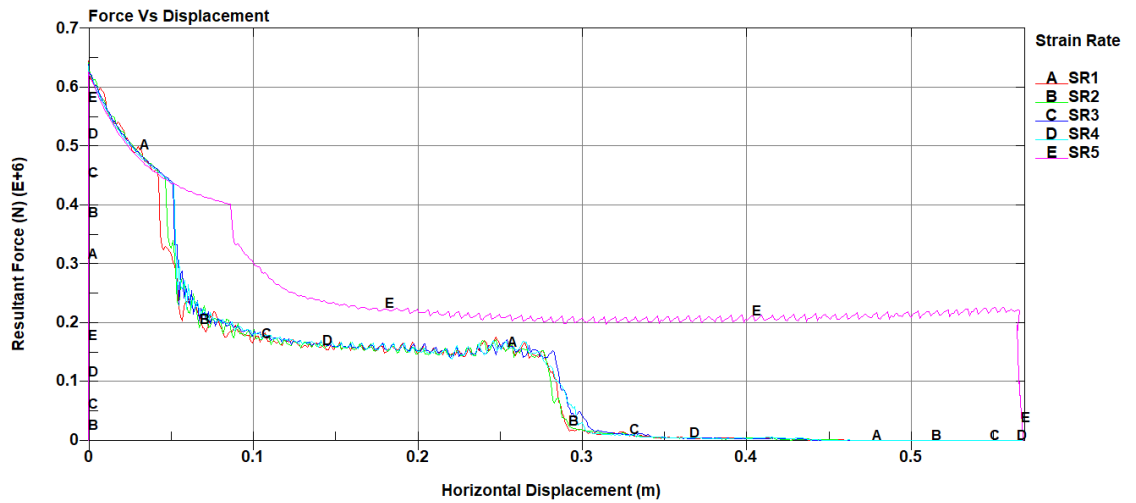
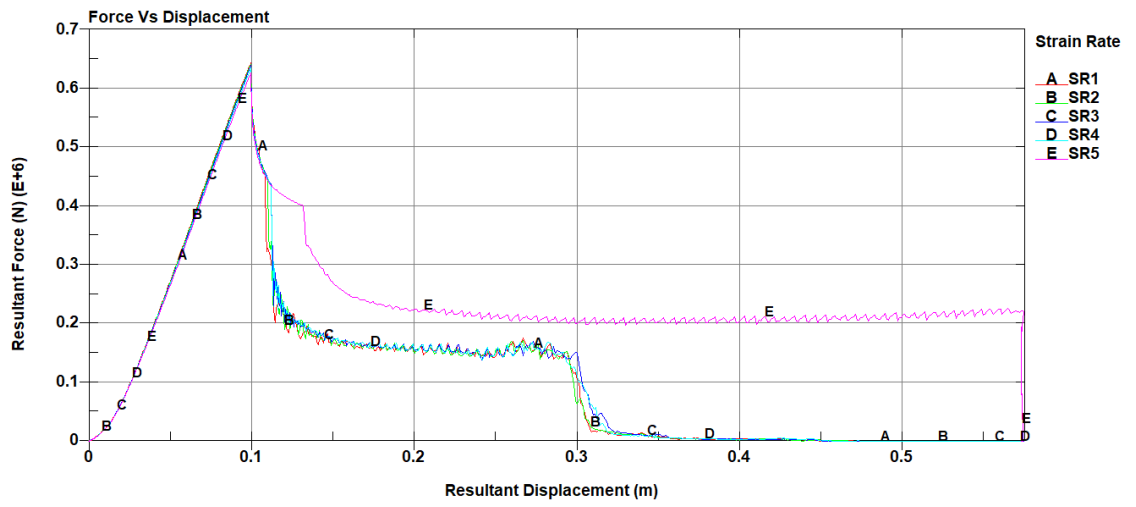
Appendix A **Simulation Results for Strain Rate Effect (Plots)**

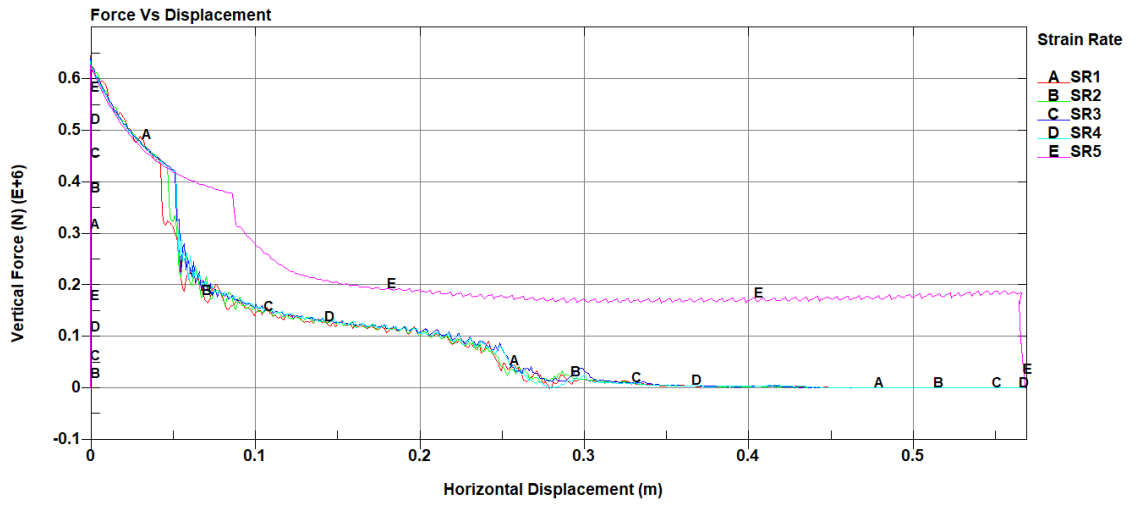
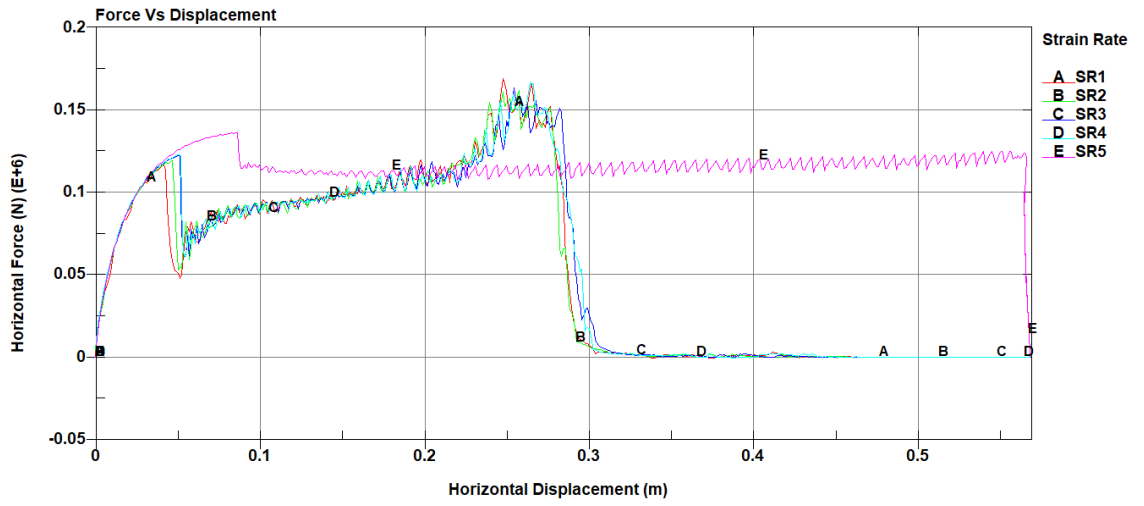
Appendix A1 Simulation Results (Plots) with Shell Elements





Appendix A2 Simulation Results (Plots) with Solid Elements

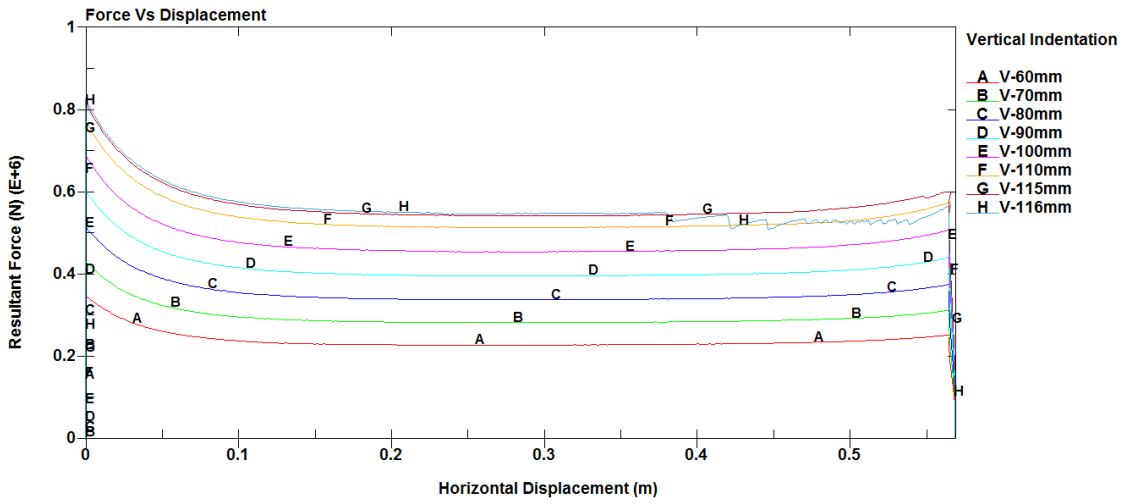
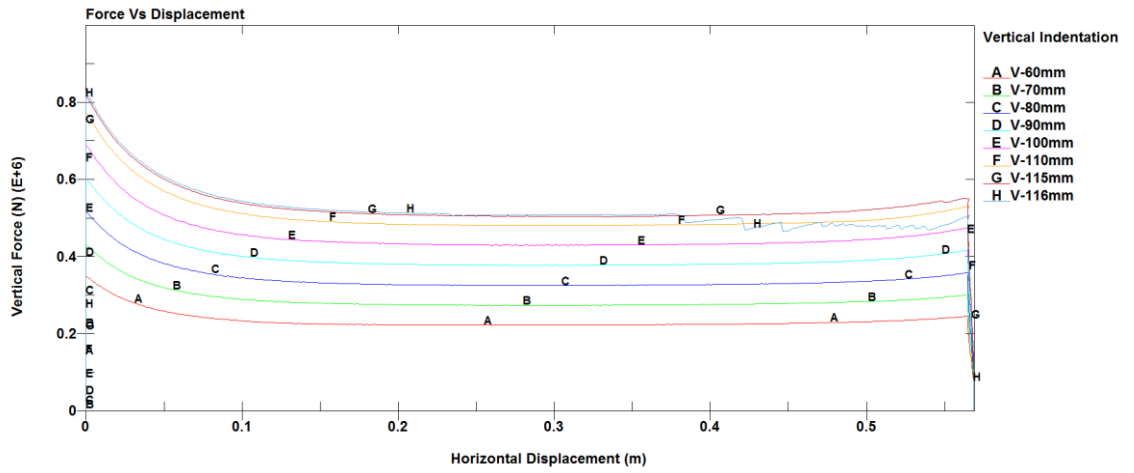


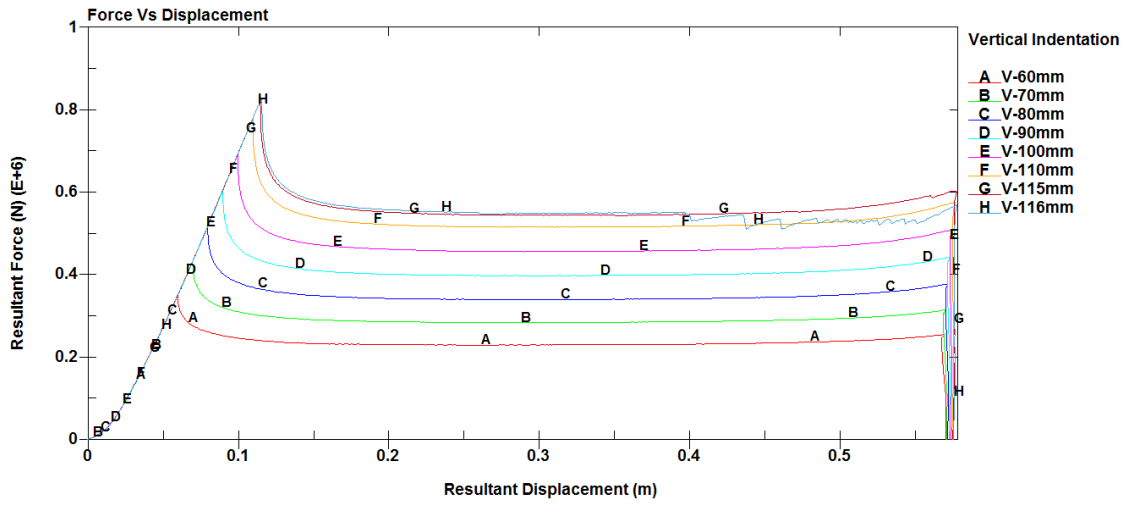
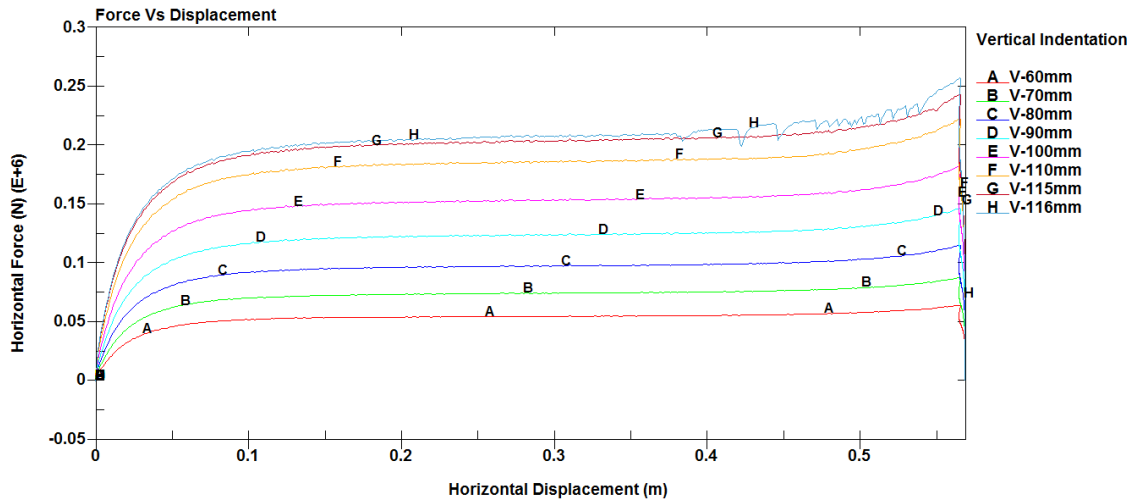


Appendix B Moving Load Capacity of the Plate Simulations Results

(Plots)

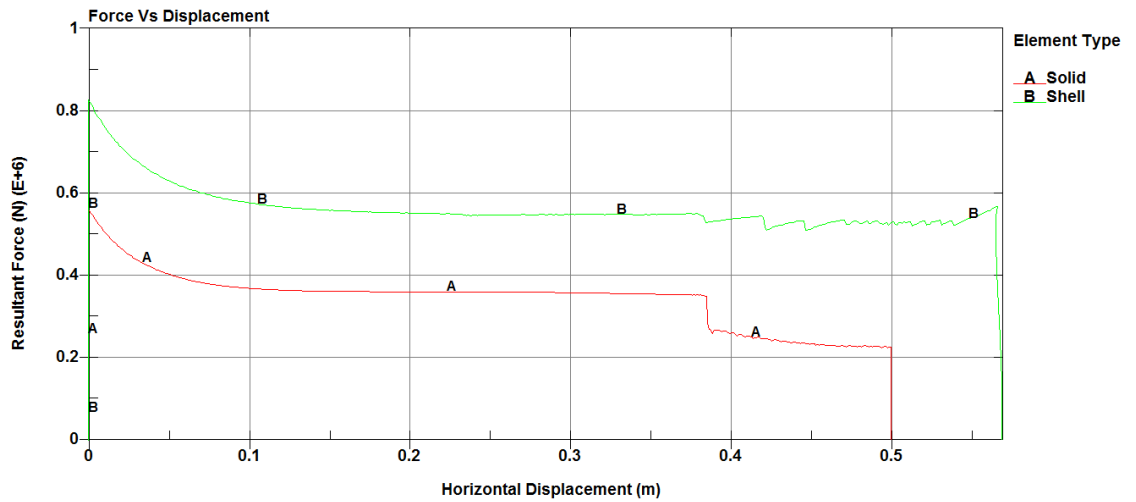
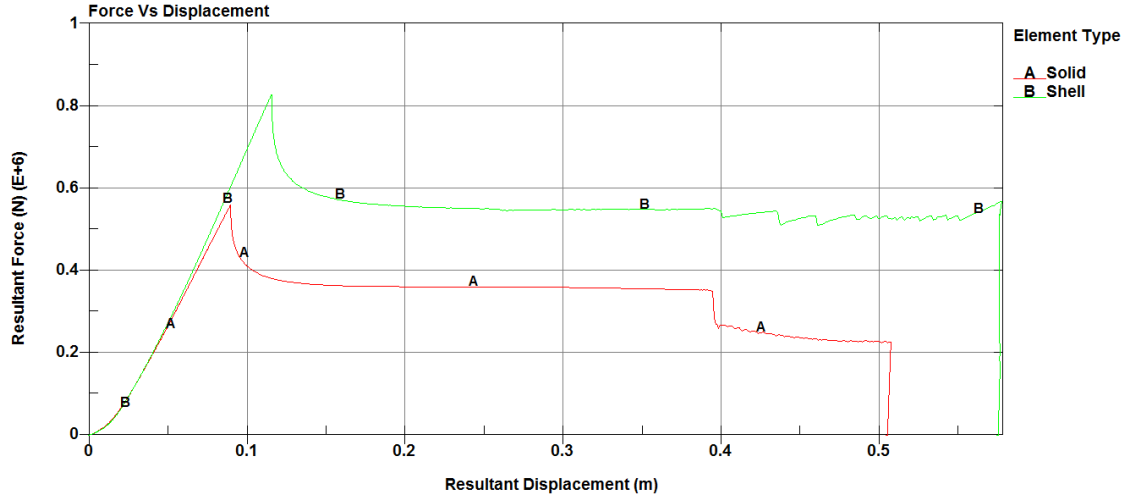
Appendix B1 Shell Elements Model Results (Plots)

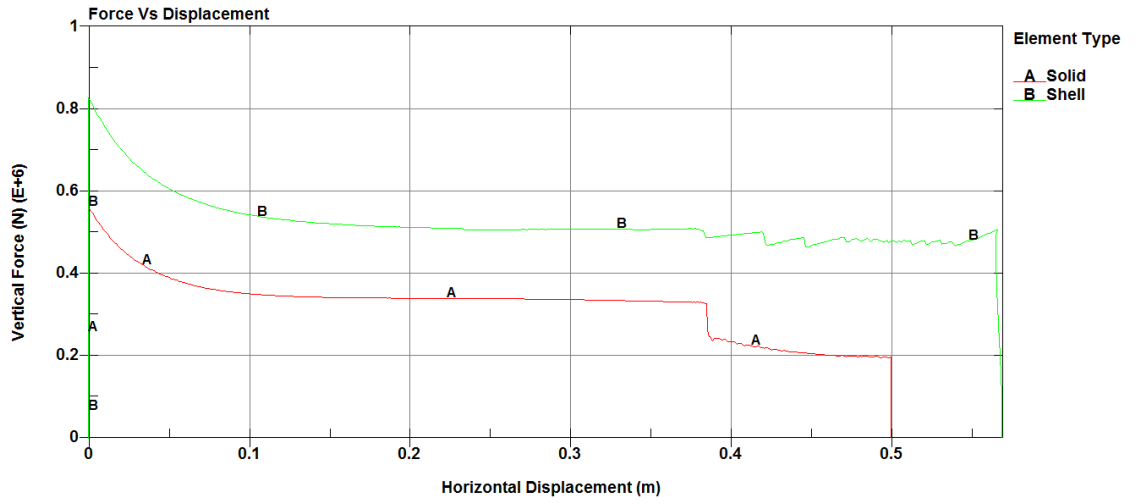
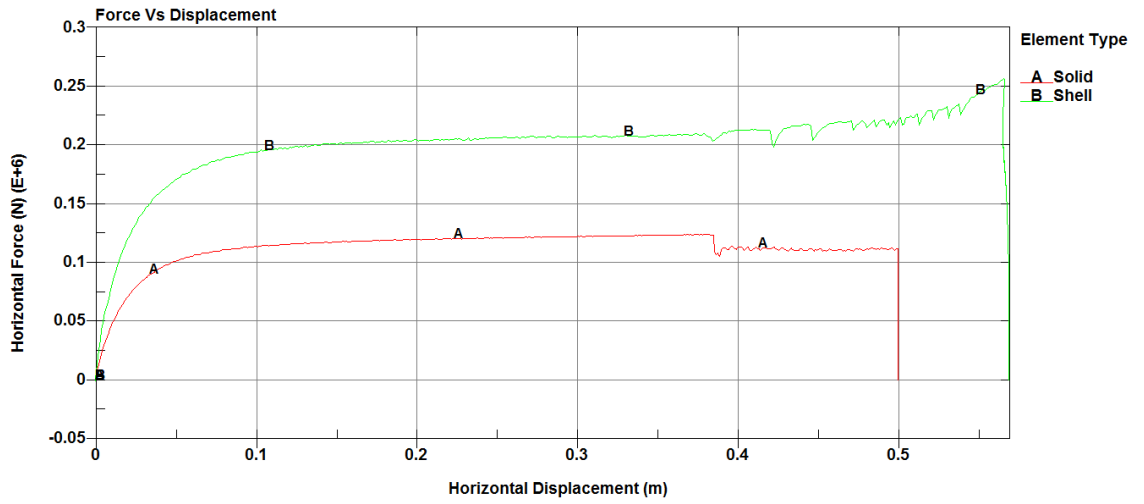




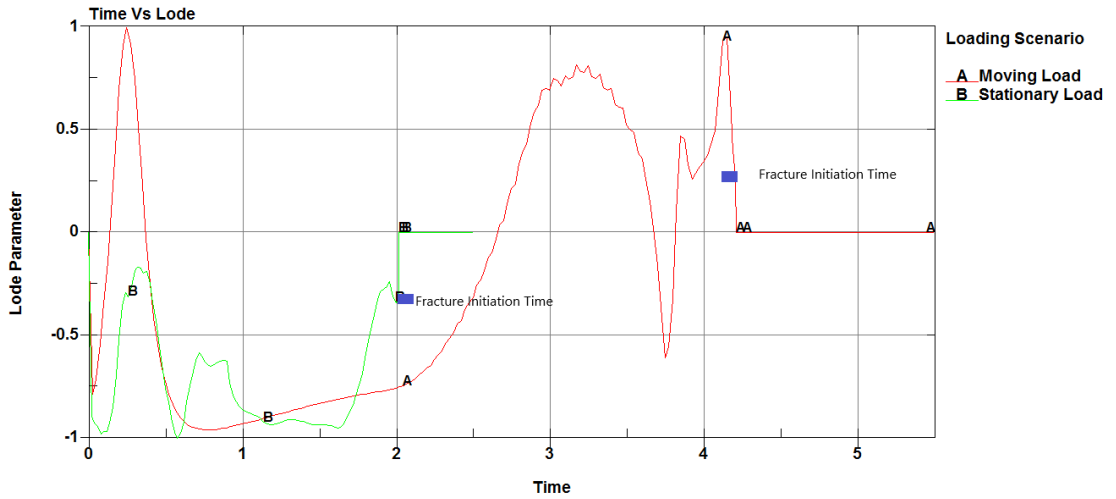
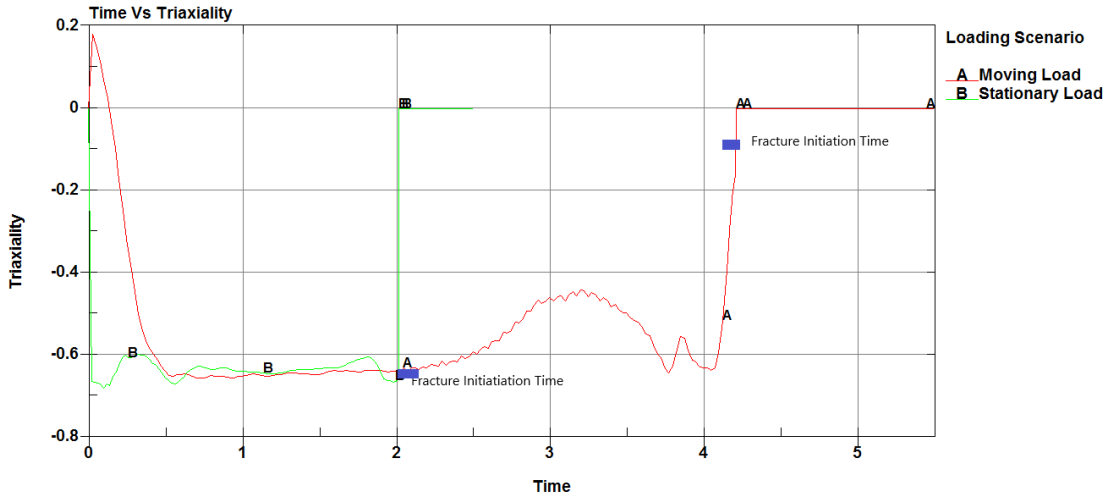
Appendix B2 Shell and Solid Elements Models Results Comparison

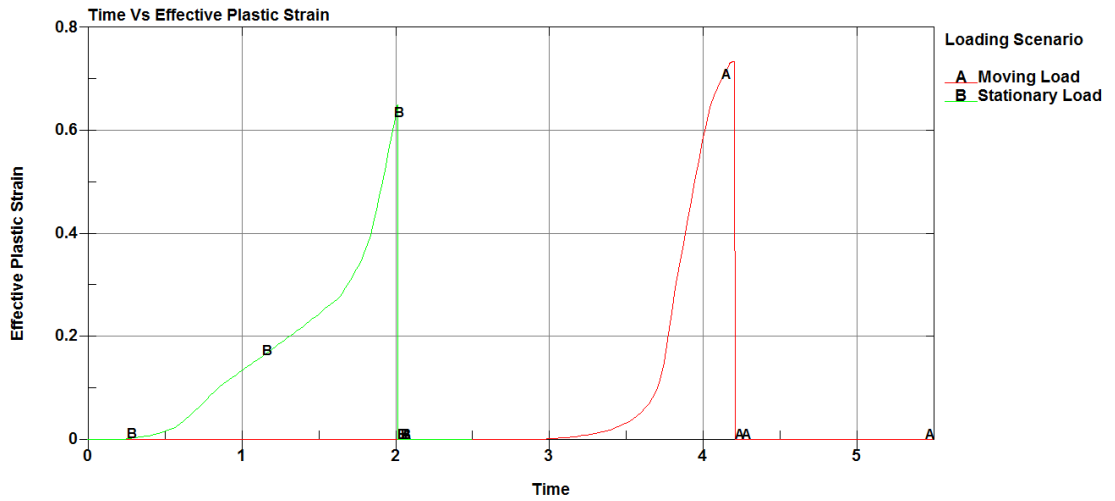
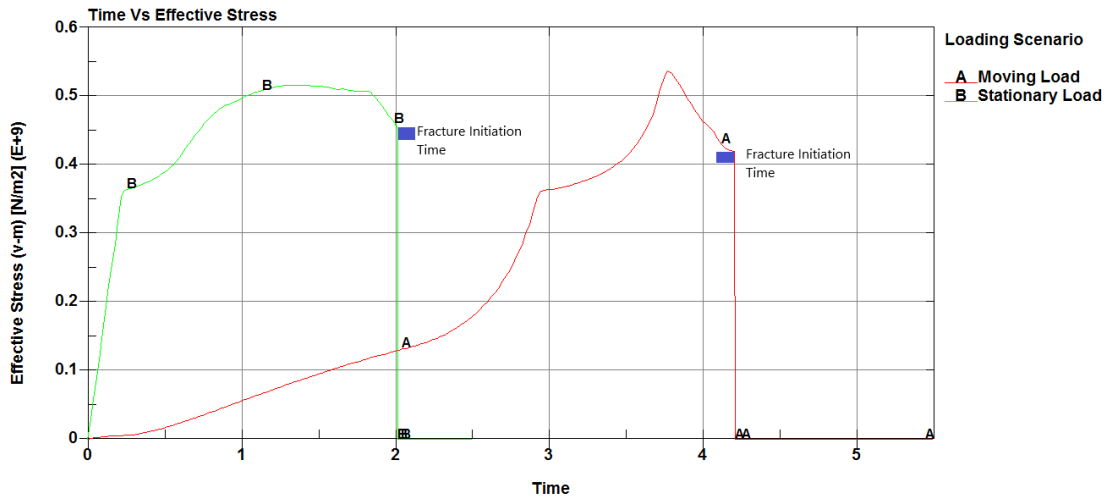
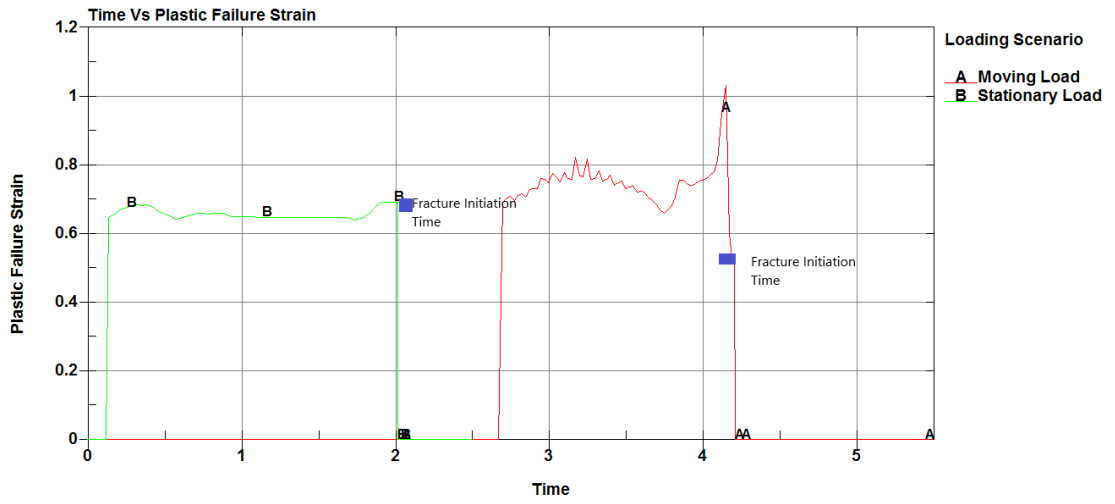
(Plots)

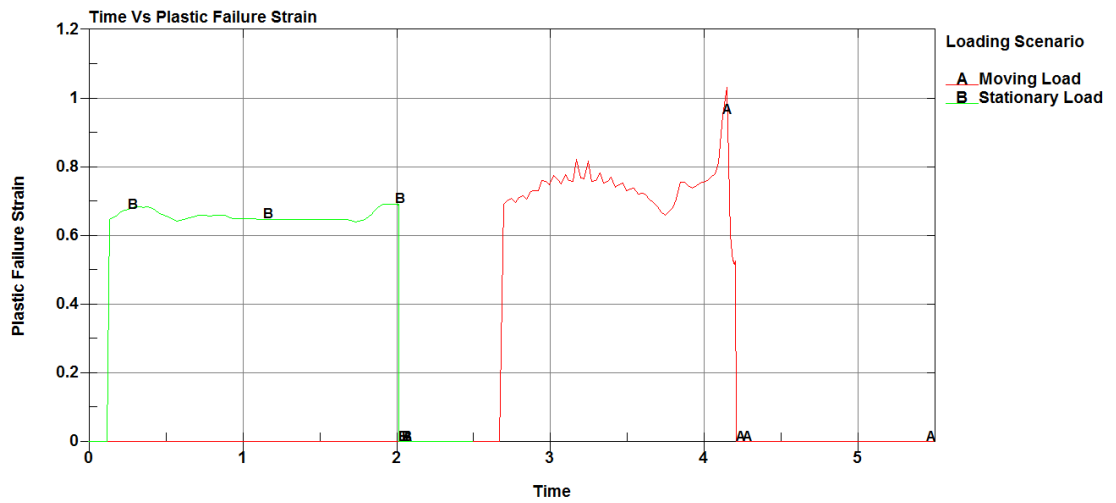
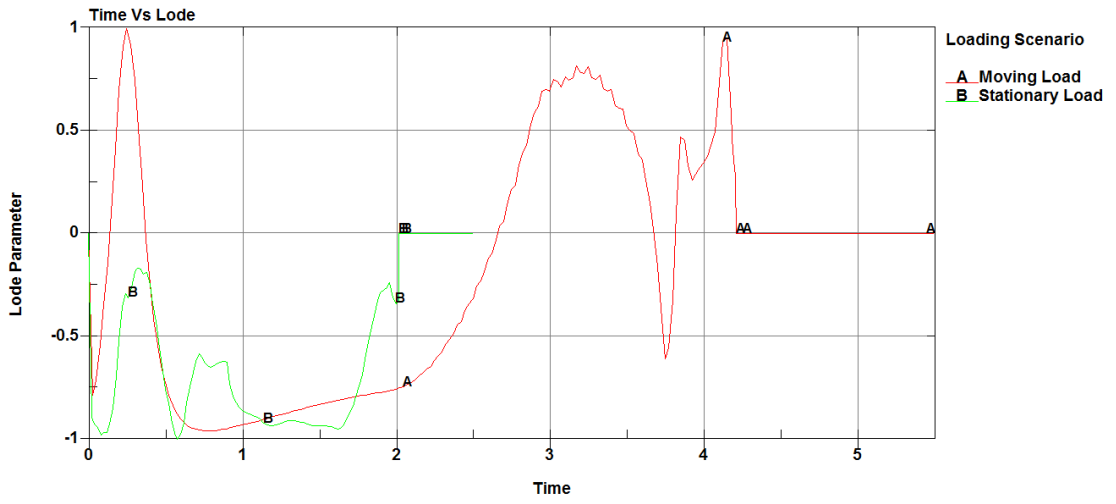
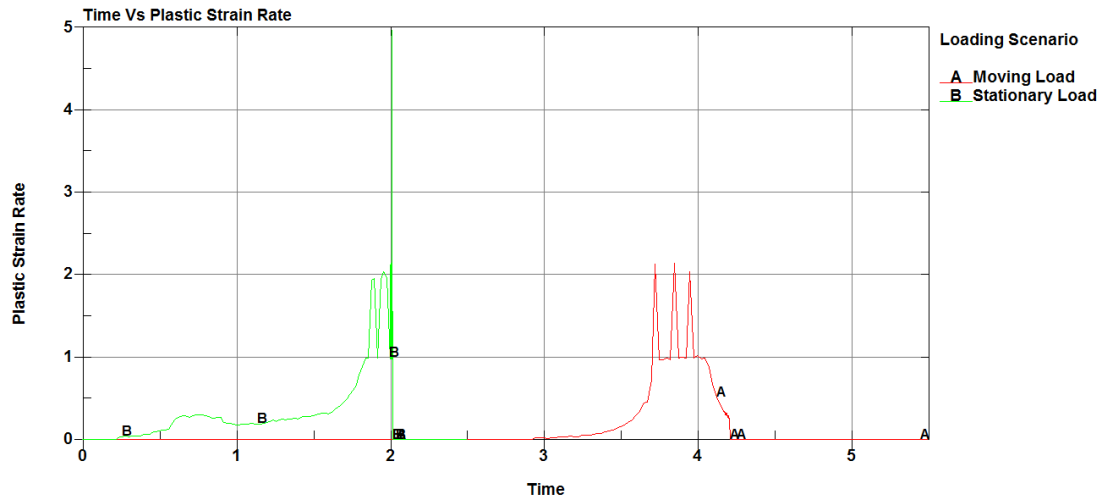


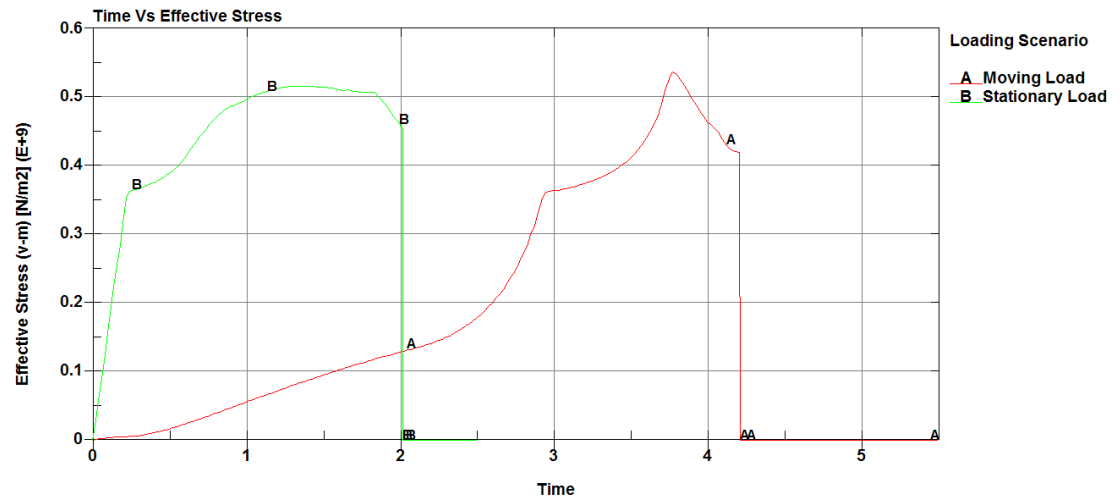
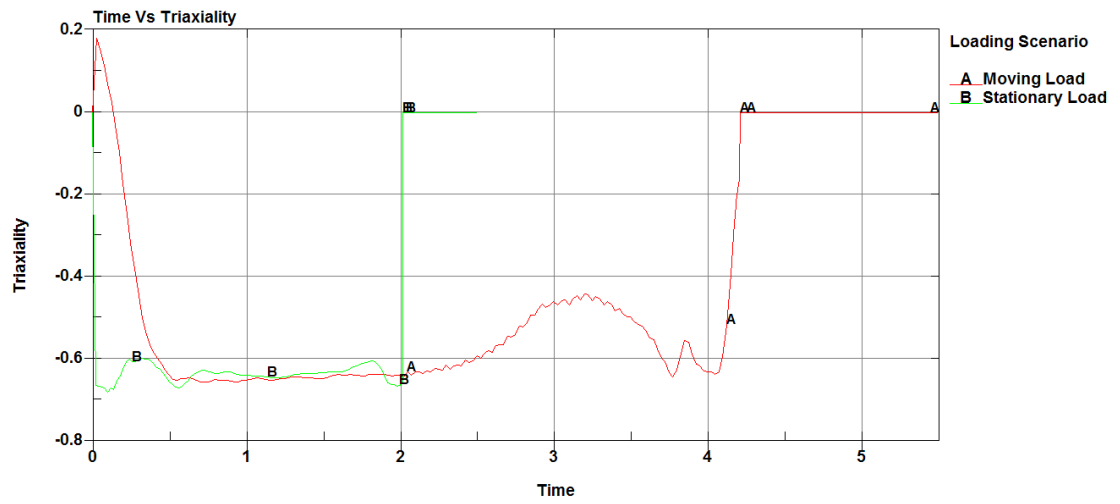


Appendix C Stress State Simulations Results (Moving Load and Stationary Load Results' Comparison Curves)

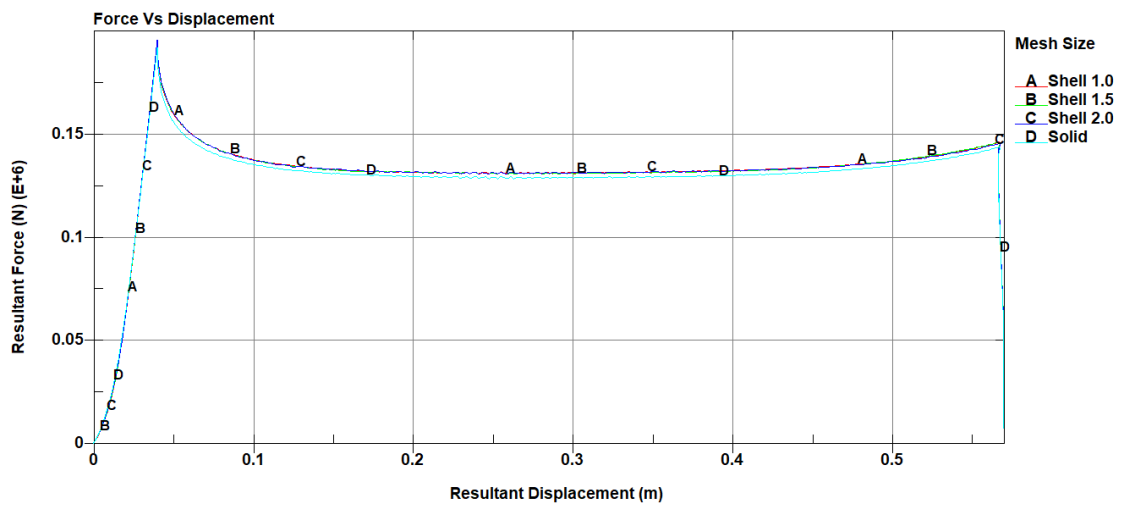
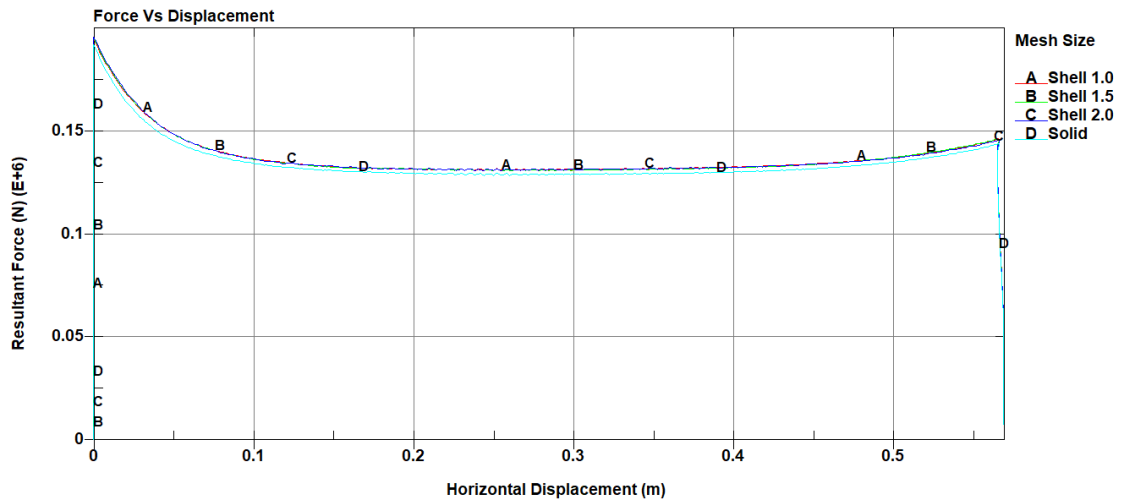
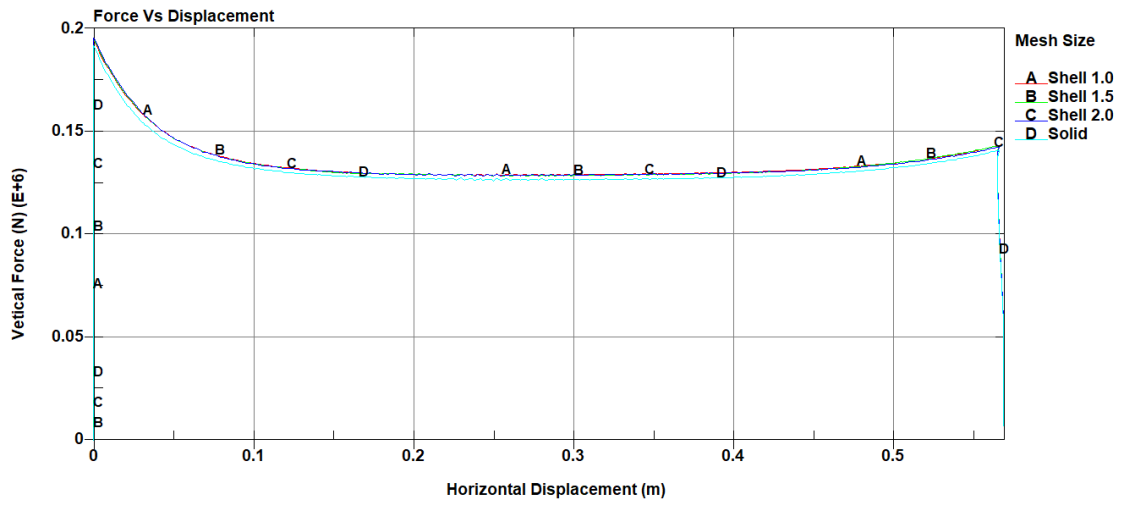








Appendix D Mesh Convergence Study Simulation Results (Plots)



[1] Quinton BWT. Progressive damage to a ship's structure due to ice loading. 2008.

- [2] Quinton BWT. Experimental and numerical investigation of moving loads on hull structures. 2015.
- [3] Alsos HS, Amdahl J. Analysis of bottom damage caused by ship grounding. 2008;2:829-36.
- [4] McClintock FA. A Criterion for Ductile Fracture by the Growth of Holes. J Appl Mech 1968;35:363.
- [5] Rice JR, Tracey DM. On the ductile enlargement of voids in triaxial stress fields*. J Mech Phys Solids 1969;17:201-17.
- [6] Bao Y. Prediction of ductile crack formation in uncracked bodies 2003.
- [7] Bao Y, Wierzbicki T. On fracture locus in the equivalent strain and stress triaxiality space. Int J Mech Sci 2004;46:81-98.
- [8] Johnson GR, Cook WH. Fracture characteristics of three metals subjected to various strains, strain rates, temperatures and pressures. Eng Fract Mech 1985;21:31-48.
- [9] Bai Y. Effect of loading history on necking and fracture 2007.
- [10] Bai Y, Wierzbicki T. A new model of metal plasticity and fracture with pressure and Lode dependence. Int J Plast 2008;24:1071-96.
- [11] Bai Y, Teng X, Wierzbicki T. On the application of stress triaxiality formula for plane strain fracture testing. J Eng Mater Technol Trans ASME 2009;131:0210021-02100210.
- [12] Bai Y, Wierzbicki T. Application of extended Mohr-Coulomb criterion to ductile fracture. Int J Fract 2010;161:1-20.
- [13] Bai Y, Wierzbicki T. A comparative study of three groups of ductile fracture loci in the 3D space. Eng Fract Mech 2014.
- [14] Bai Y, Wierzbicki T. A comparative study of three groups of ductile fracture loci in the 3D space. Eng Fract Mech 2015;135:147-67.
- [15] Wang G, Spencer J, Chen Y. Assessment of a ship's performance in accidents. Mar Struct 2002;15:313-33.
- [16] Pedersen PT. Review and application of ship collision and grounding analysis procedures. Mar Struct 2010;23:241-62.
- [17] 'Miguel Angel Gonzales Calle', 'Marcilio Alves'. Ship Collision: A Brief Survey. 21st Brazilian Congress of Mechanical Engineering October 2011.

- [18] Calle MAG, Alves M. A review- analysis on material failure modeling in ship collision. *Ocean Eng* 2015;106:20-38.
- [19] Ehlers S, Tabri K, Varsta P. Collision strength of ship structures-a state of the art review. *Mar Technol Eng* 2011;2:841-50.
- [20] Minorsky V. An analysis of ship collisions with reference to protection of nuclear power plants 1958.
- [21] Woisin G. Design against collision. : GKSS-Forschungszentrum, 1980.
- [22] Vaughan H. Damage to Ships due to Collision and Grounding. 1977.
- [23] Reardon P, Sprung J. Validation of Minorsky's ship collision model and use of the model to estimate the probability of damaging a radioactive material transportation cask during a ship collision. 1996;22:23.
- [24] Maestro M, Marino A. A predictive model for structural damages in ship collisions. *Tec Ital* 1995;60:149-62.
- [25] Petersen MJ. Dynamics of ship collisions. *Ocean Eng* 1982;9:295-329.
- [26] Simonsen BC. Ship grounding on rock - I. Theory. *Mar Struct* 1998;10:519-62.
- [27] Simonsen BC. Ship grounding on rock - II. Validation and application. *Mar Struct* 1998;10:563-84.
- [28] Pedersen PT, Zhang S. On impact mechanics in ship collisions. *Mar Struct* 1999;11:429-49.
- [29] Pedersen PT, Li Y. On the global ship hull bending energy in ship collisions. *Mar Struct* 2009;22:2-11.
- [30] Ito H, Kondo K, Yoshimura N, Kawashima M, Yamamoto S. A simplified method to analyse the strength of double hulled structures in collision. 1984;1984:283-96.
- [31] Ito H, Kondo K, Yoshimura N, Kawashima M, Yamamoto S. A simplified method to analyse the strength of double hulled structures in collision (2nd Report). *J SNAJ, Nihon zousen gakkai ronbunshu* 1985;1985:420-34.
- [32] Ito H, Kondo K, Yoshimura N, Kawashima M, Yamamoto S. A Simplified Method to Analyse the Strength of Double Hulled Structures in Collision (3rd Report). *J SNAJ, Nihon zousen gakkai ronbunshu* 1986;1986:266-74.
- [33] Paik JK, Pedersen PT. A simplified method for predicting ultimate compressive strength of ship panels. *Int Shipbuild Prog* 1996;43:139-57.

- [34] Samuel K. Skinner, William K. Reilly. The Exxon Valdez Oil Spill. 1989.
- [35] 'Ohtsubo, H.', 'Astrup, O.C.', 'Cazzulo, R.', 'Kim, O.H.', 'Lub, P.A.', Spangerberg, S.'. Structural design against collision and grounding. 1997.
- [36] Amdahl J. Energy absorption in ship-platform impacts [PhD thesis].[Trondheim (Norway)]: Department of Marine Technology. Norwegian University of Science and Technology 1983.
- [37] Kitamura O. FEM approach to the simulation of collision and grounding damage. *Mar Struct* 2002;15:403-28.
- [38] Quinton BWT, Daley CG, Gagnon RE. Effect of moving ice loads on the plastic capacity of a ship's structure. *Int Conf Exhib Perform Ships Struct Ice, ICETECH* 2010:146-53.
- [39] Quinton BWT, Daley CG, Gagnon RE. Realistic moving ice loads and ship structural response. *Proc Int Offshore Polar Eng Conf* 2012:1208-14.
- [40] Quinton BWT, Daley CG, Gagnon RE. Response of IACS URI ship structures to real-time full-scale operational ice loads. *Int Conf Exhib Perform Ships Struct Ice, ICETECH* 2012:89-95.
- [41] Quinton BWT, Daley CG, Gagnon RE. Response of IACS URI ship structures to real-time full-scale operational ice loads. *Trans Soc Nav Archit Mar Eng* 2013;120:203-9.
- [42] Alsos HS, Amdahl J. On the resistance to penetration of stiffened plates, Part I - Experiments. *Int J Impact Eng* 2009;36:799-807.
- [43] Alsos HS, Amdahl J, Hopperstad OS. On the resistance to penetration of stiffened plates, Part II: Numerical analysis. *Int J Impact Eng* 2009;36:875-87.
- [44] Chen Z. The role of heterogeneous particle distribution in the prediction of ductile fracture. , 2005.
- [45] Horstemeyer M, Ramaswamy S, Negrete M. Using a micromechanical finite element parametric study to motivate a phenomenological macroscale model for void/crack nucleation in aluminum with a hard second phase. *Mech Mater* 2003;35:675-87.
- [46] Gurland J, Plateau J. The mechanism of ductile rupture of metals containing inclusions 1963.
- [47] Gurland J. Observations on the fracture of cementite particles in a spheroidized 1.05% C steel deformed at room temperature. *Acta Metallurgica* 1972;20:735-41.

- [48] Cox TB, Low JR. An investigation of the plastic fracture of AISI 4340 and 18 Nickel-200 grade maraging steels. *Metallurgical Transactions* 1974;5:1457-70.
- [49] Brown WF. Review of developments in plane strain fracture toughness testing. : ASTM International, 1970.
- [50] Horstemeyer MF, Gokhale AM. A void-crack nucleation model for ductile metals. *Int J Solids Struct* 1999;36:5029-55.
- [51] Horstemeyer MF, Lathrop J, Gokhale AM, Dighe M. Modeling stress state dependent damage evolution in a cast Al-Si-Mg aluminum alloy. *Theor Appl Fract Mech* 2000;33:31-47.
- [52] Liu B, Qiu X, Huang Y, Hwang K, Li M, Liu C. The size effect on void growth in ductile materials. *J Mech Phys Solids* 2003;51:1171-87.
- [53] Tvergaard V. Influence of voids on shear band instabilities under plane strain conditions. *Int J Fract* 1981;17:389-407.
- [54] Gurson AL. Continuum theory of ductile rupture by void nucleation and growth: Part I—Yield criteria and flow rules for porous ductile media. *Journal of engineering materials and technology* 1977;99:2-15.
- [55] Tvergaard V, Needleman A. Analysis of the cup-cone fracture in a round tensile test bar. *Acta Metall* 1984;32:157-69.
- [56] Lou Y, Yoon JW, Huh H. Modeling of shear ductile fracture considering a changeable cut-off value for stress triaxiality. *Int J Plast* 2014;54:56-80.
- [57] Johnson GR, Cook WH. A constitutive model and data for metals subjected to large strains, high strain rates and high temperatures. 1983;21:541-7.
- [58] 'LS-DYNA Aerospace Working Group'. *MAT_224 User Guide*. 2017.
- [59] Buyuk M. Development of a tabulated thermo-viscoplastic material model with regularized failure for dynamic ductile failure prediction of structures under impact loading 2013.
- [60] 'Murat B. Development of a new material model in LS-DYNA, Part 2: Development of a tabulated thermo-viscoplastic material model with regularized failure for dynamic ductile failure prediction of structures under impact loading. 2014.
- [61] Gokhale NS. *Practical finite element analysis. : Finite to infinite*, 2008.